AD-A079 054 OAK RIDGE NATIONAL LAB TN HEALTH AND SAFETY RESEARCH DIV F/G 9/5
STUDIES OF PHOTON AND ELECTRON INTERACTIONS WITH COMMUNICATIONS--ETC(U)
OCT 79 J C ASHLEY , M W WILLIAMS

UNCLASSIFIED RADC-TR-79-234 NL

1 OF 2
AD-
A079054

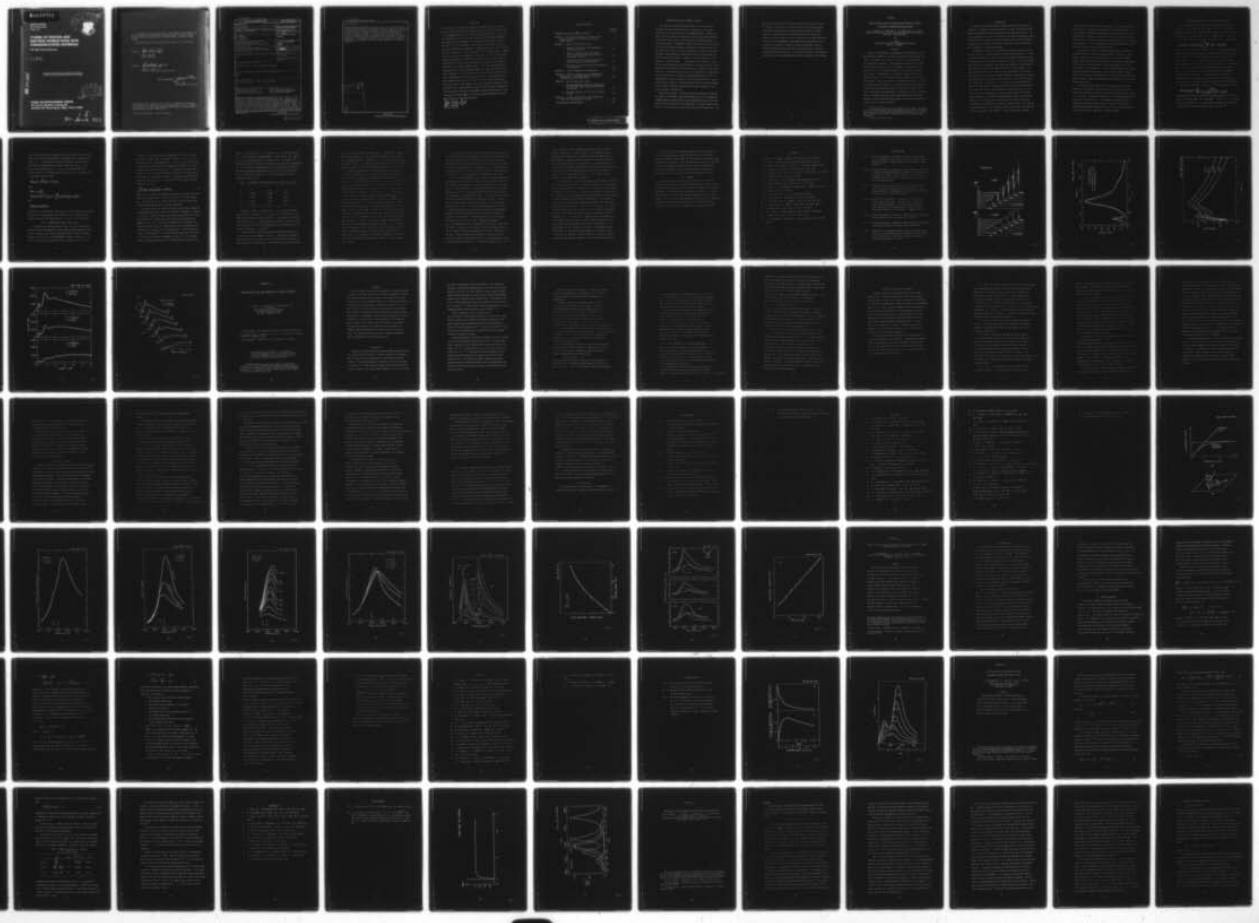

RADC-TR-79-234
Final Technical Report
October 1979

STUDIES OF PHOTON AND ELECTRON INTERACTIONS WITH COMMUNICATIONS MATERIALS

Oak Ridge National Laboratory

J. C. Ashley
M. W. Williams

ROME AIR DEVELOPMENT CENTER
Air Force Systems Command
Griffiss Air Force Base, New York 13441

This report has been reviewed by the RADC Public Affairs Office (PA) and is releasable to the National Technical Information Service (NTIS). At NTIS it will be releasable to the general public, including foreign nations.

RADC-TR-79-234 has been reviewed and is approved for publication.

APPROVED: John N Bradford

JOHN N. BRADFORD
Project Engineer

APPROVED: Robert M Barrett

ROBERT M. BARRETT
Director, Solid State Sciences Division

FOR THE COMMANDER: John P. Huss

JOHN P. HUSS
Acting Chief, Plans Office

If your address has changed or if you wish to be removed from the RADC mailing list, or if the addressee is no longer employed by your organization, please notify RADC (ESR), Hanscom AFB MA 01730. This will assist us in maintaining a current mailing list.

Do not return this copy. Retain or destroy.

UNCLASSIFIED

SECURITY CLASSIFICATION OF THIS PAGE (When Data Entered)

REPORT DOCUMENTATION PAGE

READ INSTRUCTIONS BEFORE COMPLETING FORM

1. REPORT NUMBER: RADC-TR-79-234	2. GOVT ACCESSION NO.
3. RECIPIENT'S CATALOG NUMBER	
4. TITLE (and Subtitle): STUDIES OF PHOTON AND ELECTRON INTERACTIONS WITH COMMUNICATIONS MATERIALS	5. TYPE OF REPORT & PERIOD COVERED: Final Technical Report. 1 Oct 76 - Sep 78.
	6. PERFORMING ORG. REPORT NUMBER: N/A
7. AUTHOR(s): J. C. Ashley, M. W. Williams	8. CONTRACT OR GRANT NUMBER(s): RAD80007
9. PERFORMING ORGANIZATION NAME AND ADDRESS: Oak Ridge National Laboratory, Health and Safety Research Division, Oak Ridge TN 37830	10. PROGRAM ELEMENT, PROJECT, TASK AREA & WORK UNIT NUMBERS: 61102F, 2306J320
11. CONTROLLING OFFICE NAME AND ADDRESS: Deputy for Electronic Technology (RADC/ESR), Hanscom AFB MA 01731	12. REPORT DATE: Oct 1979
	13. NUMBER OF PAGES: 142
14. MONITORING AGENCY NAME & ADDRESS (if different from Controlling Office): Same	15. SECURITY CLASS. (of this report): UNCLASSIFIED
	15a. DECLASSIFICATION/DOWNGRADING SCHEDULE: N/A

16. DISTRIBUTION STATEMENT (of this Report)

Approved for public release; distribution unlimited.

17. DISTRIBUTION STATEMENT (of the abstract entered in Block 20, if different from Report)

Same

18. SUPPLEMENTARY NOTES

RADC Project Engineer: John B. Bradford RADC/ESR

19. KEY WORDS (Continue on reverse side if necessary and identify by block number)

photon and electron interactions
communications materials
straggling and plasmon excitation
optical emission from solids
optical properties of polyethylene
optical guided wave studies

20. ABSTRACT (Continue on reverse side if necessary and identify by block number)

This report summarizes theoretical and experimental studies designed to yield information on photon and electron interactions with various communications materials. Theoretical predictions have been made for the energy-loss spectra of low-energy electrons (400 eV to 1600 eV) transmitted through thin films of carbon and comparisons made with available experimental data on 80 films. The optical properties of polyethylene have been measured over the photon energy range from 0.5 eV to 76 eV. Optical emission spectra from the solids Ag, K, Mg, and Al bombarded by low-energy electrons (20 eV to 1.5 keV) have been (Cont'd)

DD FORM 1 JAN 73 1473

UNCLASSIFIED

SECURITY CLASSIFICATION OF THIS PAGE (When Data Entered)

411525

Item 20 (Cont'd)

measured and theoretical models developed to explain the experimental data. Theoretical models combined with experimental data have resulted in tabulations of inverse mean free paths, stopping powers, "continuous-slowing-down-approximation" ranges, and straggling in the organic insulator polystyrene for electrons of energies 10 keV. Optical guided wave techniques have been employed to measure the change in refractive index of LiF films as a function of time after deposition, and a new method has been demonstrated for direct observation of the dispersion relation of optical guided waves. Studies on modifications and extensions of classical-binary-collision cross sections are summarized.

EVALUATION

This report covers research performed by the Health and Safety Research Division of Oak Ridge National Laboratory during the period 1 October 1976 to 30 September 1978 and is the Final Report for that period. The support was provided under Air Force Project Orders Y77-6, Y77-871 and RAD80007. The objective of the research is to theoretically develop the parameter pertinent to electron transport in electronic materials and to make the necessary experimental measurements to support that theory. The information derived is supplied via technical reports to the radiation effects community for use in assessing the response of electronics to nuclear and/or space radiation environments. Specifically, the low energy electron mean free paths have been determined for polystyrene and the basis established for evaluation of all carbon polymer plastics. This work has had immediate application in the dose enhancement studies of metal/semiconductor-insulation interfaces. Also, generated in this time frame was the dose distribution surrounding a cosmic ray track in silicon. That information will have immediate application in the cosmic ray-VLSI interaction analysis. The report covers a time segment of an ongoing program in support of RADC Technology Plan - Subthrust R4D entitled EM (Device) Radiation Hardening. The overall effort has been of the highest technical quality and is continuing with the development of electron transport parameters valid for whole classes of electronic materials.

John N Bradford

JOHN N. BRADFORD
Project Engineer

TABLE OF CONTENTS

PROGRAM OBJECTIVE AND SUMMARY OF RESULTS

The intent was that work performed under this contract would increase our understanding of the basic mechanisms involved when electrons interact with matter in its condensed phases. Emphasis has been placed on studying the interactions occurring in those materials which are currently used, or which are being considered for use, in electronics systems. Knowledge of quantities such as the cross sections for the various types of electron interactions in these materials and the energy-loss spectra for electrons generated by ionizing radiations incident on these materials, enable predictions to be made concerning the performance of electronics systems in various situations, such as exposure to nuclear radiation. Our approach to this general problem has been both theoretical and experimental. In our experimental program, we have made observations which can be related to electron interactions in solids. The theoretical portions of the program have included predictive calculations for a variety of interaction phenomena as well as interpretative studies in support of our experimental efforts. Results from the basic theoretical and experimental programs have been employed in more specific, applied calculations with direct relevance to electronics systems' vulnerability.

Specifically we have: (a) made theoretical predictions for energy-loss spectra of electrons transmitted through thin films of carbon and compared these predictions with available experimental data; (b) determined the optical properties of polyethylene in the photon energy range from 0.5 eV to 76 eV; (c) studied, experimentally and theoretically, the

optical emission from several metals bombarded by low-energy electrons; (d) produced a tabulation of inverse mean free paths, stopping powers, csda ranges, and straggling in polystyrene for electrons of energy $\leq$ 10 keV; (e) employed optical guided wave techniques to measure the change in refractive index of LiF as a function of time after deposition of the film; (f) demonstrated a new method for directly observing and recording the dispersion relation for optical guided waves; and (g) studied theoretically some extensions and modifications of classical-binary-collision cross sections. A detailed description of these topics, in the form of self-contained chapters, makes up the body of this report.

CHAPTER I

Straggling and Plasmon Excitation in the Energy Loss Spectra of Electrons Transmitted through Carbon*

J. C. Ashley, V. E. Anderson,† J. J. Cowan, and R. H. Ritchie
Health and Safety Research Division, Oak Ridge National Laboratory
Oak Ridge, Tennessee 37830

and

J. Hoelzl
Department of Physics, Gesamthochschule Kassel
Kassel 35, Germany

Abstract

A model is described for the calculation of differential inverse mean free paths (DIMFP's) for inelastic interactions of electrons with solids. The energy loss function, $\mathrm{Im}[-1/\varepsilon(q,\omega)]$, is represented as a sum of Drude-type functions. The adjustable parameters in the energy loss function are fixed by a fit to the energy loss function in the optical limit ($q \to 0$) obtained from data on the optical constants of glassy carbon. The extension of the optical energy loss function to arbitrary values of q in this model leads to an analytical expression for the DIMFP. Energy loss spectra for low-energy electrons (< 2000 eV) transmitted through carbon foils of various thicknesses are determined by solving the transport equation using a convolution method and the DIMFP's determined as described above. Comparisons of these calculated spectra with those measured by Jacobi show that the model provides a good description of both the broad straggling distribution and the fine structure due to plasmon excitation.

---

*Research sponsored jointly by the Deputy for Electronic Technology, Air Force Systems Command, under Interagency Agreement DOE No. 40-226-70 and the Division of Biomedical and Environmental Research, U. S. Department of Energy, under contract W-7405-eng-26 with the Union Carbide Corporation.

†Computer Sciences Division

I. INTRODUCTION

In order to fully understand the interaction of ionizing radiations with matter, one needs to be able to measure or predict theoretically what happens to both the particles and the matter with which they interact. As a basic component in solving this problem, we are applying theoretical models to predict the distribution in energy of electrons which are transmitted through layers of material for electron energies and layer thicknesses for which straggling is an important factor.

Characteristic energy loss experiments[1] typically use electrons with energies $\gtrsim$ 20 keV. At these energies, electron mean free paths are > 100 Å so electrons transmitted through films of a few hundred Angstroms thickness will undergo only a small number of energy loss events. This type of experiment allows one to study the single energy loss processes (both collective and single-particle) which are characteristic of the given medium. For lower electron energies, say $\lesssim$ 2000 eV, mean free paths are much smaller and multiple energy loss events become important in determining the spectra of transmitted electrons even in rather thin films. Such multiple energy loss events lead to straggling as is evident in the experimental work of Jacobi[2] on transmission of low-energy electrons through thin carbon films. His results for the energy distributions of electrons, $N_T(E)$ vs E, are shown in Fig. 1 for monoenergetic, primary electron beams with energies ranging from 400 eV to 1600 eV transmitted through carbon foils 80 Å and 230 Å thick. The energy scale in the figure (horizontal axis) may be delineated by the positions of the elastic scattering peaks. The structure at electron energies $\gtrsim$ 20 eV below the elastic peak results from Auger and plasmon excitations in the material. At very low energies, secondary

electrons also contribute to the distributions. The above contributions are also seen in the energy distributions of reflected electrons. The broad asymmetric component, which appears only in transmission, has the characteristic of becoming narrower and shifting to higher energies as either the foil thickness is decreased or the primary energy is increased. This component is due to straggling of the primary electrons as they are degraded in energy in passing through the foil.

Employing the simple Bohr impact parameter model for electron-electron interactions and the straggling theory of Landau, the straggling distributions could be accounted for in a reasonable manner.[3] However, the structure due to multiple plasmon excitations superimposed on the broad straggling distributions was not accounted for in the simple model used in reference 3. Since the experimental energy spectra indicate substantial contributions from plasmon excitation, a more realistic description of the interaction of the incident electrons with the foil should include the plasmon excitation process as well as single particle collisions.

In the work presented here we will concentrate on the electron energy loss region where plasmon excitations are important in determining the structure of the energy loss spectrum (electron energy losses up to ~ 200 eV). The theory and models used in the calculations will be described in the next section. The theoretical predictions will be compared with the experimental results for carbon[2] in Section III followed by some general observations on the validity and usefulness of these calculations for predictions in applied problems.

II. THEORETICAL DESCRIPTION OF ELECTRON ENERGY LOSSES

A basic component of the theory is a suitable description of the differential inverse mean free path (DIMFP), $d\Lambda^{-1}/d\omega$, for inelastic interactions of an electron with the solid. Since we are interested in the distribution of energy losses only, the DIMFP, or the probability per unit path length per unit energy for an energy loss ω, is given by[4]

$$d\Lambda^{-1}/d\omega \equiv \tau(E,\omega) = \frac{1}{\pi E}\int_{q_-}^{q_+}\frac{dq}{q}\ Im[-1/\varepsilon(q,\omega)]\ , \qquad (1)$$

where $E = v^2/2$ is the energy of the electron, v is the electron velocity, and the limits on the integration over momentum transfer q are given by $q_\pm = v \pm \sqrt{v^2 - 2\omega}$. In the discussion here we work in atomic units (a.u.) where $\hbar = m = e = 1$; conversions to other units will be given where appropriate. The energy loss function $Im[-1/\varepsilon(q,\omega)]$, the imaginary part of the negative reciprocal of the complex dielectric response function, ε, of the solid, describes the response of the medium to energy and momentum transfers. A simple model for the dielectric response function which emphasizes the influence of single-particle interactions for large momentum transfer and interactions with plasmons for small momentum transfer is given by a sum of Drude-type functions as

$$Im[-1/\varepsilon(q,\omega)] = \sum_i \frac{A_i\gamma_i\omega}{[(\omega_{oi}+q^2/2)^2-\omega^2]^2+(\gamma_i\omega)^2}\ . \qquad (2)$$

An energy loss function of this form was used by Hamm et al.[5] for calculations of electron DIMFP's in liquid water. In the limit $q \to 0$ (optical limit), the constants A_i, γ_i, and ω_{oi} may be obtained from optical data for the medium or from characteristic energy loss data.[1,6]

Using Eq. (2), where $q \neq 0$, the integration over momentum transfer to obtain the DIMFP may be performed analytically to give

$$\tau(E,\omega) = \frac{1}{\pi V^2} \sum_i \frac{A_i \gamma_i \omega}{(\omega_{oi}^2 - \omega^2)^2 + (\gamma_i \omega)^2} \left\{ \ln(q_+^2/q_-^2) - [T_i(c_i) - T_i(-c_i)]/2\gamma_i \omega c_i \right\}, \quad (3)$$

where

$$T_i(c_i) \equiv [a_i(\omega_{oi}\alpha_i + c_i) - \omega_{oi}\beta_i(\omega_{oi}^2 - \omega^2)]\, L_i + [(\omega_{oi}\alpha_i + c_i)(\omega_{oi}^2 - \omega^2) + a_i \omega_{oi} \beta_i]\, B_i$$

with the definitions

$$a_i = \gamma_i \omega \quad ,$$

$$c_i = (\omega^4 + a_i^2)^{1/4} \quad ,$$

$$\alpha_i = [\tfrac{1}{2}(1 + \omega^2/c_i^2)]^{1/2} \quad ,$$

$$\beta_i = [\tfrac{1}{2}(1 - \omega^2/c_i^2)]^{1/2} \quad ,$$

$$L_i = \tfrac{1}{2} \ln [(x_{i+}^2 + y_i^2)/(x_{i-}^2 + y_i^2)] \quad ,$$

$$B_i = \tan^{-1}(y_i/x_{i+}) - \tan^{-1}(y_i/x_{i-}) \quad ,$$

$$y_i = -c_i \beta_i \quad , \quad x_{i\pm} = \omega_{oi} + q_\pm^2/2 - c_i \alpha_i \quad .$$

In the equation for B_i, the angles $\theta_i^\pm \equiv \tan^{-1}(y_i/x_{i\pm})$ must lie in the region $-\pi < \theta_i^\pm \leq \pi$.

Having obtained values for $\tau(E,\omega)$, one can calculate the energy loss distribution $f(t,\omega)$ which gives the probability that an electron of energy E will have lost energy ω on traversing a thickness t of the

solid. The energy loss distribution is a solution of the transport equation

$$\partial f(x,\omega)/\partial x = \int_0^\infty \tau(E,\omega') f(x,\omega-\omega')\, d\omega' - f(x,\omega)\Lambda^{-1}(E) , \tag{4}$$

where $\Lambda^{-1}(E)$ is the inverse mean free path given by

$$\Lambda^{-1}(E) = \int_0^E \tau(E,\omega)\, d\omega . \tag{5}$$

Values of $f(t,\omega)$ were obtained using a convolution technique developed by Williams.[7] This technique has been employed recently in a detailed study of straggling distributions for protons in aluminum.[8] The solution of the transport equation may be written in the form[8]

$$f(2x,\omega) = \int_0^\omega f(x,\omega-\omega') f(x,\omega')\, d\omega' , \tag{6}$$

that is, the distribution after traversing a thickness 2x of the solid is obtained as a convolution of the distribution of electrons which have lost energy $\omega - \omega'$ in thickness x with the distribution for energy loss ω' in x. We start with a thickness x_0 for which the probability of a single energy loss event is quite small. The distribution for this situation is taken to be

$$f(x_0,\omega) = (1 - x_0\Lambda^{-1})\,\delta(\omega) + x_0\tau(E,\omega) . \tag{7}$$

In this distribution the zero energy loss term [given by the Dirac delta function $\delta(\omega)$] has been decreased by the probability for any energy loss event, $x_0\Lambda^{-1}$. That energy loss event was assigned to the energy loss distribution as determined by the DIMFP through the term $x_0\tau$. Given this initial distribution, Eq. (7), $f(t,\omega)$ may be obtained for any desired value of t by repeated application of Eq. (6). The result after n convolutions may be written

$$f(t,\omega) = b^{2^n}\delta(\omega) + F_n(\omega) \quad , \tag{8}$$

where

$$b \equiv 1 - x_0\Lambda^{-1} \quad ,$$

$$F_n(\omega) = 2b^{2^{n-1}}F_{n-1}(\omega) + \int_0^{\omega} F_{n-1}(\omega')\,F_{n-1}(\omega-\omega')\,d\omega' \quad ,$$

and

$$F_0(\omega) \equiv x_0\tau(E,\omega) \quad .$$

The energy loss distributions calculated using this procedure are expected to be valid for energy losses small compared to the incident electron energy E since the DIMFP determined for E is used in the convolutions.

III. CALCULATIONS OF ENERGY LOSS SPECTRA

To evaluate the constants required in Eq. (2), we used the optical data of Williams and Arakawa[9] on glassy carbon for photon energies up to 80 eV. The energy loss function determined from this data is shown as the solid curve in Fig. 2 and corresponds to carbon of density ρ = 1.47 g/cm^3. The energy loss in electron volts is given by 27.2 x ω (a.u.).

The peaks in this function are well understood in terms of collective oscillations of the σ and π electrons.[9] Using Eq. (2) for $q = 0$, we determined values of the parameters A_i, γ_i, and ω_{oi} using a sum of four functions and fitting to the optical energy loss function. The result is shown as the dashed curve on Fig. 2. At energies below the K-edge in carbon at ~ 282 eV, the optical energy loss function is determined by the response of the valence electrons. As a check on the fitting procedure, we require that Eq. (2) account for all the valence electrons through the sum rule

$$\int_0^\infty \omega \, \mathrm{Im}[-1/\varepsilon(0,\omega)] \, d\omega = 2\pi^2 n_v \quad , \tag{9}$$

where n_v is the valence electron density assuming a contribution of four electrons per carbon atom. From Eq. (9) with Eq. (2), we have $\sum_i A_i = 4\pi n_v$. Energy losses due to K-shell ionization are not included since they are outside the energy loss range studied here.

Solid carbon occurs in several forms with a wide range of densities. The evaporated films used in the work of Jacobi[2] correspond to a density $\rho = 2.0$ g/cm^3. Ideally, we would use optical data obtained on the same form and density of carbon used in this experiment to determine the parameters in Eq. (2). Since such information is not available, the energy loss function, Eq. (2), determined from glassy carbon data must be modified to correspond to this higher density. From characteristic energy loss experiments,[10] it is found that the peaks due to excitation of collective oscillations or plasmons, as seen in Fig. 2 for glassy carbon, are predicted quite well for different densities assuming the

position is proportional to $\sqrt{\rho}$. The values of ω_{oi} have each been scaled to $\rho = 2$ g/cm^3 using this proportionality. Since, from Eq. (9), $\sum_{i=1}^{4} A_i = 4\pi n_v$, we have scaled each A_i by the factor 2/1.47. The values of γ_i, which are related to the widths of the peaks, are assumed to be proportional to ρ as indicated by arguments based on a free-electron approximation.[11] The set of parameters determined by the fit to the glassy carbon data, Fig. 2, and scaled to a density $\rho = 2.0$ g/cm^3 are shown in Table I, expressed in atomic units.

Table I. Parameters Used in Calculations of Energy Loss Spectra

i	A_i	ω_{oi}	γ_i
1	0.00736	0.245	0.100
2	0.3755	0.9005	0.400
3	0.2796	1.458	0.9007
4	0.08463	2.573	1.00

Examples of DIMFP's calculated from Eq. (3) using the parameters given in Table I are shown in Fig. 3, with τ and ω in atomic units, for electrons of energy 500, 1000, and 2000 eV. The structure in the energy loss function, Fig. 2, is also present in the DIMFP with maxima at $\sim$0.25 (6.8 eV) and at $\sim$0.93 (25.3 eV) corresponding to the plasmon losses in carbon at the density $\rho = 2.0$ g/cm^3.

Electron inelastic mean free paths have been calculated from Eqs. (5) and (3) using the parameters in Table I. The results are given by the solid line in Fig. 4 where we plot Λ in Angstroms as a function of electron energy in electron volts. The dashed curve was calculated from

Penn's electron gas model[12] for carbon with $\rho = 2$ g/cm^3; Penn's values fall about 40% below ours. The experimental values of electron attenuation lengths shown in the figure are 7.5 ± 1.5 Å at 263 eV from Jacobi and Hoelzl[13] and the points at 920 eV and 1169 eV are from Steinhardt, Hudis, and Perlman;[14] no error limits were assigned to the latter values.

The DIMFP's predicted by this model were used to calculate the distribution of energy losses for electrons transmitted through carbon foils of various thicknesses using the convolution method described in Section II. In the following figures we show the energy loss distribution $f(t,\omega)$ as a function of energy loss ω for electrons of energy E transmitted through a carbon foil of thickness t. In Figs. 5 and 6 we can see the changes in the energy loss distribution for E = 1000 eV as the thickness of the carbon layer increases from 10 Å through 115 Å. The contribution to $f(t,\omega)$ from zero energy-loss electrons, $b^{2^n}\int\delta(\omega)d\omega$, is given approximately by $e^{-t/\Lambda}$. Even for the small thickness t = 10 Å, over 30% of the electrons have lost energy on transmission through the carbon. In Fig. 5, the plasmon loss peak at ~0.93 at first grows with increasing t but then decreases as maxima begin to develop at multiples of this loss. For a thickness of 20 Å, slightly less than one electron mean free path (Λ = 26 Å at E = 1000 eV), a shoulder corresponding to electrons that have undergone two losses is seen at $\omega \simeq 1.9$. Multiples of the 0.25 energy loss are too small to be seen in these curves. Multiple plasmon losses become more evident for the larger values of t shown in Fig. 6. The growth of the straggling distribution, with structure associated with multiple plasmon excitations, is clearly shown in these figures.

It is important to point out that our theoretical model assumes the thin films are uniform and homogeneous, and the dielectric properties of the carbon are the same as for the bulk material of a given density. Figures 5 and 6 illustrate the development of the energy loss distribution based on these assumptions. Experimentally, it is quite difficult to obtain a uniform film with a thickness $\lesssim$ 100 Å; this problem should be kept in mind when making comparisons of theory with experiment.

In Fig. 7 we have compared our calculations with some representative experimental results of Jacobi[2] (dashed curves) with 80-Å carbon foils for incident electron energies from 600 eV through 1600 eV. Data taken from Fig. 1 on the number of transmitted electrons of 1600-eV incident energy were scaled by a factor which made the overall maximum roughly the same height as predicted by the theory. The same factor was used to scale the transmitted intensities for the lower energies. Electron energy loss was measured from the elastic peak. As one goes toward zero energy loss in Fig. 7, the experimental data begin to rise into a slightly-broadened elastic peak while the theoretical calculations approach zero [since the theoretical model assumes the elastically scattered electrons appear at exactly zero energy loss as given by the delta-function term in Eq. (8)]. Remarkably good agreement is found between theory and experiment for the 1600-, 1400-, 1200-, and 1000-eV comparisons. The positions of the plasmon peaks and the overall shapes of the data are predicted quite well by the theory. As one goes to lower incident electron energies, the positions of the maxima in the broad straggling distributions are predicted quite closely by the theory down through 600 eV. At 400 eV (not shown in Fig. 7), the

position of the maximum is predicted to occur at ~193 eV, while the experimental data give a value of ~160 eV. This represents quite an improvement over the results of reference 3 where the peak positions predicted from a simple theoretical model were about twice as large as those found experimentally for the 80-Å foil. Our calculations for a 230-Å carbon foil predict the position of the maximum in the energy loss spectrum, or the most probable energy loss, to occur at a value ~1.8 times that found experimentally (see Fig. 1) for incident electron energies of 1000, 1200, 1400, and 1600 eV.

The calculated $f(t,\omega)$ tend to overestimate the experimental intensities at the lower electron energies. The ratio of theoretical to experimental values (at the maxima) is 1.3 at 800 eV, 1.6 at 600 eV, and 3.8 at 400 eV for the 80-Å foil (see Fig. 7). As pointed out earlier, the theory used for calculation of the straggling distributions assumes that energy losses are small compared to the incident electron energy. This condition is most nearly fulfilled for the highest energy (1600 eV) for the range of energy losses shown in Fig. 7 (from zero up to ~ 163 eV). For example, a 1600-eV electron which has lost 100 eV has its mean free path reduced by 6% while this energy loss reduces the mean free path of a 600-eV electron by 13%. This results in a larger increase in the probability for a further energy loss event to occur for the electron of initial energy 600 eV than for the electron of initial energy 1600 eV. This would account for the increase in the ratio of the theoretically predicted maximum to that observed experimentally as one goes to lower incident electron energies, since the theory uses a constant value of electron mean free path corresponding to the incident electron energy.

The analytic form of the DIMFP described in this work should be useful in conjunction with a Monte Carlo solution of the transport equation to account for the change in DIMFP after each energy loss event experienced by an electron. Using this approach we could also study the build-up of secondary and Auger electrons and their contributions to the energy loss spectra. We plan to investigate this approach for calculation of energy loss distributions for low-energy electrons.

IV. SUMMARY

A model has been described for the calculation of differential inverse mean free paths of electrons interacting with a medium. Optical data for glassy carbon was used to determine the parameters in the model. The DIMFP's thus determined were employed in calculations of energy loss distributions for electrons transmitted through thin layers of carbon. Comparisons with available experimental data indicated that the theoretical description of the energy loss spectra accounts quite well for the structure in the straggling distributions due to plasmon excitation.

REFERENCES

1. See, e.g., H. Raether, Springer Tracts Mod. Phys. 38, 81 (1965).
2. K. Jacobi, "Elektronenspektroskopie dünner Kohlenstoff-folien in Reflexion und Transmission," Thesis, T. U. Clausthal, Germany (1970).
3. J. J. Cowan and J. Hoelzl, Thin Solid Films 32, 355 (1976).
4. J. Lindhard, K. Dan. Vidensk. Selsk. Mat.-Fys. Medd. 28(8), 1-57 (1954); R. H. Ritchie, Phys. Rev. 114, 644 (1959).
5. R. N. Hamm et al., Fifth Symposium on Microdosimetry, Verbania, Pallanza, September 1975, EUR-5452 d-e-f, pp. 1037-1053.
6. J. Daniels, C. v. Festenberg, H. Raether and K. Zeppenfeld, Springer Tracts Mod. Phys. 54, 77 (1970).
7. E. J. Williams, Proc. R. Soc. Lond. A 125, 420 (1929).
8. H. Bichsel and R. P. Saxon, Phys. Rev. A 11, 1286 (1975).
9. M. W. Williams and E. T. Arakawa, J. Appl. Phys. 43, 3460 (1972).
10. L. B. Leder and J. A. Suddeth, J. Appl. Phys. 31, 1422 (1960).
11. P. Nozières and D. Pines, Phys. Rev. 113, 1254 (1959).
12. D. R. Penn, J. Electron Spectrosc. Relat. Phenom. 9, 29 (1976),
13. K. Jacobi and J. Hoelzl, Surf. Sci. 26, 54 (1971).
14. R. G. Steinhardt, J. Hudis, and M. L. Perlman, Phys. Rev. B 5, 1016 (1972).

FIGURE CAPTIONS

Fig. 1. Energy distributions of electrons transmitted through carbon foils (thicknesses 80 Å and 230 Å) for primary electron energies from 400 to 1600 eV. These curves are from the work of Jacobi, reference 2.

Fig. 2. The optical energy loss function for glassy carbon (solid curve) as derived from experimental data, reference 9, vs photon energy in atomic units (bottom scale) or electron volts (top scale). The dashed curve shows our fit to the experimental result using a sum of Drude-type terms.

Fig. 3. Differential inverse mean free paths as a function of energy loss for electrons of energy 500, 1000, and 2000 eV. These curves are based on the parameters obtained from the theoretical fit shown in Fig. 2 (see text for details).

Fig. 4. Electron mean free paths, Λ in Angstroms, as a function of electron energy for carbon. The solid curve is the result of this work, the dashed curve is based on an electron gas model (reference 12), and experimental values of electron attenuation lengths are from references 13 (●) and 14 (○).

Fig. 5. Calculated energy loss spectra for 1000-eV electrons transmitted through carbon layers of thickness 10, 20, and 40 Å.

Fig. 6. Calculated energy loss spectra for 1000-eV electrons transmitted through carbon layers of thickness 57.5, 80, and 115 Å.

Fig. 7. Comparisons of calculated electron energy loss spectra (solid curves) with experimental data from reference 2 (dashed curves) for 600-, 800-, 1000-, 1200-, 1400-, and 1600-eV electrons transmitted through 80 Å of carbon.

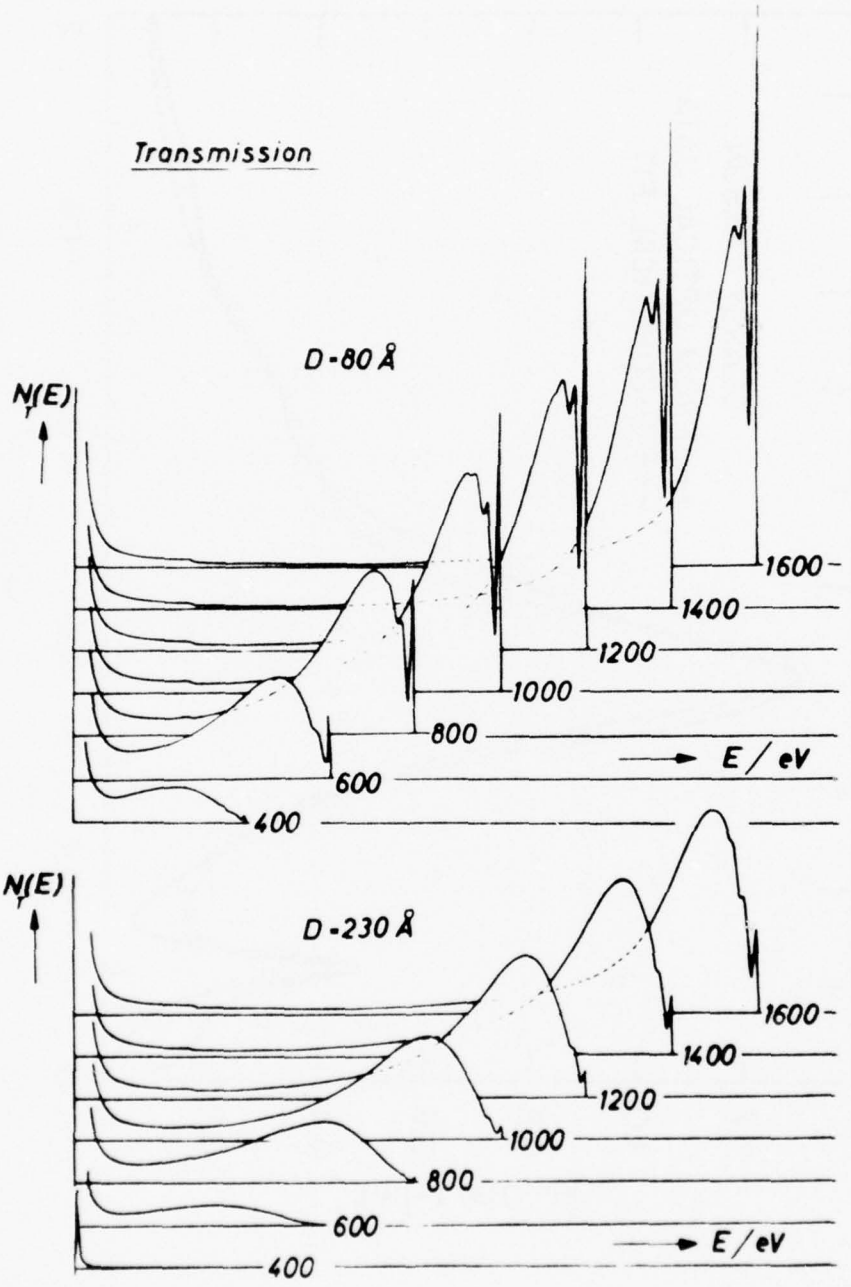

Fig. 1

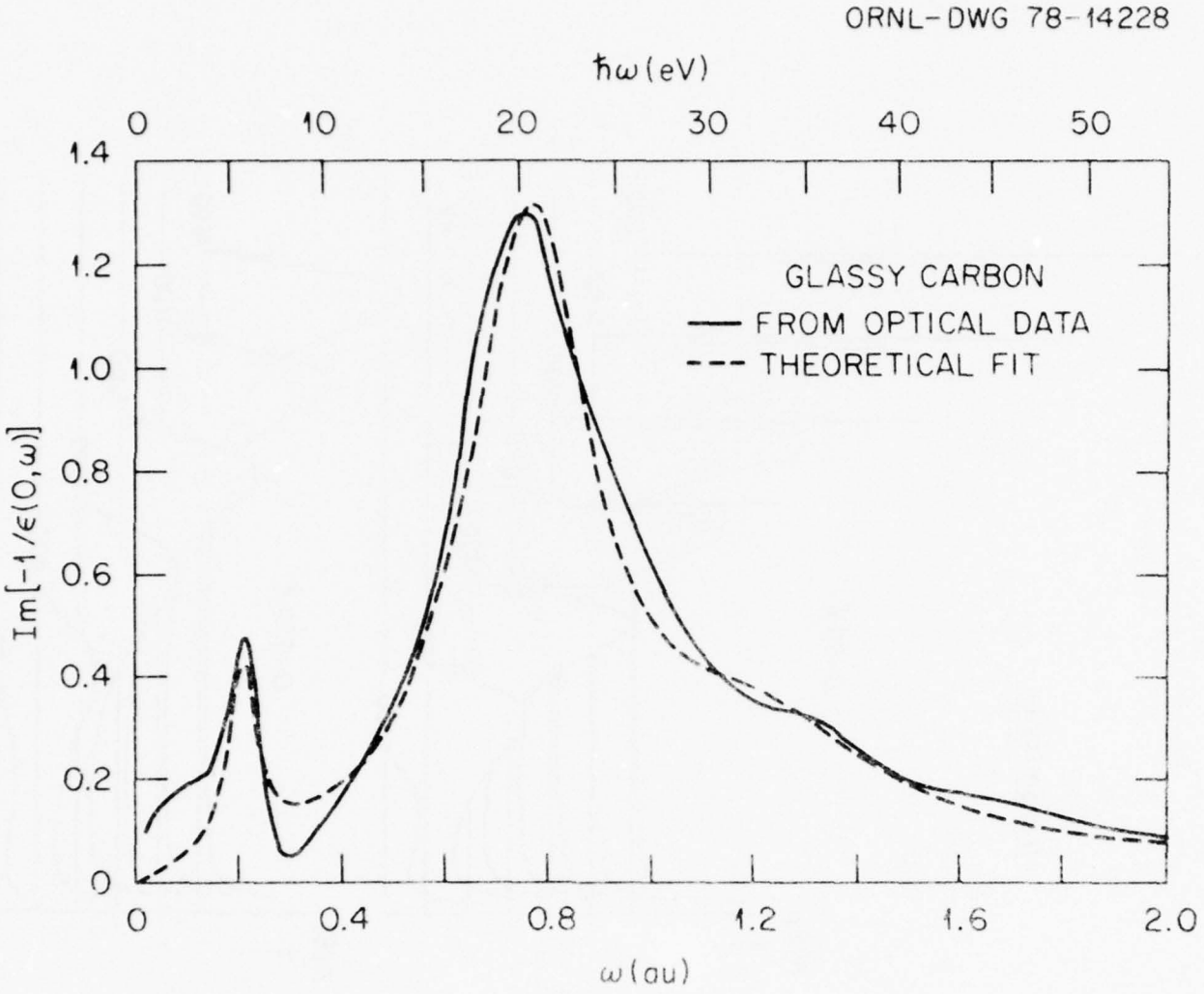
ORNL-DWG 78-14228
ħω(eV)
0
10
20
30
40
50
1.4
1.2
1.0
0.8
0.6
0.4
0.2
0
Im[-1/ε(0,ω)]
GLASSY CARBON
FROM OPTICAL DATA
THEORETICAL FIT
0
0.4
0.8
1.2
1.6
2.0
ω(au)

Fig. 2

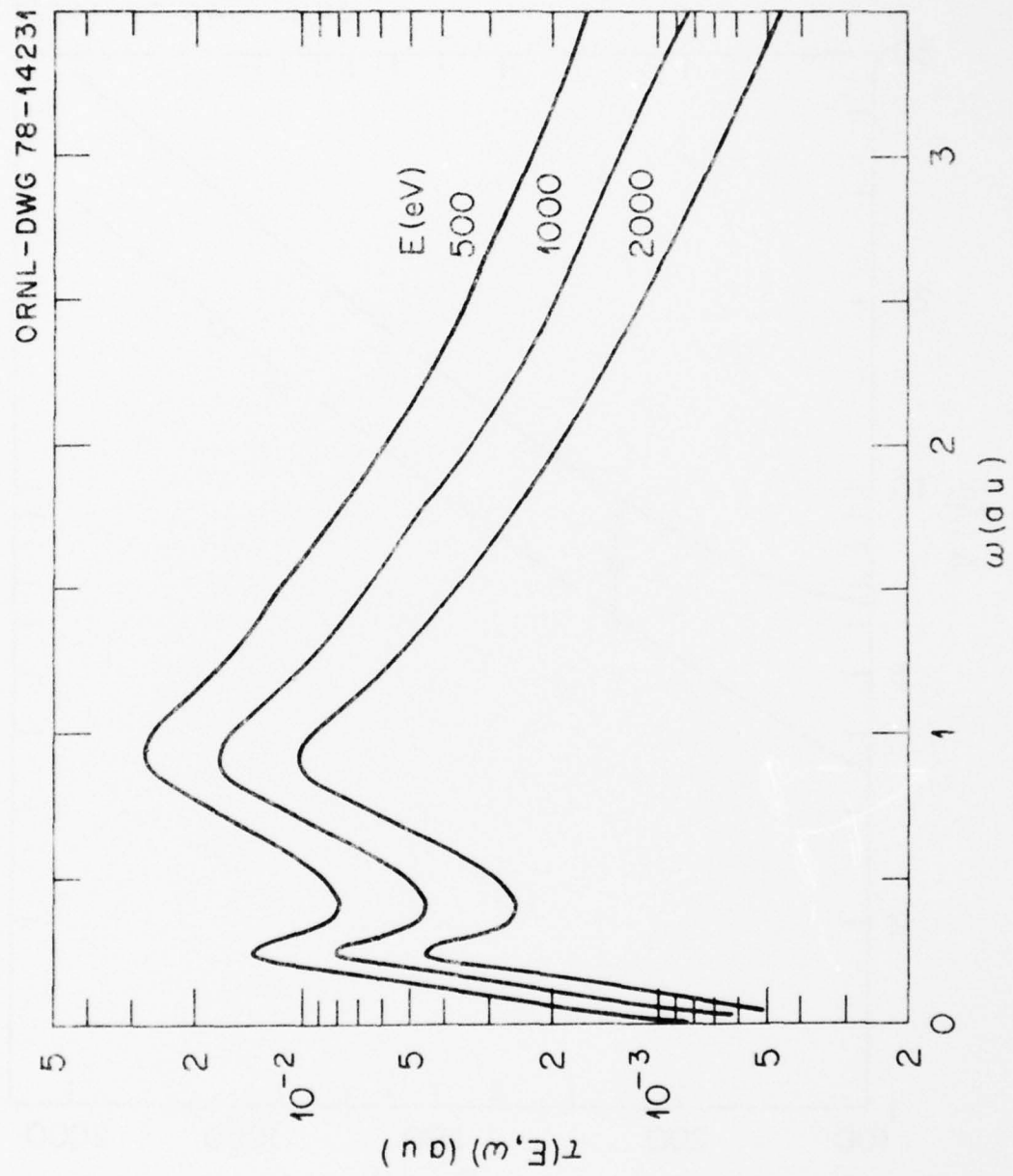
ORNL-DWG 78-14231
E(eV)
500
1000
2000
$\tau(E,\omega)$ (a.u.)
10^{-2}
10^{-3}
5
2
5
2
5
2
0
1
2
3
ω(a.u.)

Fig. 3

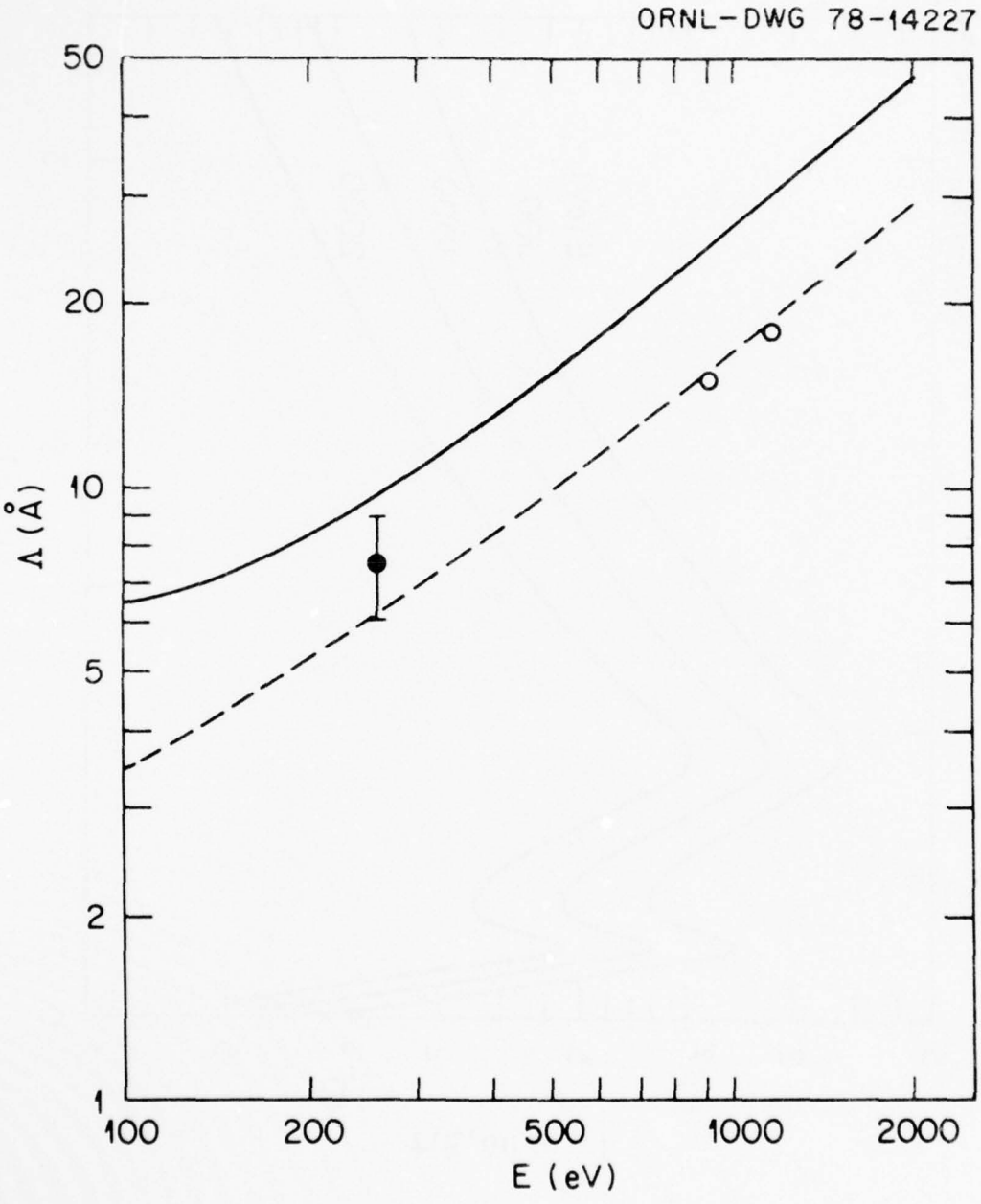

Fig. 4

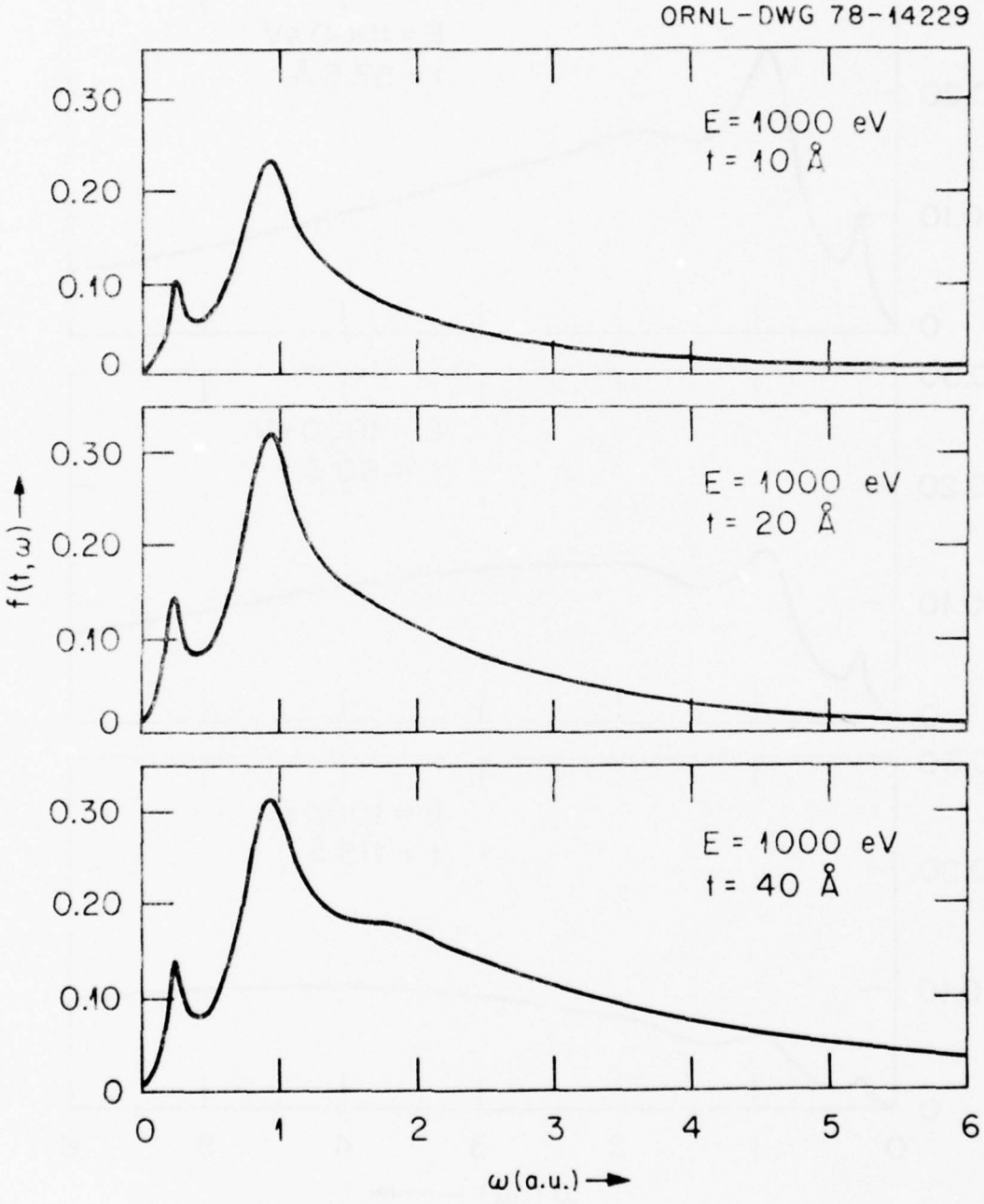
ORNL-DWG 78-14229
E = 1000 eV
t = 10 Å
E = 1000 eV
t = 20 Å
E = 1000 eV
t = 40 Å
f(t, ω)
ω(a.u.)
0.30
0.20
0.10
0
0
1
2
3
4
5
6

Fig. 5

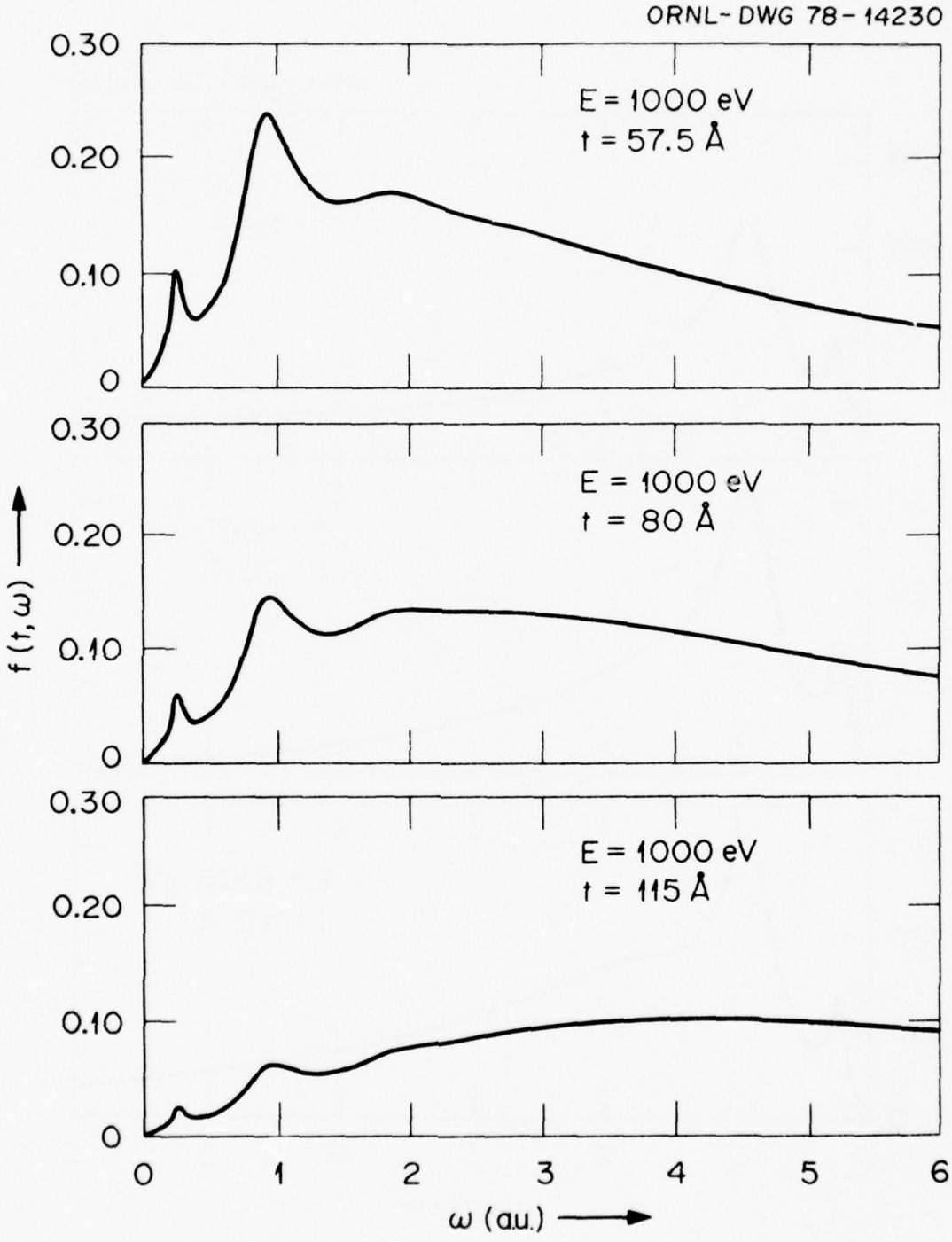
ORNL-DWG 78-14230
E = 1000 eV
t = 57.5 Å
E = 1000 eV
t = 80 Å
E = 1000 eV
t = 115 Å
f(t, ω)
ω (a.u.)
0.30
0.20
0.10
0
0
1
2
3
4
5
6

Fig. 6

ORNL-DWG 78-15224R

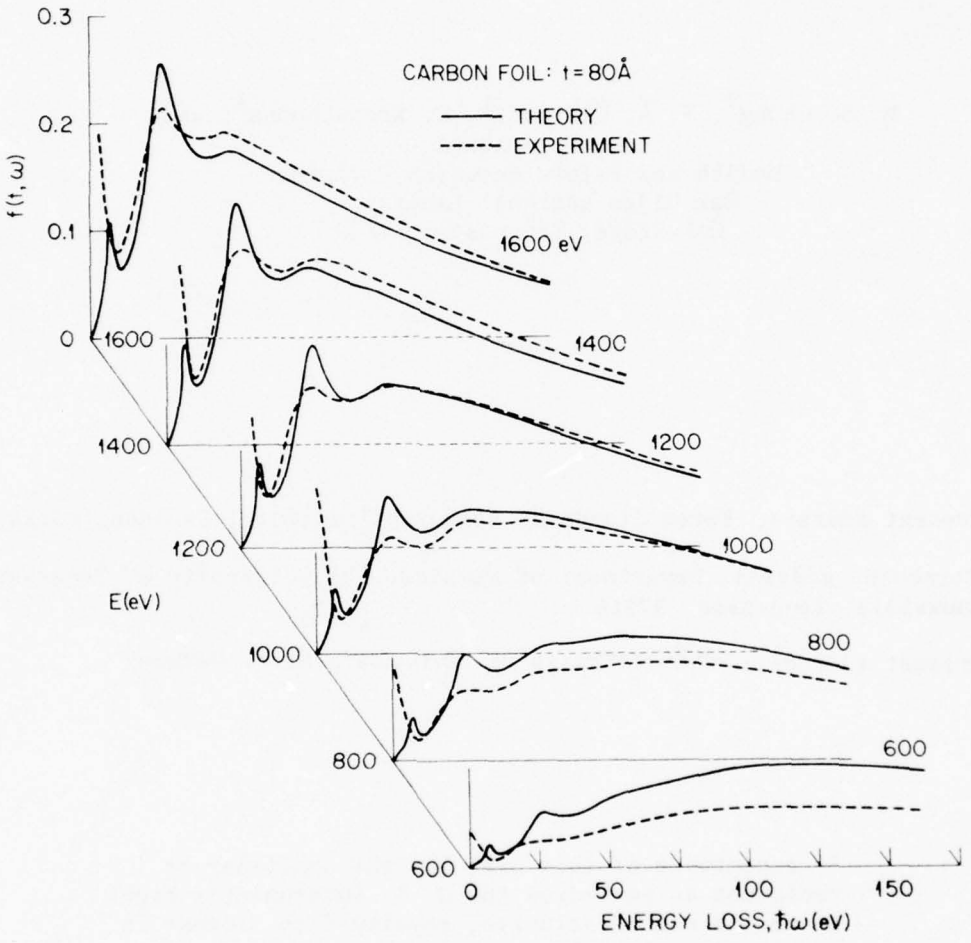

Fig. 7

CHAPTER II-A

RADIATION FROM SILVER FILMS BOMBARDED BY LOW-ENERGY ELECTRONS*

M. S. Chung[†], T. A. Callcott[‡], E. Kretschmann[§], and
E. T. Arakawa
Health and Safety Research Division
Oak Ridge National Laboratory
Oak Ridge, Tennessee 37830

† Present address, Korea Standards Research Institute, Daejeon, Korea.

‡ Permanent address, Department of Physics, The University of Tennessee, Knoxville, Tennessee 37916

§ Present address, Schäferstrasse 28, 2 Hamburg 6, W. Germany

*Research sponsored jointly by the Deputy for Electronic Technology, Air Force Systems Command, under interagency Agreement DOE No. 40-226-70 and the Division of Biomedical and Environmental Research, U. S. Department of Energy, under contract W-7405-eng-26 with the Union Carbide Corporation.

ABSTRACT

Emission spectra from Ag films irradiated by low energy electrons (20-1500 eV) have been measured, and the results compared with theory. For relatively smooth films, two peaks in the spectra are resolved. One at 3.73 eV, the volume plasmon energy, is attributed to transition radiation and/or bremsstrahlung. The second, at about 3.60 eV, is very sensitive to surface roughness in both position and magnitude and is produced by roughness-coupled radiation from surface plasmons. For rough films, the roughness-coupled radiation dominates the emission. In addition to spectral shapes, the polarization of the radiation and its intensity as a function of electron energy were measured. The experimental results are compared with new calculations of roughness-coupled emission which account for most of our observations. They indicate that high wavevector roughness components play the dominant role in the emission process.

Introduction

Energetic electrons incident on a metal surface produce radiation via several physical processes. Transition radiation is produced by the collapsing dipole field generated as the particle enters the surface,[1-4] and bremsstrahlung is produced by electron scattering in the metal.[3-5] These processes produce spectra characterized by a peak or shoulder at the volume plasma frequency (ω_V) of the electron

gas with a continuum of radiation extending to lower frequencies. They may be distinguished experimentally since transition radiation produces P-polarized light only (electric vector in plane defined by the incident beam and the surface normal), while bremsstrahlung produces light with both P and S polarizations. The electrons also excite surface plasma waves that do not radiate so long as the surface is smooth.[6] A rough surface allows the plasmons to de-excite by roughness-coupled surface-plasmon radiation (RCSPR).[7-11]

Other experiments provide information about one or the other of the two physical processes giving rise to RCSPR from Ag. Energy losses suffered by electrons scattered from the metal surface provide information about the plasmon production process,[12] while reflectivity,[13-17] light scattering[18-20] and absorption[21] experiments yield information about the roughness coupling of plasmons to photons.

Radiation produced by high energy electrons ($\gtrsim$ 20 keV) incident on Ag has been studied by several workers.[22-27] In this energy range, transition radiation dominates the spectra observed by most workers,[22-26] although RCSPR has been observed for sufficiently rough films.[25-27] In this paper we report measurements of the radiation spectra produced by low-energy electrons (20-1500 eV) incident on Ag. For sufficiently smooth surfaces, both volume-plasmon radiation (transition radiation and/or bremsstrahlung) and RCSPR were observed, but for most surfaces the RCSPR dominates the observed spectra.

The formal aspects of the theory we use to describe our results are given in a separate paper that precedes this one.[28] We will describe here some of the physical processes contributing to the formal results.

A dispersion curve ω (k) for surface plasmons is shown in Fig. 1a along with the dispersion line of light. The plasmon curve approaches the light line in the retarding region ($k \lesssim 0.5$) where the plasmon phase velocities become comparable with the velocity of light in vacuum, and approaches a limiting value ω_s in the normal plasmon region ($k \gtrsim 2$). Wavevectors k in the figure are given in units of $\frac{\omega_s}{c} = \frac{2\pi}{\lambda_s}$ ($\simeq 1.8 \times 10^{-3}$ Å^{-1} for Ag.). For a free-electron gas with no damping, RCSPR would have a sharp upper limit at ω_s. An important feature of surface plasmons for a real metal however, is that they are strongly lifetime broadened, particularly at high k-vectors where ω (k) approaches ω_s.[29] We will cite the presence of large amounts of RCSPR with $\omega > \omega_s$ as evidence of the importance of high k-vector plasmons to the observed spectra.

The surface roughness is described in terms of an autocorrelation function which may be fourier analyzed into components of wavevector q.[10,17] Each q represents a periodic structure that can couple plasmons and photons of the same frequency when

$$\vec{k}_{\ell 11} + \vec{q} = \vec{k}_{p1}, \qquad (1)$$

where $\vec{k}_{\ell 11}$ is the component of the wavevector of light lying in the radiating surface. The coupling is shown schematically in Figure 1b. For an observation angle θ from the normal, each roughness component

q can couple plasmons with wavevector magnitudes $q-k_\ell \sin\theta \leq k_{pl} \leq q+k_\ell \sin\theta$ to the radiation field. For high q-vector roughness components ($q \gg k_\ell$) or photon emitted near normal ($\sin\theta \cong 0$), $k_{pl} \cong q$ so that the observed RCSPR spectrum is determined in large measure by the distribution and magnitude of the surface roughness components.

The other important factor determining the RCSPR spectrum is the distribution of plasmons in 2-D k-space produced by an electron of energy E incident at an angle ϕ to the surface normal. The formalism of Kretschmann et al in the accompanying paper is valid for all regions of the dispersion curves but a more transparent result can be obtained from an earlier treatment of Wilems and Ritchie which is valid for the normal plasmon region where $\omega(k) \cong \omega_s$ at all k-vectors.[4] For normally incident electrons of energy E, the probability of producing a plasmon of wavevector k may be written in the form

$$P(k) = \text{const} \frac{v_o/c^2\ k^2}{(v_o^2/c^2 + 1/k^2)^2} = \text{const}\left(\frac{2E}{mc^2}\right)\frac{1/k^2}{(2E/mc^2 + 1/k^2)^2} \qquad (2)$$

where v_o is the electron velocity, m the electron mass and k is written in units of $\frac{\omega}{c}$. For a given electron energy P(k) is proportional to k^2 for $k \ll (mc^2/2E)^{1/2}$, reaches a peak at $k = (mc^2/2E)^{1/2}$ and decreases for higher values of k. Since $(mc^2/2E)^{1/2} = 16$ for E = 1000 eV, relatively few small k plasmons are produced by electrons with the energies used in this study.

We find that our experimental data can be accounted for quite satisfactorily if we assume that the RCSPR spectra are produced primarily by a relatively narrow distribution of high q-components in the roughness

spectrum. The well known presence of another peak centered at $q = 0$ has little effect on our results since few small k plasmons are generated by low energy electrons. Assuming a high q roughness peak, equation (1) shows that the peak of the RCSPR spectrum observed near normal results from the decay of plasmons with wavevector $k_{pl} \simeq q_h$, where q_h is the dominant roughness component. Thus the peak intensity of the RCSPR spectrum is proportional to the probability of producing a plasmon of wavevector $k_{pl} = q_h$. By fitting equation (2) to a plot of peak intensity versus electron energy, it is possible to obtain an estimate of q_h, the dominant component of the high q roughness peak. The theory of Kretschmann et al. in the accompanying paper developes the above ideas in a consistent formalism which allows us to obtain an estimate of the dominant high q roughness component of a Ag film from the experimental data.

An important extension of the present theory, however, is the inclusion of the effect of roughness in coupling plasmons to each other as well as to the photon field.[28,30] For a single roughness component, the calculations predict a prominent splitting of the RSCPR peak at ω_s. The splitting is not resolved in the RCSPR spectra of Ag reported here, presumably due to the finite width of the roughness peak and to the lifetime broadening of the plasmons, but it does account in a natural way for a shift in the position of the peak of the RCSPR spectrum that is observed as the surface is roughened. A double-peaked RCSPR spectrum of potassium [31] has been observed in our laboratory that is consistent with the prediction of the Kretschmann theory.

Experimental Techniques and Results

A schematic diagram of the apparatus used in the studies is shown in Fig. 2. The angle between the electron beam and monochromator port is fixed at 35°. Most of the results reported here were obtained with near-normal incidence electrons and an observation angle of $\leq 40°$. Silver films were prepared in situ by evaporating Ag onto various substrates with the film thickness monitored by a quartz crystal thickness monitor. Photons emitted by the films were analyzed in the wavelength range between 3000 Å and 5500 Å using a grating monochromator and photomultiplier. The experiments were performed in an unbaked, ion-pumped vacuum system operated with a base pressure of about 5×10^{-7} torr which rose to the 10^{-6} torr range during evaporation.

Film preparation and treatment had a very strong effect on the radiation produced by the electrons. Substantially different results were obtained for Ag films deposited on shiny Ag sheet, shiny Ta plate, Mo plate with a matte finish, and glass slides. The rate of Ag deposition and local heating of the electron beam also affected the radiation observed.

Fig. 3 shows the emission spectra from a specularly reflecting Ag plate irradiated with electrons of 500 eV and 1000 eV both before (dashed curve) and after (solid curve) the rapid (∿1000 Å/min) evaporation of a 2000 Å-thick Ag layer. A double-peaked spectrum is observed with peaks located at approximately 3320 Å (3.73 eV) and 3440 Å (3.60 eV). Note that the magnitude of the 3440 Å peak is enhanced for the evaporated film. The positions of the volume plasmon oscillation ($\hbar\omega_V$ = 3.76 eV, λ_V = 3300 Å) and of the limiting surface plasmon excitation ($\hbar\omega_S$ = 3.66 eV, λ_S = 3390 Å) are indicated by arrows on this and most of the following figures.[32]

Fig. 4 shows results from a Ag film evaporated on a matte Mo plate. The double-peaked spectrum is retained, with one peak located at about 3300 Å as before, but the dominant peak is now centered at about 3500 Å.

Fig. 5 shows the results obtained with 300 eV electrons on a rapidly evaporated thick film of Ag on Ag sheet along with spectra obtained when additional Ag is evaporated very slowly (∿100 Å/min) onto the surface. The results on the original film can best be interpreted as two poorly resolved peaks of about equal magnitude located at 3320 Å and 3440 Å. During the slow evaporation, the intensity at 3320 Å remains virtually unchanged, but the 3440 Å peak grows dramatically in magnitude and shifts to slightly longer wavelengths.

Fig. 6 shows the emission from Ag on glass for films of increasing thickness. A rather broad peak centered at 3440 Å

grows in magnitude and shifts to longer wavelength with increasing film thickness. In these curves the surface-plasmon radiation completely dominates the spectra, and the short-wavelength peak is barely visible as a shoulder.

If excessive electron beam power was dissipated in the Ag on glass films, the appearance of the films changed with time from shiny to frosty as a result of film damage by local heating. The frosty spots on such films were rough when viewed through an optical microscope. Fig . 7 shows the accompanying change in the emission as a Ag film was subjected to a high-intensity (~1 mA) electron beam. The peak is shifted to longer wavelengths as film roughening proceeds. A fresh evaporation of Ag on such a damaged region does not move the emission peak back to its original position as would be the case if the shift were due to the formation of an oxide or other contaminant layer on the surface.

In nearly all curves of Figs. 3 through 6, there is evidence for a high-energy component at about 3300 Å which changes little with changes in the surface condition. This is the volume plasmon radiation composed of transition radiation and bremsstrahlung radiation that was described briefly in the introduction. It produces a peak or shoulder at the volume plasmon energy (3.76 eV or 3300 Å). The remaining radiation which dominates most of the spectra in Figs. 3 through 7, is roughness-coupled emission from the decay of surface plasmons.

The different shapes of RCSPR spectra are related primarily to the roughness coupling of plasmons to photons and not to the

production process of the plasmons. The most general qualitative conclusion that we draw is that any mechanism that produces a rougher surface has two effects. It increases the intensity of the RCSPR and shifts its maximum to longer wavelengths and lower frequencies. In Fig. 3, where Ag was rapidly evaporated onto a specularly reflecting Ag substrate, the surface plasmon peak is relatively weak and has its maximum near the asymptotic energy, $\hbar\omega_s$, of the surface plasmon dispersion curve for Ag ($\hbar\omega_s$ = 3.66 eV, λ = 3390 Å).[32] In Fig. 4, where the emission is from Ag on a matte finish Mo substrate, the dominant surface-plasmon peak is centered at a longer wavelength. We will argue below that this indicates a rougher surface. In Figs. 5 and 6, the very slow evaporation of Ag results in increasingly rougher surfaces. Such an increase in roughness with film thickness has been observed previously.[20,24,25] The effect seems to be enhanced in our experiments when the electron beam is incident on the radiating region as new Ag is deposited.

A satisfactory explanation of the above results, and particularly of Figs. 5 and 6, must account for the increase in intensity and shift in spectral maximum of the RCSPR that occurs as the roughness is increased. It should also account for the spectral width and the fact that a nearly constant fraction of the radiation is observed at frequencies above the asymptotic surface plasmon frequency ω_s even after the spectral maxima has shifted to a lower frequency.

In Fig. 8, we show emission spectra from a rough Ag film as a function of incident electron energies. Smooth surface volume plasmon radiation is negligible in the spectra. The curves are normalized to the incident electron current. In Fig. 9, the peak emission intensity is plotted as a function of electron energy. The data points are fitted by a theoretical curve discussed in the following section.

Fig. 10 shows emission spectra for P- and S-polarized radiation (P polarization has the E vector in the plane determined by the incident beam and the sample normal) from a Ag film. The spectra have been corrected for the sensitivity of the monochromator and optical system to the two polarizations. In the results shown, the electron beam was incident at 5° to the sample normal, and the photons were detected at 30° from normal. Similar results were obtained with electrons incident at 65° from normal and the same observation angle. This indicates that the observed polarization does not depend strongly on the angle of incidence of the electrons.

These measurements of the polarization dependence of the emission spectra support our assertion that two separate emission mechanisms contribute to the observed spectra. The P- and S-polarized spectra are strikingly different with the P-polarization curve peaking near the volume-plasmon wavelength (3300 Å) and the S-polarization curve peaking near the surface plasmon wavelength (3440 Å). The dashed curve is the P-S difference curve and represents the excess of P over S emission.

The intensity of the volume plasmon peak using smooth-surface transition-radiation theory should increase from zero in the direction of the sample normal to a maximum about 30° away from the sample normal, all radiation being P-polarized. Bremsstrahlung is less completely polarized since electrons are randomly scattered in the surface. It is not clear in the present data whether all of the excess P radiation at longer wavelength should be attributed to the long tail that is known to exist for the smooth-surface transition radiation or whether some of it may represent an excess P-polarized emission component in the RCSPR.

Ritchie[10] has derived expressions for the polarization dependence of roughness-coupled emission for plasmons produced by high-energy grazing-incidence electrons. The results are complex and strongly dependent on the roughness spectrum but do indicate an excess of P-polarized radiation. In our experiments, electrons are incident near normal and plasmons are produced by both the incident electrons and by scattered electrons with randomized directions. These factors all serve to reduce the probability of generating plasmons with k-vectors in the plane of incidence of the electron beam, which will, in turn, reduce the excess of P to S polarized light. For the present experiment, where the electron beam is incident near normal, it appears that nearly all of the excess P radiation can be assigned to the smooth surface volume plasmon radiation.

Qualitatively, then, the difference curve can probably be taken as representing smooth-surface volume plasmon radiation and the S-polarized curve as representing RCSPR.

Referring to Fig. 10, we see that the ratio of the maxima of the P-S curves to the maxima of the S curves decreases with decreasing electron energy. In practice we found it impossible to monitor the smooth-surface transition radiation at electron energies much below 500 eV. Attempts to increase the emission intensity by increasing the electron flux roughened the film and enhanced the surface-plasmon radiation at the expense of the smooth-surface transition radiation.

Discussion of Results

We wish to compare the experimental results on spectral shape and intensity with the theory of RCSPR outlined in the previous paper.[28] Much of this discussion is necessarily qualitative since we do not have independent measurements of the frequency spectrum of the roughness auto-correlation function. Some proposed experiments for obtaining independent measurements of this function are discussed briefly at the end of the paper. For the present, however, any knowledge we may gain about the roughness spectra must be extracted from the emission spectra themselves. A similar approach has usually been taken by workers measuring the effect of roughness in producing a dip in the reflectance of metals near the surface plasmon frequency. There, the decrease in reflectance becomes

larger and shifts to lower frequencies as the surface becomes rougher.

The usual explanation of the increase in emission intensity with increasing roughness is that the vertical roughness, as measured by the r.m.s. deviation of the true surface from the ideal smooth surface, is increased. This is the quantity $\langle s^2 \rangle$ appearing in the theory paper.[28]

The shift of the emission peak to lower frequencies (longer wavelengths) might be explained by attributing the radiation to relatively small q roughness components which couple plasmons in the retarding region to the radiation field and by assuming that the roughness spectrum shifts to lower q values with increasing roughness. But this mechanism is not consistent with our observation of strong radiation above ω_s, nor does such an assumption lead to reasonable predictions of the dependence of the radiation intensity on electron energy. In the retarding region, ($k<2$) equation (2) shows that plasmon production is (nearly) linear in electron energy in contrast to the data shown in Fig. 9. The second possibility for explaining the shift to lower frequencies is that the peak radiation is produced by high q roughness components, but that increasing roughness somehow decreases the frequency of high k-vector plasmons. Other workers have also obtained experimental results which they attribute to a shift of the surface plasmon curve to lower frequencies (or equivalently to a reduction in plasmon phase velocities) as the surface is roughened.[21] An alternative explanation for this shift can be given by assuming that the rough surface

acts as a surface layer with a refractive index intermediate between that of air and Ag, but to our knowledge no rigorous theory accounting for the shift has been given.

The attractive feature of the calculations of Kretschmann et al. is that they provide explanations for the major features of the RCSPR spectra both as a function of electron energy and as a function of increasing vertical roughness using standard surface plasmon and surface roughness theory and the single additional assumption that the roughness spectrum has a prominent peak at high q-vector that is responsible for the RCSPR in the vicinity of its spectral peak.

For simplicity, the high q-vector roughness peak has been modeled as a delta function. Fig. 1a of the theory paper shows the decrease of the ratio of the RCSPR to the volume plasmon emission with increasing electron energy. This is in agreement with our observation that RCSPR increasingly dominates the radiation at low electron energies.

Fig. 2 of the theory paper shows the emission spectrum as a function of $q_h^2 \ \langle s^2 \rangle$ where q_h is the dominant roughness component and $\langle s^2 \rangle$ the r.m.s. height of the roughness. The surprising result is that the single high-q roughness component produces a double peaked radiation spectrum with one peak lying above ω_s and the second and much larger peak lying below ω_s. Both the intensity and the splitting increase with increasing $\langle s^2 \rangle$. If the delta function in the roughness spectrum is replaced by a high q-vector peak of finite width, additional broadening is introduced so that the splitting is no longer so well resolved. The shift of the dominant peak position to lower frequencies and larger wavelengths with increasing $\langle s^2 \rangle$ is retained however. Similar splittings

have been noted for experiments on diffraction gratings,[33] but the effects are much larger for large q-vector roughness peaks since the splitting scales with q_h^2.[28]

The splitting is not resolved in Ag, which is not surprising since the model does not include a finite width for the roughness spectrum nor does it treat the lifetime broadening of the surface plasmon in Ag adequately. It would be difficult to observe a splitting for Ag in any case, because ω_v and ω_s occur very close together. But the theory does provide suggestive explanations for the dependence of peak radiation intensity on electron energy, and for the shift in peak position as roughness is increased. Neither of these results of the calculations is changed significantly if a roughness peak of finite width is assumed.

As indicated in Eq. 6 and Fig. 1b of Kretschmann et al. the peak intensity versus electron energy is scaled along the horizontal axis by q_h^2 where q_h^2 designates the dominant roughness component. Using this universal curve, we can fit the experimental values of the peak intensity versus electron energy shown in Fig. 9 if we assume that $q_h = 1.12 \times 10^{-2}$ $\mathring{A}^{-1}$, which corresponds to a wavelength of $\lambda_h = 560$ $\mathring{A}$, for the dominant roughness component. This is equivalent to a value of $q_h = 6.25$ in the reduced units of (ω/c) that were used in the introduction of this paper and by Kretschmann et al. As we saw in the introduction the dependence of peak intensity on the electron energy results primarily from the energy dependence of the probability of producing plasmons of wavevector $k \approx q_h$.

Fitting the data of Fig. 9 with Eq. 2 of this paper gives very nearly the same value of q_h ($q_h \simeq k = 8$) as the more exact treatment.

The Kretschmann et al. theory also predicts a shift in the dominant peak position which is analytically related to the change in peak height. As may be seen from Eqs. 6 and 7 of the theory paper, a plot of emission intensity versus $4[(1 + \epsilon_p)/(1 - \epsilon_p)]^2$, where ϵ_p is the location of the spectral peak measured in terms of the real part of the dielectric constant, should give a straight line as the r.m.s. height $\langle s^2 \rangle$ of the dominant roughness component is increased. This has been done for the data of Fig. 6 and is shown in Fig. 11. The observed straight line plot provides support for our contention that a single dominent high q-vector component of roughness can account satisfactorily for most of our data.

There are some independent indications that a large high q-vector peak occurs in the roughness autocorrelation function. The growth process can easily lead to such a result, since these evaporated films usually develop from isolated islands which grow with the addition of material until they touch.[21,34] It seems reasonable that there is a dominant horizontal roughness component whose scale is set by the average size of the islands when they first touch, and in fact most photomicrographs of sufficient resolution show regular microstructure with lateral dimensions of a few hundred Å.[21,36] Autocorrelation functions obtained from interferometric[35] and light scattering[36] measurements are sensitive primarily to small

q roughness components and can not give evidence of a high-q roughness peak. The photomicrographic technique of Dobberstein[37] does indicate the presence of a high-q peak in the roughness spectrum. For Ag, Dobberstein found a peak at 7×10^{-3} $\mathring{A}^{-1}$ and Kaspar and Kriebig[21] found peaks at 7×10^{-3} $\mathring{A}^{-1}$ and 15×10^{-3} $\mathring{A}^{-1}$. Braundmeier and Hall found it necessary to assume an autocorrelation function with a peak at 2×10^{-3} $\mathring{A}^{-1}$ in order to explain the radiation patterns of optically excited surface plasmons on Ag films.[19] These values may be compared with the value of 11×10^{-3} $\mathring{A}$ obtained from fitting the data of Fig. 9.

It would be desirable to perform experiments on surfaces with completely characterized roughness functions. By combining methods sensitive to small q[35,36] components with photomicrographic methods[37] sensitive to high-q components, it may be possible to specify the roughness spectrum over the full region of interest. To confirm the splitting predicted theoretically, it would be better still to prepare surfaces with a single dominant q-vector as has been done for small q-vectors using diffraction gratings.[33] We hope to pursue both approaches in the future.

Acknowledgements

The authors thank R. H. Ritchie and A. J. Braundmeier for enlightening discussions concerning the interpretation of our data.

FIGURE CAPTIONS

Fig. 1. (a) Dispersion curve for surface plasmons

(b) Wavevector conservation for roughness-coupled surface-plasmon radiation

Fig. 2. Schematic of experimental apparatus

Fig. 3. Emission spectrum for Ag on Ag showing both surface- and volume-plasmon peaks (--- before evaporation; —— after evaporation). Volume-plasmon and limiting surface-plasmon wavelengths are indicated on this and most subsequent figures.

Fig. 4. Emission spectrum for Ag on matte Mo substrate

Fig. 5. Growth of low-energy emission peak with slow evaporation of additional Ag on Ag

Fig. 6. Growth of emission intensity with Ag thickness for deposits of Ag on glass

Fig. 7. Shift of emission peak as the roughness of a Ag film is increased by electron beam heating

Fig. 8. Emission spectra for various incident electron energies

Fig. 9. Peak intensity as a function of electron energy. Smooth curve is from theory of Kretschman et al. described in text.

Fig. 10. P and S polarized emission spectra from relatively smooth surface showing both volume-plasmon radiation and roughness-coupled surface-plasmon radiation.

Fig. 11. Plot of peak intensity versus $4[(1 + \varepsilon)/(1 - \varepsilon)]^2$, a function of peak position. The plot should be a straight line in the theory of Kretschmann et al.

REFERENCES

1. R. A. Ferrell, Phys. Rev. 111, 1214 (1958).
2. R. H. Ritchie and H. B. Eldridge, Phys. Rev. 126, 1935 (1962).
3. R. H. Ritchie, J. C. Ashley and L. C. Emerson, Phys. Rev. 135, A759 (1964).
4. R. E. Wilems and R. H. Ritchie, Ph. D. Thesis, Univ. of Tenn, 1968. Available as ORNL Report - ORNL-TM-2101.
5. I. M. Frank, Sov. Phys. Usp. 8, 729 (1965).
6. R. H. Ritchie, Phys. Rev. 106, 874 (1957).
7. E. A. Stern, Phys. Rev. Lett. 19, 1321 (1967).
8. E. Kroger and E. Kretschmann, Z. Phys. 237, 1 (1970).
9. E. Kretschmann and E. Kroger, J. Opt. Soc. Am. 65, 150 (1975).
10. R. H. Ritchie, Phys. Status Solidi 39, 297 (1970).
11. G. Sauerbrey, E. Woeckel and P. Dobberstein, Phys. Status Solidi B60, 665 (1973) and Erratum B 72 845 (1975).
12. P. Zacharias, Z. Phys. 238, 172 (1970).
13. S. N. Jasperson and S. F. Schnatterly, Phys. Rev. 188, 759 (1969).
14. A. J. Braundmeier and E. T. Arakawa, J. Phys. Chem. Solids 35, 517 (1974).
15. L. J. Cunningham and A. J. Braundmeier, Phys. Rev. B14, 479 (1976).
16. R. Orlowski and H. Raether, Surf. Sci. 54, 303 (1976).
17. J. Crowell and R. H. Ritchie, J. Opt. Soc. Amer. 60, 794 (1970).
18. J. M. Elson and R. H. Ritchie, Phys. Status Solidi B 62, 461 (1974).
19. A. J. Braundmeier and D. G. Hall, Surf. Sci. 49, 376 (1975).
20. D. L. Hornauer, Opt. Commun. 16, 76 (1976).

21. W. Kaspar and U. Kreibig, Surf. Sci. 69, 619 (1977).

22. E. T. Arakawa, N. O. Davis and R. D. Birkhoff, Phys. Rev. 135, A224 (1964).

23. G. E. Jones, L. S. Cram and E. T. Arakawa, Phys. Rev. 147, 515 (1966).

24. L. S. Cram and E. T. Arakawa, Phys. Rev. 153, 455 (1967).

25. H. Boersch and G. Sauerbrey in Optical Properties and Electronic Structure of Metals and Alloys, ed. by F. Abeles (North Holland, Amsterdam, 1966) p. 386.

26. H. Boersch, P. Dobberstein, D. Fritsche and G. Sauerbrey, Z. Phys. 187, 97 (1965).

27. D. Heitman and U. Permien, Opt. Commun. 25, 196 (1978).

28. E. Kretschmann, T. A. Callcott and E. T. Arakawa, Surf. Sci. _____ (1979). (preceding paper).

29. J. M. Elson and R. H. Ritchie, Surf. Sci. 30, 178 (1972).

30. E. Kretschmann, T. Ferrell and J. C. Ashley (submitted to Phys. Rev. Lett.).

31. M. W. Williams, J. C. Ashley, E. Kretschmann, T. A. Callcott, M. S. Chung and E. T. Arakawa (submitted to Physics Letters)

32. R. H. Huebner, E. T. Arakawa, R. A. MacRae and R. N. Hamm, J. Opt. Soc. Am. 54, 1434 (1964).

33. R. H. Ritchie, E. T. Arakawa, J. J. Cowan and R. N. Hamm, Phys. Rev. Lett. 21, 1530 (1968).

34. A useful review of older work is given by J. W. Matthews in Physics of Thin Films, ed. by G. Hass and R. E. Thuu (Academic Press, New York, 1967) Vol. 4, pp 137-187.

35. J. M. Bennett, Appl. Opt. 15, 2705 (1976).

36. D. Heitman and U. Permien, Opt. Commun. 23, 131 (1977).

37. P. Dobberstein, Phys. Lett. A31, 307 (1970).

ORNL DWG 78-17742

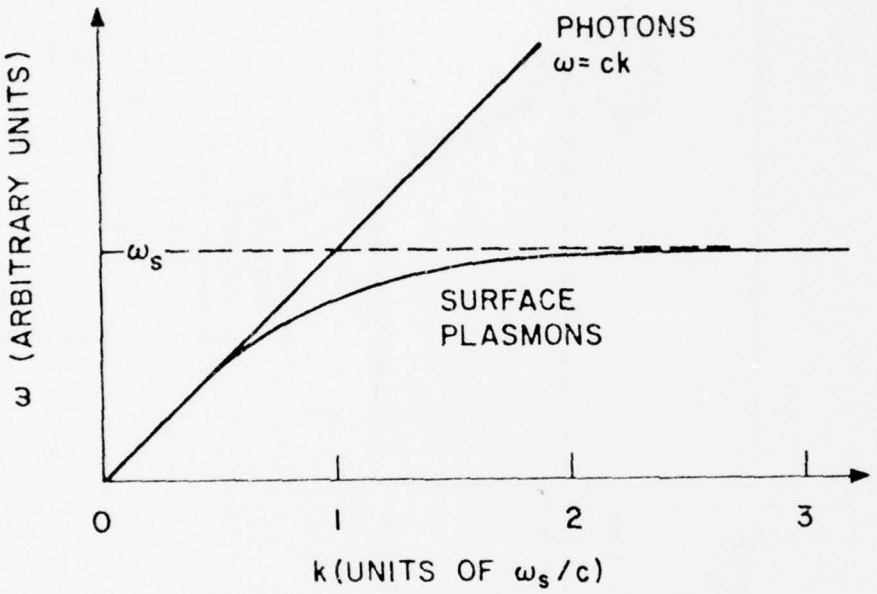

(a)

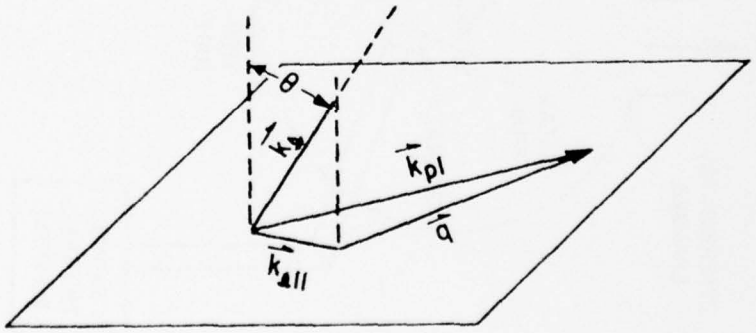

(b)

Fig. 1

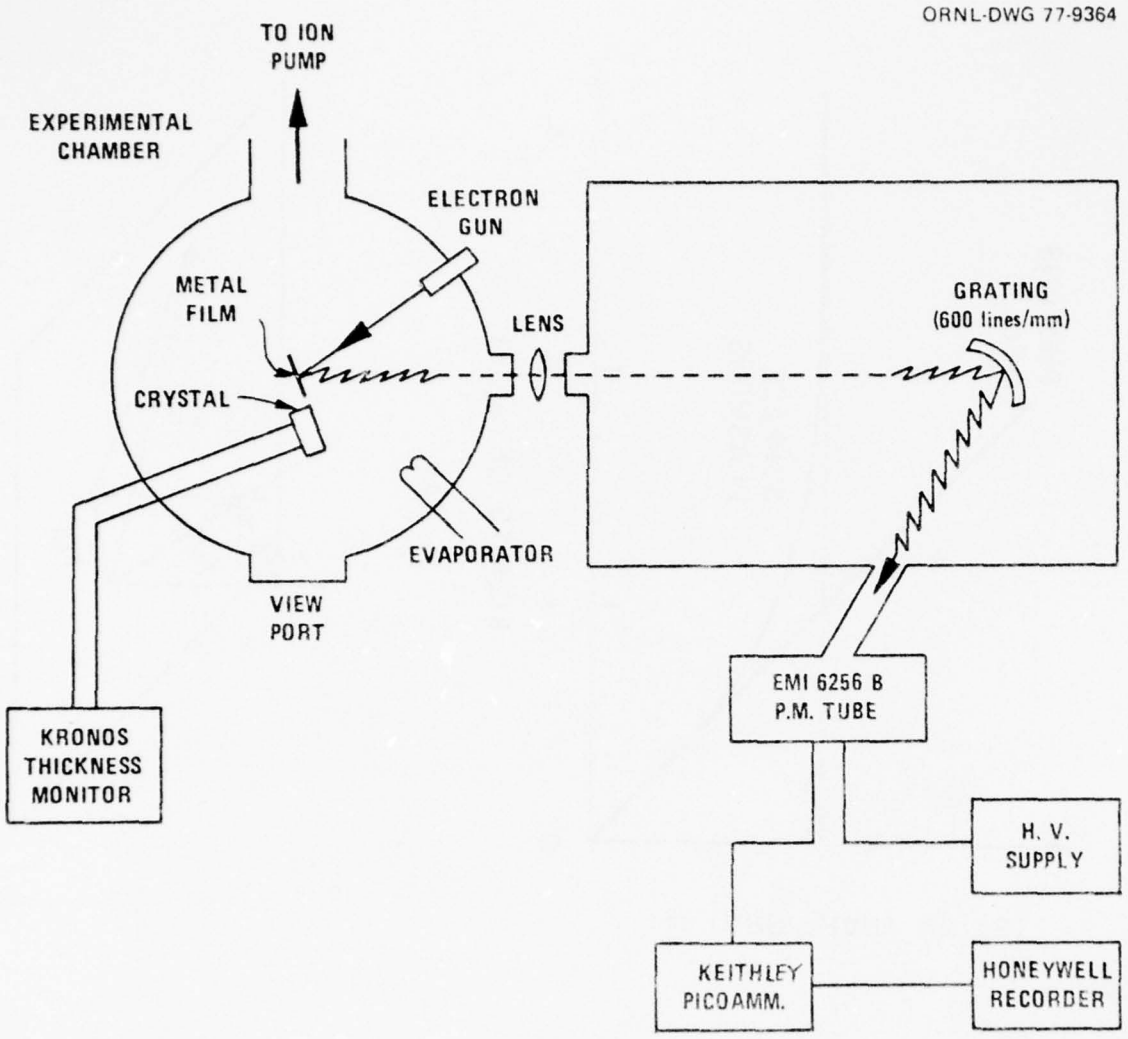
ORNL-DWG 77-9364
TO ION PUMP
EXPERIMENTAL CHAMBER
ELECTRON GUN
METAL FILM
LENS
GRATING (600 lines/mm)
CRYSTAL
EVAPORATOR
VIEW PORT
KRONOS THICKNESS MONITOR
EMI 6256 B P.M. TUBE
H. V. SUPPLY
KEITHLEY PICOAMM.
HONEYWELL RECORDER

Fig. 2

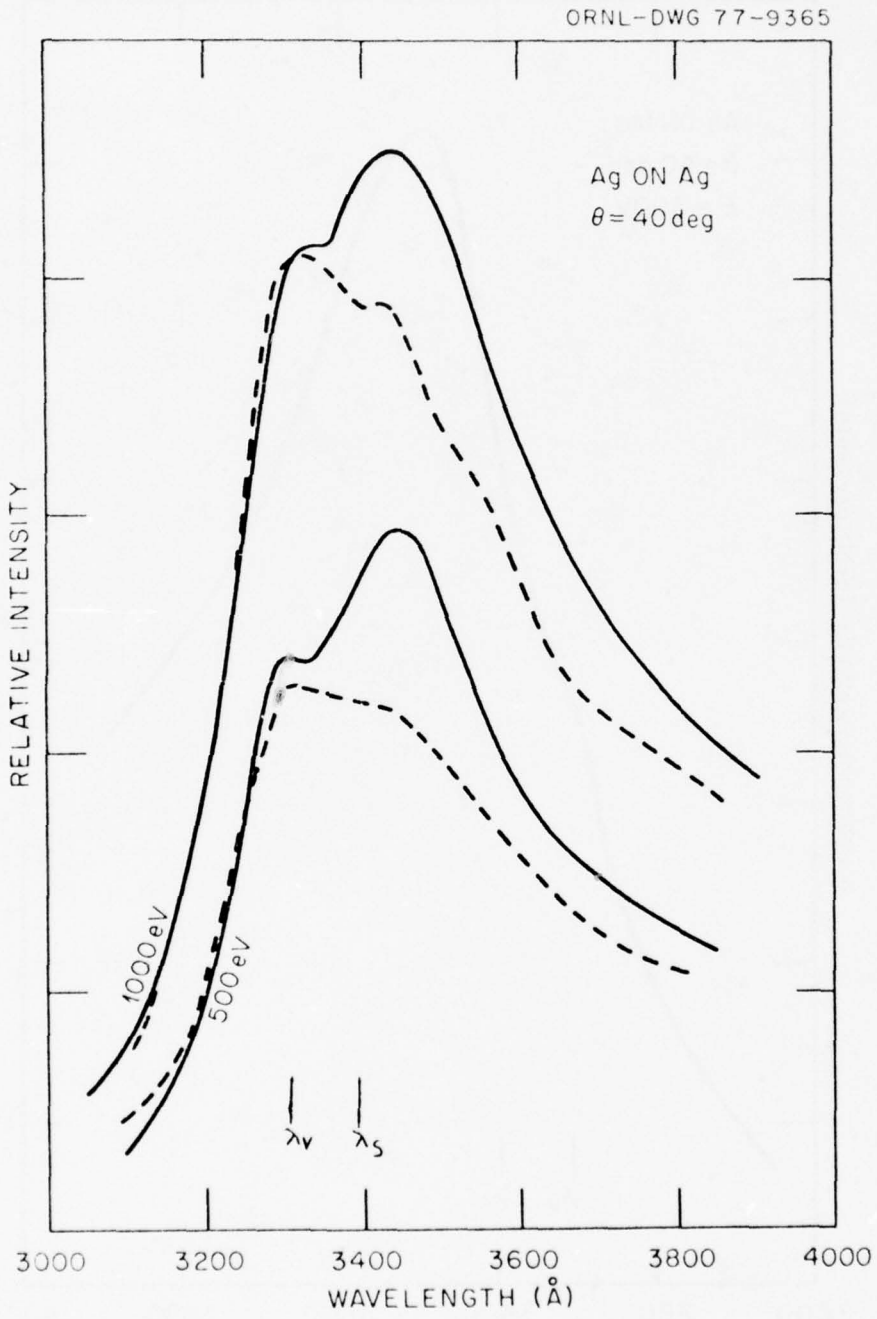
ORNL-DWG 77-9365
Ag ON Ag
θ = 40 deg
RELATIVE INTENSITY
1000 eV
500 eV
λV
λS
3000
3200
3400
3600
3800
4000
WAVELENGTH (Å)

Fig. 3

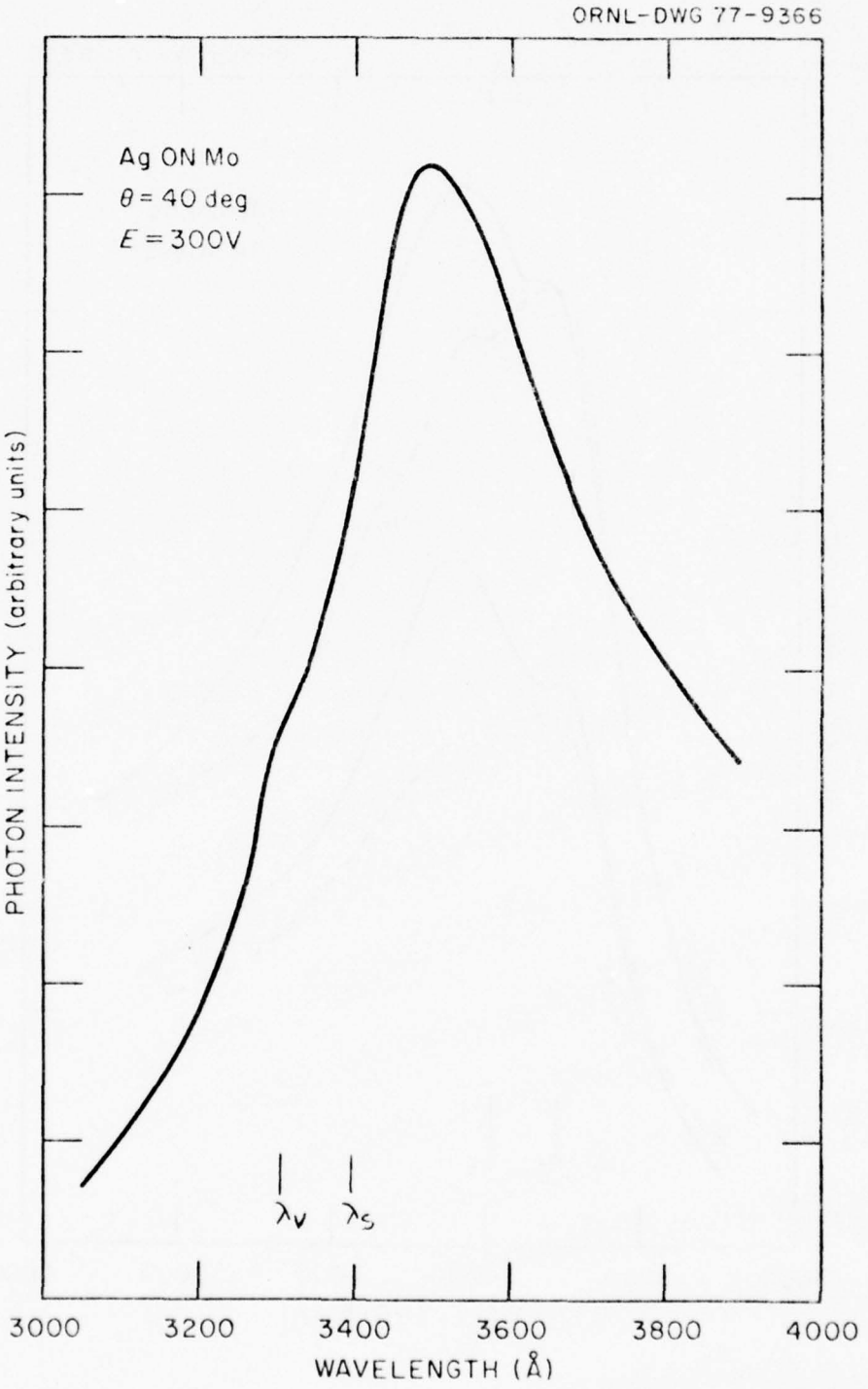
ORNL-DWG 77-9366
Ag ON Mo
θ = 40 deg
E = 300V
PHOTON INTENSITY (arbitrary units)
λV
λS
3000
3200
3400
3600
3800
4000
WAVELENGTH (Å)

Fig. 4

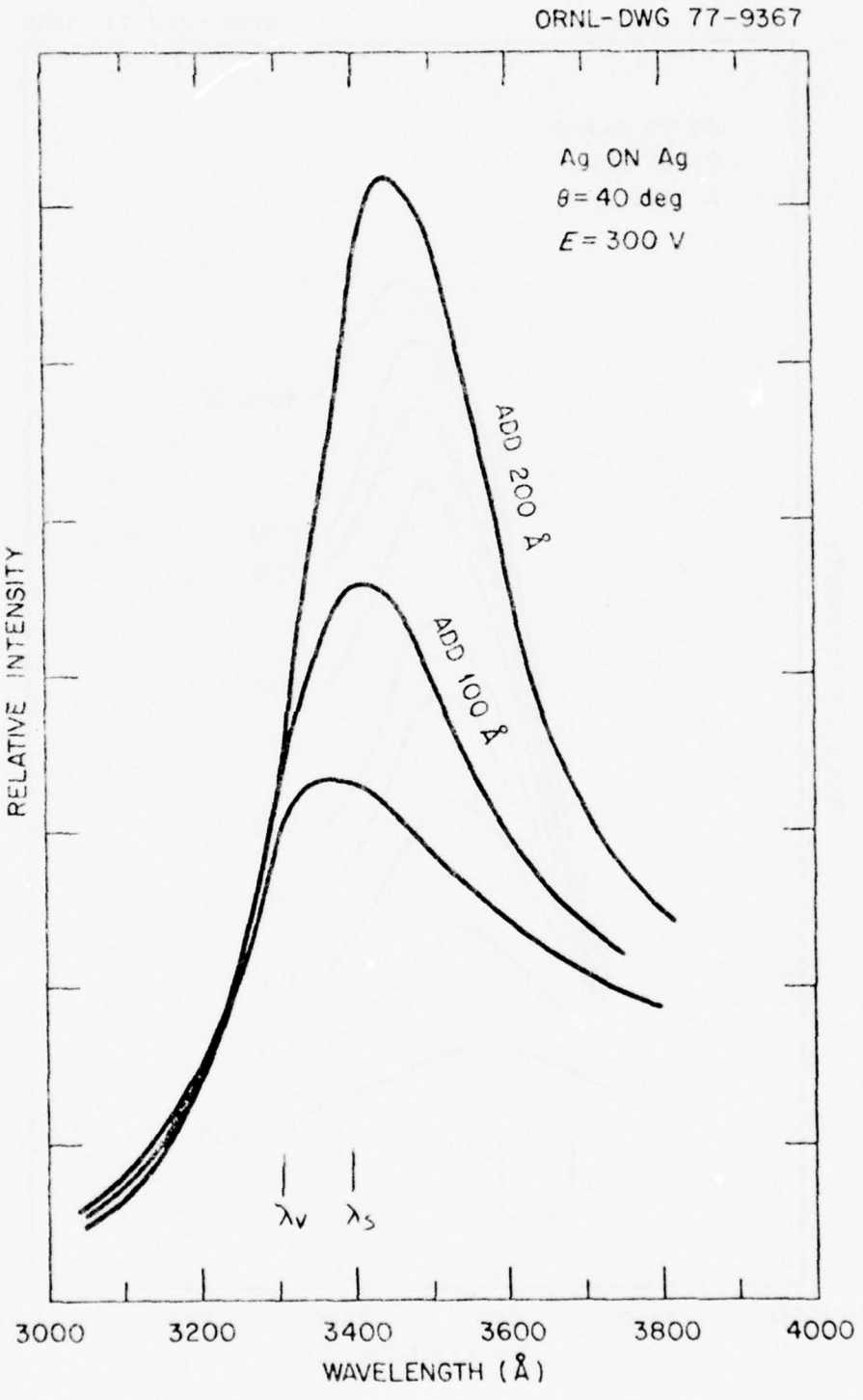
ORNL-DWG 77-9367
Ag ON Ag
θ = 40 deg
E = 300 V
ADD 200 Å
ADD 100 Å
RELATIVE INTENSITY
λV
λS
3000
3200
3400
3600
3800
4000
WAVELENGTH (Å)

Fig. 5

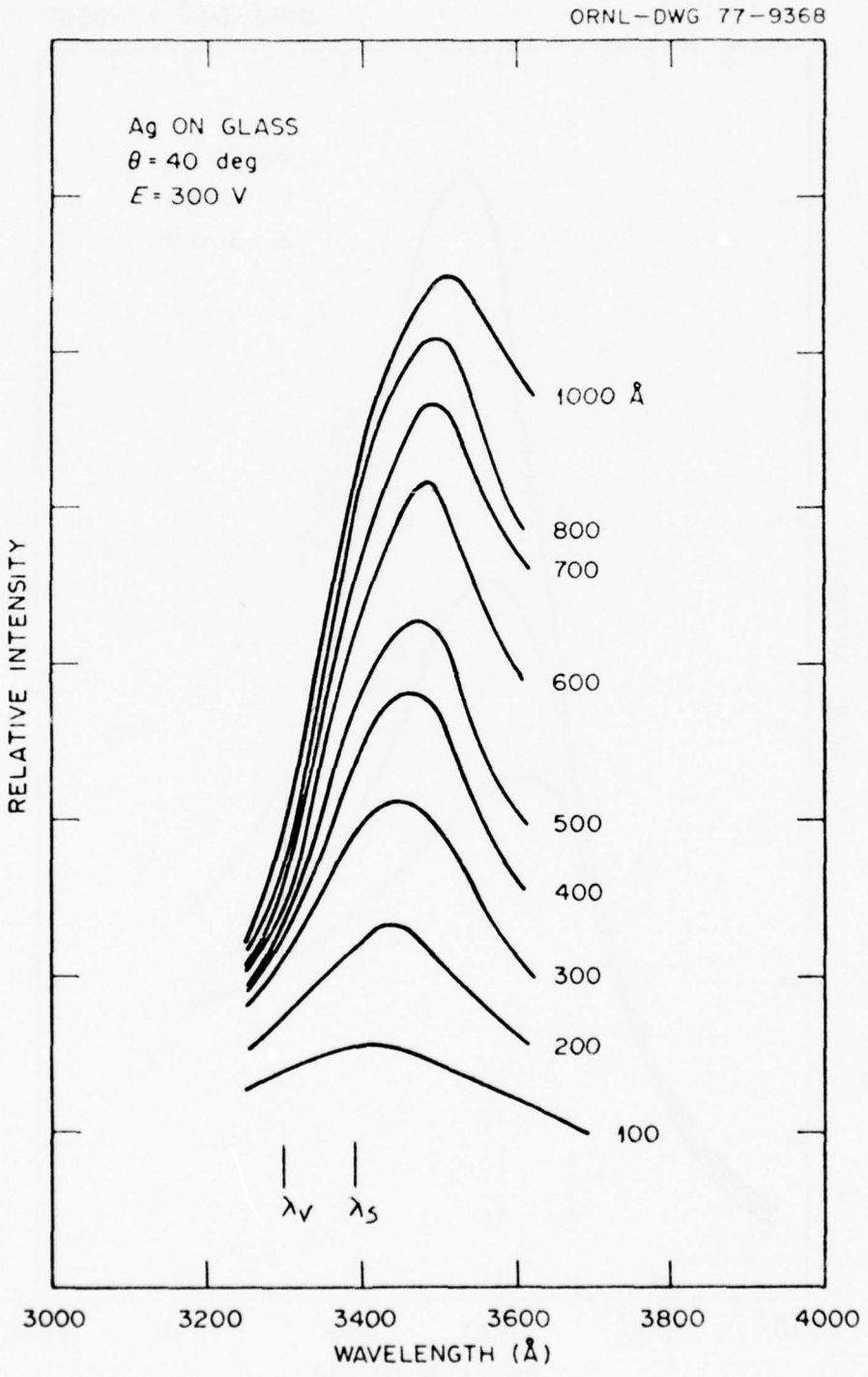
ORNL-DWG 77-9368
Ag ON GLASS
θ = 40 deg
E = 300 V
1000 Å
800
700
600
500
400
300
200
100
λV
λS
RELATIVE INTENSITY
3000
3200
3400
3600
3800
4000
WAVELENGTH (Å)

Fig. 6

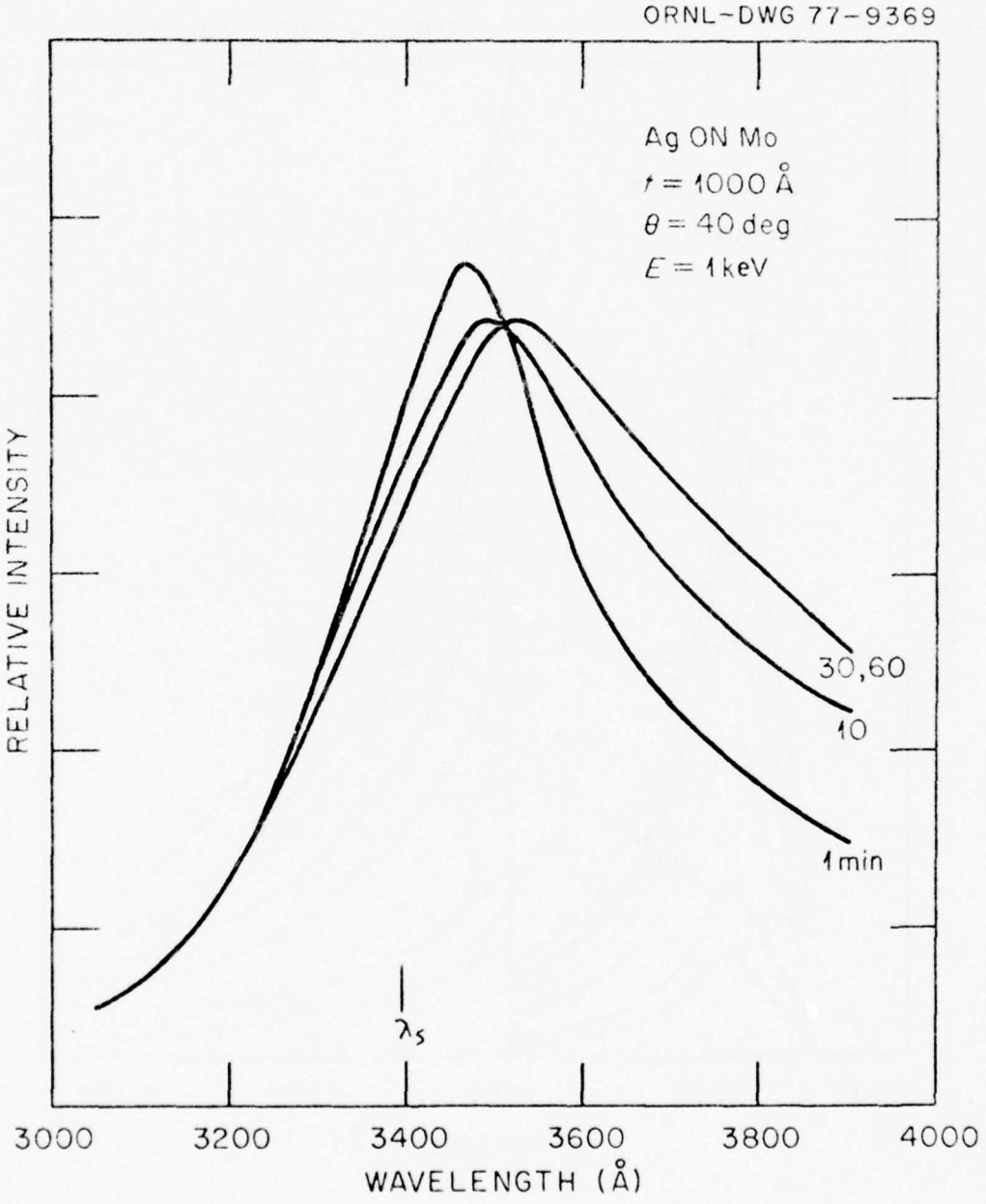
ORNL-DWG 77-9369
Ag ON Mo
t = 1000 Å
θ = 40 deg
E = 1 keV
30,60
10
1 min
λs
RELATIVE INTENSITY
3000
3200
3400
3600
3800
4000
WAVELENGTH (Å)

Fig. 7

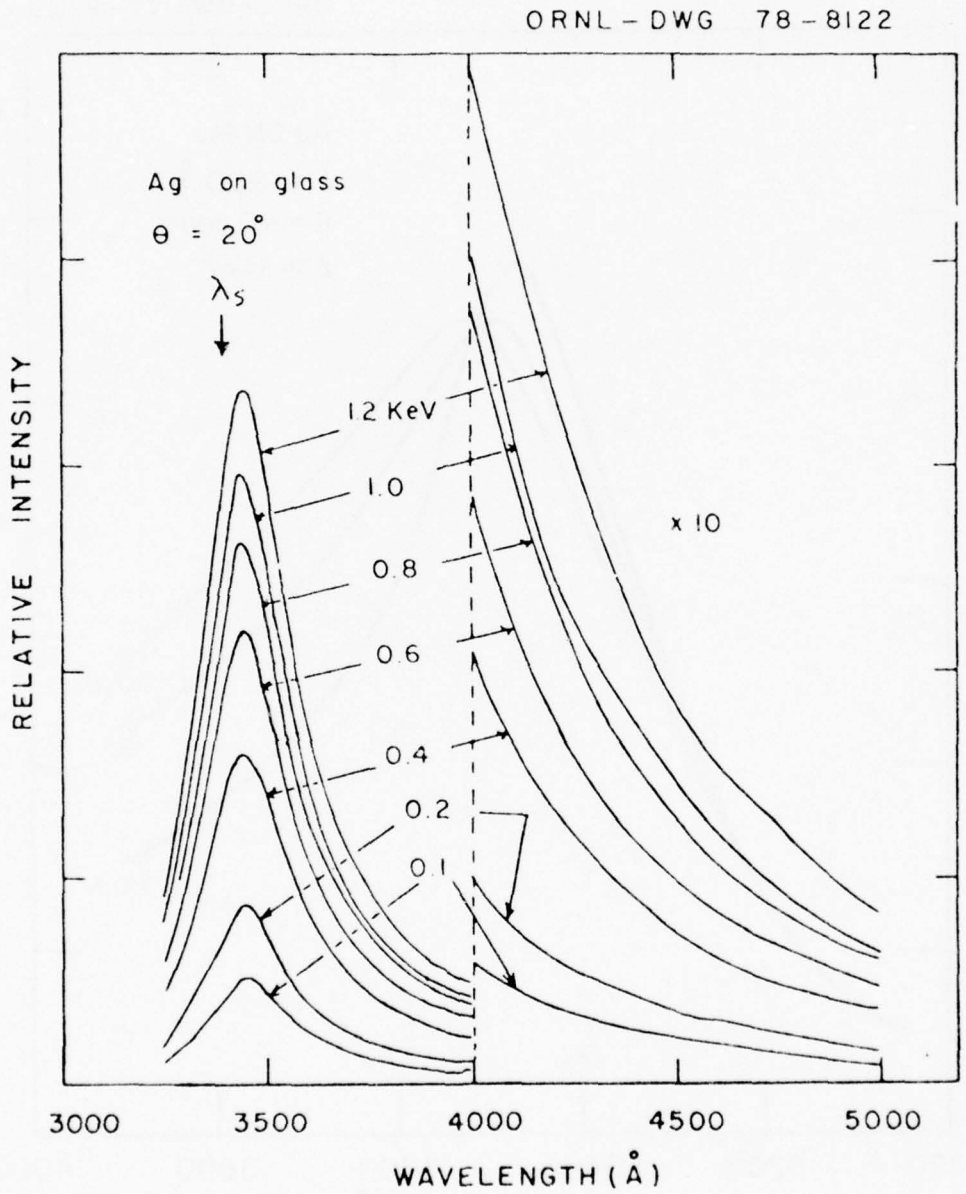
ORNL – DWG 78 – 8122
Ag on glass
θ = 20°
λs
12 KeV
1.0
0.8
0.6
0.4
0.2
0.1
x 10
RELATIVE INTENSITY
3000
3500
4000
4500
5000
WAVELENGTH (Å)

Fig. 8

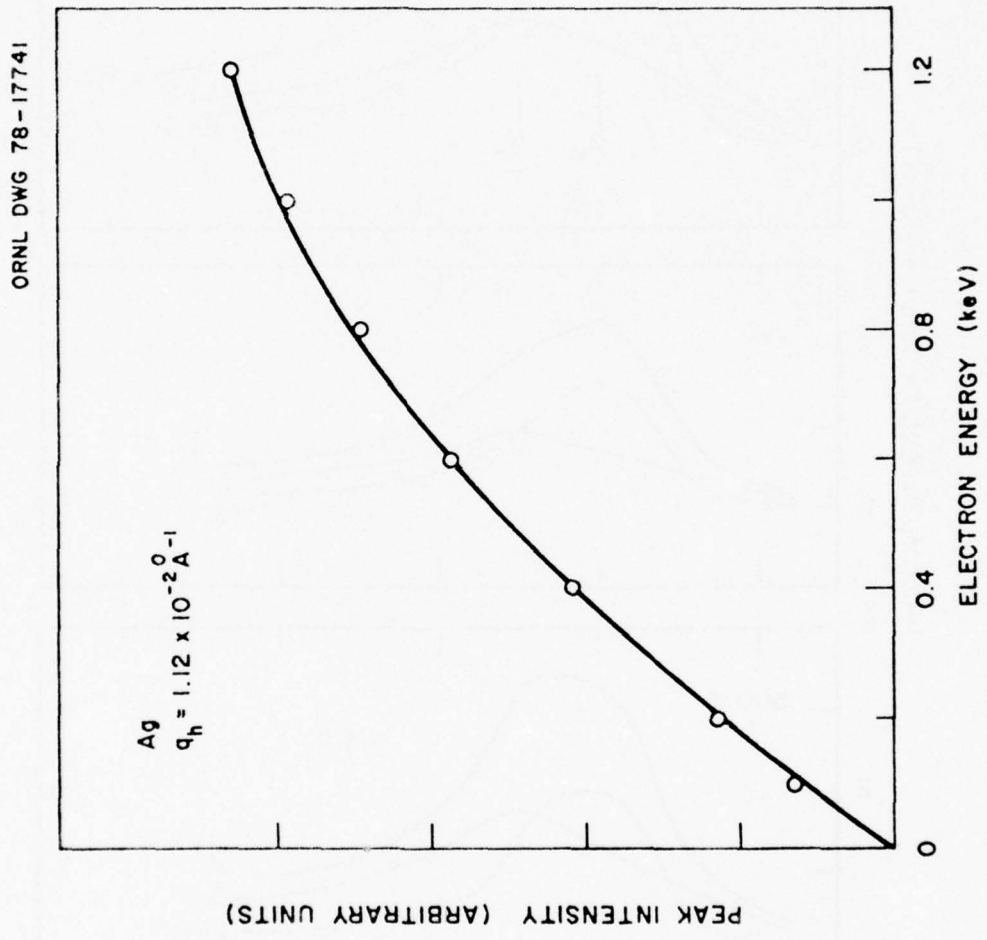
ORNL DWG 78-17741
Ag
$q_h = 1.12 \times 10^{-2} \text{ Å}^{-1}$
PEAK INTENSITY (ARBITRARY UNITS)
0
0.4
0.8
1.2
ELECTRON ENERGY (keV)

Fig. 9

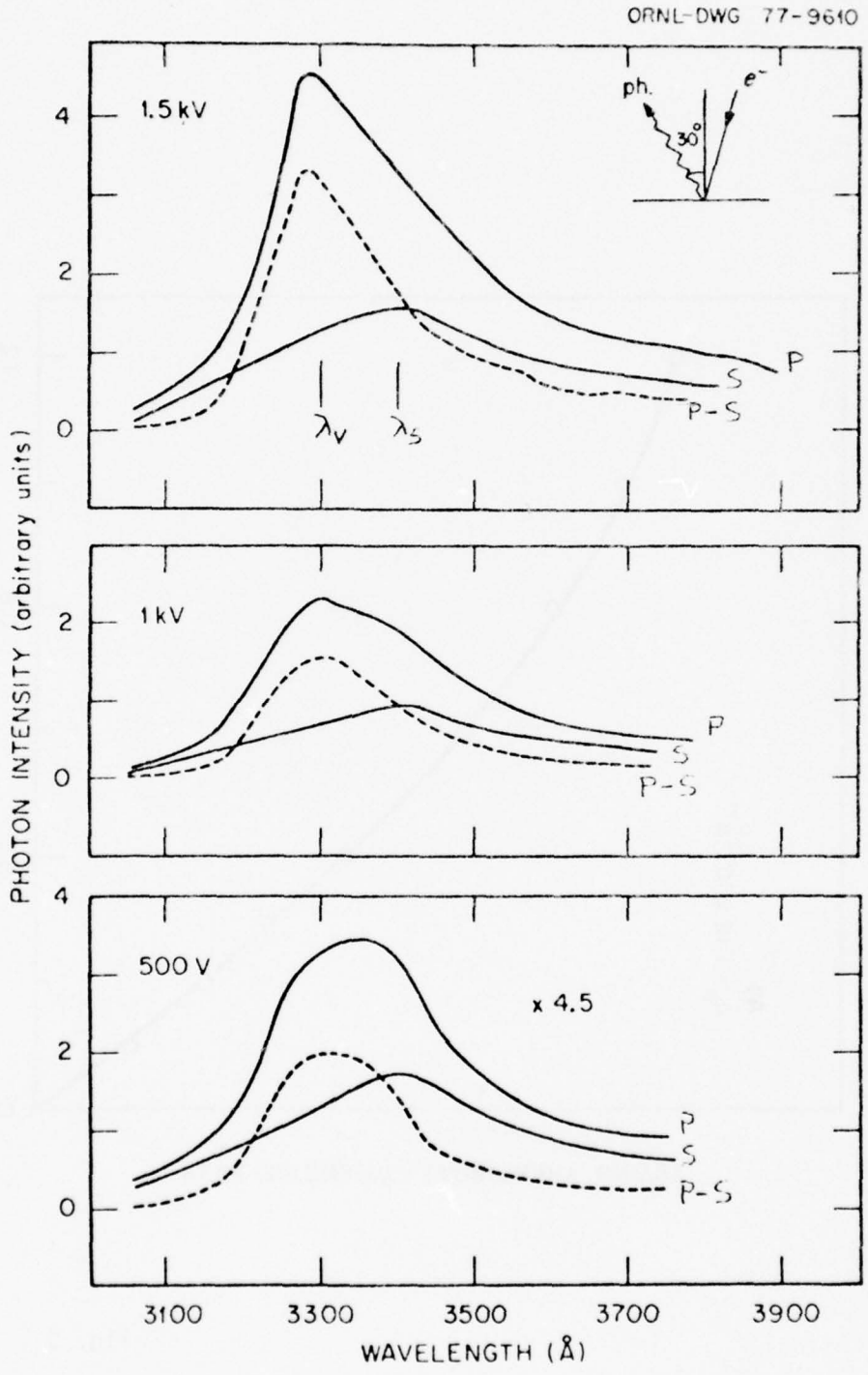
ORNL-DWG 77-9610
1.5 kV
ph.
e⁻
30°
P
S
P-S
λV
λS
1 kV
P
S
P-S
500 V
x 4.5
P
S
P-S
PHOTON INTENSITY (arbitrary units)
0
2
4
3100
3300
3500
3700
3900
WAVELENGTH (Å)

Fig. 10

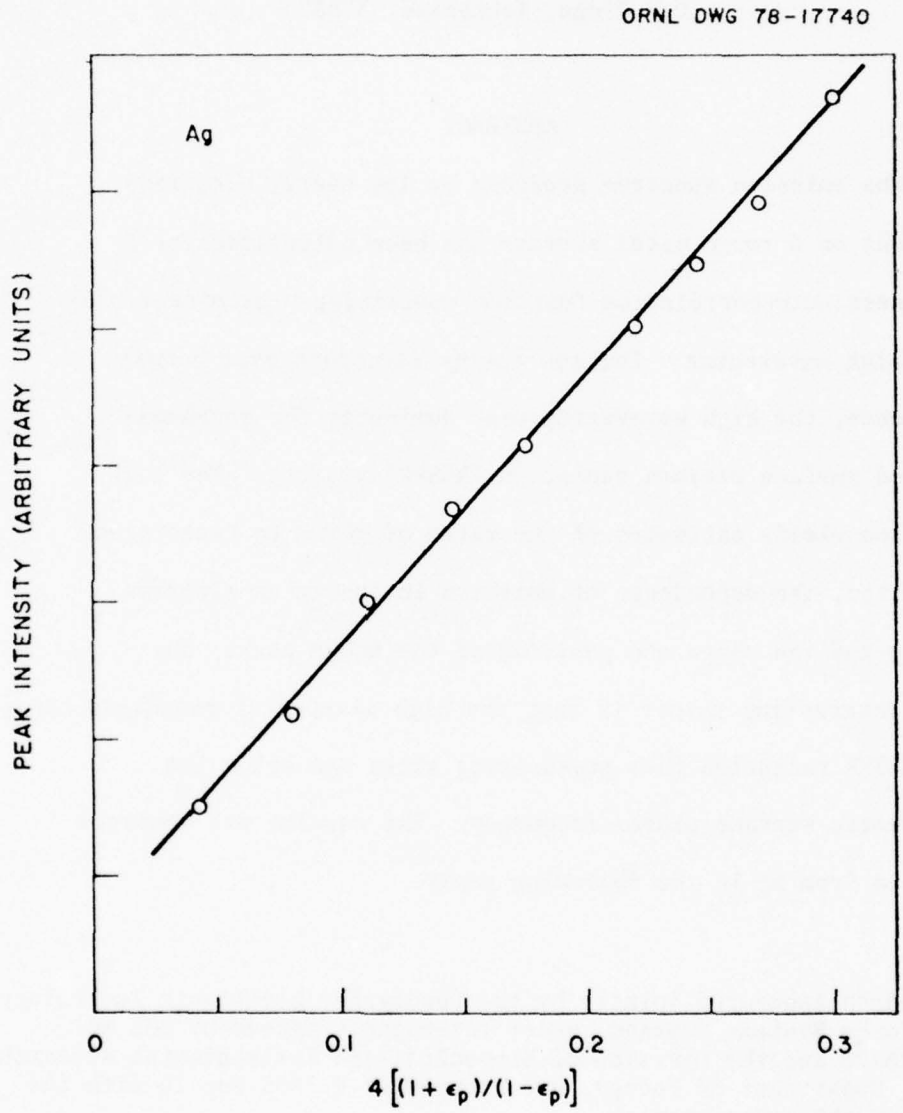
ORNL DWG 78-17740
Ag
PEAK INTENSITY (ARBITRARY UNITS)
0
0.1
0.2
0.3
4 [(1 + ϵp)/(1 − ϵp)]

Fig. 11

CHAPTER II-B

Theory of Emission Spectra from Metal Films Irradiated by Low Energy Electrons near Normal Incidence*

E. Kretschmann,† T. A. Callcott,†† and E. T. Arakawa
Health and Safety Research Division, Oak Ridge National Laboratory
Oak Ridge, Tennessee 37830

ABSTRACT

The emission spectrum produced by low energy electrons incident on a rough metal surface has been calculated for a roughness auto-correlation function containing a prominent peak at a high wavevector. For low energy electrons near normal incidence, the high wavevector peak dominates the roughness coupled surface plasmon radiation (RCSPR) process. The calculation yields estimates of the ratio of RCSPR to transition radiation, the dependence of emission intensity on electron energy and the shape and position of the RCSPR peak. The most interesting result is that the high wavevector roughness can split the RCSPR radiation into peaks lying above and below the asymptotic surface plasma frequency. The results are compared to data from Ag in the following paper.

*Research sponsored jointly by the Deputy for Electronic Technology, Air Force Systems Command, under Interagency Agreement DOE No. 40-226-70 and the Division of Biomedical and Environmental Research, U. S. Department of Energy, under contract W-7405-eng-26 with the Union Carbide Corporation.

†Present address: Schäferstrasse 28, 2 Hamburg 6, W. Germany.

††Also Department of Physics, University of Tennessee, Knoxville, Tennessee 37916.

I. INTRODUCTION

A large number of experimental and theoretical studies of the emission of light from metal surfaces irradiated by electrons have been performed in the last two decades. The most recent ones are cited here; the earlier ones are listed in references 1-4. In the emission spectra an edge or weak maximum is generally found experimentally near $\omega = \omega_p$ (the volume plasma frequency of the metal). Under certain conditions an additional maximum is found near $\omega = \omega_s$ (the surface plasma frequency). Theoretically the edge at ω_p can be described by transition radiation (and/or Bremsstrahlung) at a smooth surface,[5] and the maximum near ω_s by roughness coupling of nonradiative "surface plasmons" to the radiation field.[6]

There are three published theoretical treatments of the latter effect. In one quantum mechanical calculation[7] and in a classical calculation,[4] based on earlier theoretical work,[8] the electrons are assumed to have nearly grazing incidence and only the radiation from high wavevector surface plasmons are calculated. The change of the dispersion relation of surface plasmons due to the roughness is not included. A more general calculation has been carried out recently[3] which involves all angles of incidence as well as the influence of surface roughness on the dispersion relation. But in that study only the case of nearly grazing incidence electrons was discussed in detail because till now most experiments have been done in this

configuration in order to enhance the surface plasmon radiation. Recently transition radiation experiments at rough metal surfaces have been performed with low energy electrons[1] ($E_{el} \lesssim 1$ keV). It was found that the natural roughness of evaporated metal films causes the intensity of the surface plasmon radiation to be much greater than that of the transition radiation even for normally incident electrons. We include in the calculation the effect of the roughness on the dispersion relation, which has been shown to cause splitting of the high wavevector part of the dispersion relation into two branches.[9]

The model used, the results of the calculations, and a discussion of the results for a particular correlation function will be given here. A comparison of experimental data on Ag with this theory will be given in the following paper.

II. MODEL AND RESULTS

An electron of charge -e penetrates the metal-vacuum boundary at an angle α with the surface normal with a constant velocity v. Electron velocity is small compared to the velocity of light ($\beta \equiv v/c << 1$). The metal is described by the dielectric function $\varepsilon(\omega)$. For a smooth surface the emission spectrum is calculated as follows. The homogeneous fields associated with the moving electron in both vacuum and the metal are calculated by the Maxwell equations. Homogeneous fields in the metal and the vacuum are added in order to satisfy the usual boundary conditions at an interface. The fields have radiative parts (transition radiation) where the

wavevector along the boundary is smaller than ω/c, the wavevector of light, and nonradiative parts (surface plasmons). Additional details of the method and the results of the smooth surface calculation can be found in ref. 10. From these zero order fields, which are present at a smooth surface, the scattered fields due to the surface roughness up to the second order in the roughness height are calculated with a method given in ref. 11.

From the zero order fields we get for the power of the emitted electromagnetic radiation in the plane of incidence per frequency interval, $d\omega$, observed at the angle θ within an element of solid angle $d\Omega$

$$\frac{d^2I^\circ}{d\Omega d\omega} = \left(\frac{e^2}{\pi^2 c}\right) \cos^2\alpha \sin^2\theta \cos^2\theta |\varepsilon-1|^2 \beta^2 / |\varepsilon \cos\theta + \sqrt{\varepsilon-\sin^2\theta}\,|^2. \quad (1)$$

The Eq. (1) can be found in ref. 5 also. It predicts a weak maximum near the plasma frequency when $\varepsilon = 0$, which is usually called the "volume plasmon peak." From the scattered fields we get for the special case of normally incident electrons ($\alpha = 0$) and for the detection angle $\theta = 0$

$$\frac{d^2I^1}{d\Omega d\omega} = 2\pi \left(\frac{e^2}{\pi^2 c}\right) |\sqrt{\varepsilon} - 1|^2 \left(\frac{\omega}{c}\right)^4 \langle s^2\rangle \int dk\, k^3\, g\left(\frac{\omega}{c} \cdot k\right) \left| \frac{k_1 + k_2}{k_1 + \varepsilon k_2} \right|^2 \frac{\beta^2}{(1 + k^2\beta^2)^2} \quad (2)$$

Here $k_1 \equiv \sqrt{\varepsilon - k^2}$, $k_2 = \sqrt{1 - k^2}$ ($\mathrm{Im}k_1, \mathrm{Im}k_2 > 0$) and k is the wavevector of the zero order waves along the surface in units of ω/c. The surface properties enter through $\langle s^2\rangle$,

the mean square roughness height, and $g(\frac{\omega}{c} \cdot k)$ the normalized correlation function of the roughness. (For a definition of $g(\frac{\omega}{c} \cdot k)$ see ref. 11.) In Eq. (2) terms with β^2 (but not with $\beta^2 k^2$) are neglected and only the transverse magnetic (TM) zero order fields are taken into account. The TM fields are associated with surface plasmons and are of much larger amplitude than transverse electric (TE) fields.

III. DISCUSSION

We will discuss Eq. (2) for frequencies where surface plasmons may be present ($\varepsilon(\omega) < 0$.) For the discussion we will use a special roughness correlation function with features that we believe roughly approximate the true correlation function. The correlation function of a rough surface can be determined in this low roughness k-vector region by light scattering experiments.[12] It has been generally assumed that the correlation function has a strong maximum for $k = 0$ and falls monotonically with increasing $k(\omega/c)$. However, there are indications that in the high k-region the correlation function has a second maximum at some $k = k_h >> 1$.[4,13,14] Here $k_h = \lambda_s/\lambda_h$ with λ_h the dominant wavelength of the statistical roughness and λ_s the wavelength of light at the surface plasma frequency ω_s. Therefore, we divide $g(\frac{\omega}{c} \cdot k)$ into a low k-vector part, $g_\ell(k)$, and a high k-vector part, $g_h(k)$ which will be approximated by a δ-function.

$$\langle s^2\rangle\, g\left(\frac{\omega}{c}\cdot k\right) = \langle s_\ell^{\,2}\rangle\, g_\ell\left(\frac{\omega}{c}\cdot k\right) + \frac{1}{2\pi}\langle s_h^{\,2}\rangle \frac{1}{\left(\frac{\omega}{c}\right)^2 k_h}\,\delta\,(k - k_h), \quad (3)$$

where $\langle s^2\rangle = \langle s_\ell^{\,2}\rangle + \langle s_h^{\,2}\rangle$ and $k_h = \lambda_s/\lambda_h$. More generally we may introduce a sum of δ-functions to describe the high k-vector part.

Equation (2) can be simplified since $\left|\frac{k_2 + k_1}{\varepsilon k_2 + k_1}\right|^2$ has a pole if $k = k_{sp} = \sqrt{\varepsilon/(\varepsilon + 1)}$, the normalized k-vector of surface plasmons. For the scattered power of "low k-vector" surface plasmons ($\varepsilon < -1.5$, $k_{sp} \leq 2$, $\mathrm{Im}\varepsilon \ll \mathrm{Re}\,\varepsilon$), we approximate the integral in Eq. (2) by the integral over the pole and obtain

$$\frac{d^2 I^{\ell}}{d\omega d\Omega} = 4\pi^2 \left(\frac{e^2}{\pi^2 c}\right) \cdot \frac{1 - \mathrm{Re}\,\varepsilon}{\mathrm{Im}\varepsilon} \cdot k_o^{\,6} \left(\frac{\omega}{c}\right)^4 \langle s^2\rangle\, g\left(\frac{\omega}{c}\cdot k_o\right) \quad (4)$$

where $k_o = \sqrt{\mathrm{Re}\,\varepsilon/(\mathrm{Re}\,\varepsilon + 1)}$. Equation (4) is similar to the equation which has been developed to describe the dip in the reflection near the surface plasma frequency. For the scattered power of "high k-vector" surface plasmons ($\varepsilon \simeq -1$, $k \gg 1$) we get

$$\frac{d^2 I^{h}}{d\omega d\Omega} = 8\pi \left(\frac{e^2}{\pi^2 c}\right) \left(\frac{\omega}{c}\right)^4 \langle s_h^{\,2}\rangle \cdot \frac{|\sqrt{\varepsilon} - 1|^2}{|\varepsilon + 1|^2} \int dk\, k^3\, g_h\left(\frac{\omega}{c}\cdot k\right) \frac{\beta^2}{(1 + k^2\beta^2)^2} \quad (5)$$

In order to get Eq. (5) we set $ik \simeq k_1 \simeq k_2$ which is appropriate for large k.[9] With the special choice of $g\left(\frac{\omega}{c}\cdot k\right)$ in Eq. (3) we get

$$J^h = \frac{d^2 I^h}{d\omega d\Omega} = 4 \left(\frac{e^2}{\pi^2 c}\right) \cdot \frac{|\sqrt{\varepsilon} - 1|^2}{|\varepsilon + 1|^2} \quad \langle s_h^2 \rangle \left(\frac{}{c}\right)^2 \frac{\beta^2 k_h^2}{|1 + k_h^2 \beta^2|^2} \qquad (6)$$

Equations (2) to (6) are still inconsistent since they do not include the effect of roughness on the surface plasmon dispersion relation. To include this effect k_o in Eq. (4) has to be replaced by $\bar{k}_o$, the wavevector of the surface plasmons at the rough surface. The value of $\bar{k}_o$ is larger than k_o, the wavevector at a smooth surface. In ref. 16 experimental and in ref. 17 theoretical determinations of $\bar{k}_o$ are made.[16,17] The inconsistency in Eq. (6) can be removed if $(\varepsilon + 1)$ appearing in the denominator of Eq. (6) is replaced. In ref. 9 it is shown that one has to replace $1/(\varepsilon + 1)$ by

$$\frac{1}{(1-a^2)} \quad \frac{\varepsilon + 1}{(\varepsilon + \varepsilon_1)(\varepsilon + 1/\varepsilon_1)} \qquad (7)$$

where $\varepsilon_1 = \frac{1 + a}{1 - a}$ and

$$a^2 = \langle s_h^2 \rangle \left(\frac{\omega}{c}\right)^2 \int d^2\underset{\sim}{k}' g_h\left(\frac{\omega}{c} |\underset{\sim}{k}' - \underset{\sim}{k}|\right) kk' \left(1 - \frac{\underset{\sim}{k} \cdot \underset{\sim}{k}'}{kk'}\right)^2$$

and $\underset{\sim}{k}$, $\underset{\sim}{k}'$ are the two dimensional wavevectors of the electromagnetic waves along the surface in units of $\frac{\omega}{c}$. If we use the δ-function for $g_h(k \cdot \frac{\omega}{c})$ and set $k \simeq k_h$ in the above integral we obtain

$$a^2 = \left(\frac{\omega}{c}\right)^2 \langle s_h^2 \rangle k_h^2 \cdot \frac{1}{8.2}$$

$$= \left(\frac{2\pi\lambda_s}{\lambda}\right)^2 \cdot \frac{\langle s_h^2 \rangle}{\lambda_h^2} \cdot \frac{1}{8.2} \qquad (8)$$

For further discussion we will perform some numerical calculations which treat aspects of the theory that can be compared to experiment. We calculate:

1. The intensity relation between "surface plasmon" and "volume plasmon" peaks.
2. The electron energy dependence of the surface plasmon peak intensity.
3. The shape (half width and maximum position) of the surface plasmon peak.
4. The relation between maximum position and intensity of the surface plasmon peak.

1. For $\theta = 30°$, $\alpha = 0$, $\varepsilon = 0$, Eq. (1) gives $J^\circ = \frac{d^2I^\circ}{d\Omega d\omega} = \frac{3}{4}\frac{e^2}{\pi^2 c}\beta^2$ as the maximum of the volume plasmon peak. The ratio of the intensity of the surface plasmon peak (Eq. (6) for $\varepsilon = -1 + i\varepsilon_2$) and the volume plasmon peak, is given in Fig. 1a. Figure 1a shows clearly that a small β value (or a low electron energy) is necessary in order to enhance the surface plasmon peak relative to the volume plasmon peak. If we take E = 1 keV and $\mathrm{Im}\varepsilon = \varepsilon_2 = 0.3$ we need $\langle s_h^2 \rangle^{1/2}/\lambda_h > 1/15.2$ to get $J^h > 10\ J^\circ$. If we took E = 10 keV we would get $J^h \simeq J^\circ$ for the same roughness parameter.

The energy dependence of the surface plasmon peak intensity is shown in Fig. 1b. For small β, J^h is a linear function of β^2. It peaks for $\beta = 1/k_h$. If one fits the curvature of the experimentally determined energy dependence with the theoretical one, one can calculate the dominant wavelength of the roughness.

3. In Fig. 2 roughness coupled surface plasmon spectra as predicted by Eq. (6) with the replacement (7) are shown. The $\mathrm{Re}\varepsilon$ values of silver determined in ref. 18 are assumed and $\mathrm{Im}\varepsilon$ is set equal to 0.3.[18] Spectra for different values of the roughness parameter $b = \sqrt{\langle s_h^2 \rangle}\ /\lambda_h$ are plotted. The denominator $(1 + k_h^2\beta^2)^2$ has been neglected. Whereas one peak is predicted near $\varepsilon = -1$ for $b = 0$, a double peak is predicted for $b \neq 0$. The high energy peak is always smaller in intensity. The splitting increases with b. Recently this double peak structure was found[19] in the emission spectrum of potassium. There is also a report in the literature[20] which shows double peaks in reflection measurements of sodium and potassium. Because the splitting changes with the value of k it may be smeared out since in real physical systems $g_h[(\omega/c)k]$ contains more than one Fourier component. A broad peak which is shifted to smaller ε-value (larger wavelength) may be seen in this case. This is the situation that we believe to be appropriate to the Ag data presented in the following paper.

4. In Fig. 2 it can be seen that an increase of the intensity is always connected with a shift in the position of the maximum to longer wavelength. According to Eq. (6) the intensity is proportional to $\langle s_h^2 \rangle k_h^2$ and according to Eqs. (7) and (8) $(\varepsilon_1 - 1)/(\varepsilon_1 + 1) = a$ is proportional to $\sqrt{\langle s_h^2 \rangle k_h^2}$. This result should be valid for all experimental situations where roughness coupling to high k-vector surface plasmons takes place. This relation between intensity and shift was found in the reflection measurement at rough surfaces,[21] and is demonstrated for emission from Ag in the following paper.

The results obtained in the numerical calculations associated with paragraphs 1 through 4 above are consistent with experimental results on emission spectra from rough silver films reported in the accompanying paper.

REFERENCES

1. M. S. Chung, T. A. Callcott, E. Kretschmann, and E. T. Arakawa Surface Science _____ (1979) (preceding paper).
2. D. Heitmann and V. Permieu, Opt. Commun. 25, 196 (1978).
3. A. M. Marvin, F. Toigo, Trieste July 1977 - private communication.
4. G. Sauerbrey, E. Woeckel and P. Dobberstein, Phys. Status Solidi B 60, 665 (1973) and Erratum B 72, 845 (1975).
5. I. M. Frank, Sov. Phys.-Usp. 8, 729 (1965).
6. E. A. Stern, Phys. Rev. Lett. 19, 1321 (1967).
7. R. H. Ritchie, Phys. Status Solidi 39, 297 (1970).
8. E. Kröger and E. Kretschmann, Z. Phys. 237, 1 (1970).
9. E. Kretschmann, T. L. Ferrell, and J. C. Ashley (submitted to Phys. Rev. Lett.).
10. R. H. Ritchie and H. B. Eldridge, Phys. Rev. 126, 1935 (1962).
11. E. Kretschmann and E. Kröger, J. Opt. Soc. Am. 65, 150 (1975).
12. D. Hartmann and V. Permieu, Opt. Cummun. 23, 131 (1977).
13. W. Kaspar and U. Kreibig, Surf. Sci. 69, 619 (1977).
14. A. J. Braundmeier and D. G. Hall, Surf. Sci. 49, 376 (1975).
15. J. M. Elson and R. H. Ritchie, Phys. Status Solidi B 62, 461 (1974).
16. D. Hornauer, H. Kapitza and H. Raether, J. Phys. D7, 100 (1974).
17. E. Kröger and E. Kretschmann, Phys. Status Solidi B 76, 515 (1976).
18. R. H. Huebner, E. T. Arakawa, R. A. MacRae, R. N. Hamm, J. Opt. Soc. Am. 54, 1434 (1964).
19. M. W. Williams, J. C. Ashley, E. Kretschmann, T. A. Callcott, M. S. Chung and E. T. Arakawa -(submitted to Phys Letters A)

20. R. E. Palmer and S. E. Schnatterly, Phys. Rev. B 4, 2329 (1971).

21. J. L. Stanford, H. E. Bennett, J. M. Bennett, E. J. Ashley, and E. T. Arakawa, Bull. Am. Phys. Soc. 12, 399 (1967).

FIGURE CAPTIONS

Fig. 1a Ratio of the intensities of the "surface plasma" peak J^h to the "volume plasma" peak J^v.

Fig. 1b Intensity of the "surface plasma" peak J^h versus incident electron energy.

Fig. 2 Wavelength dependence of the emission intensity J^h (Eq. 6, 7, 8) from high k-vector surface plasmons. The values of Re ε are shown below the wavelength scale; Imε is assumed to be 0.3. The curves are labeled by values of the relevant roughness parameter $\sqrt{\langle s^2_h \rangle}\,/\lambda_h$.

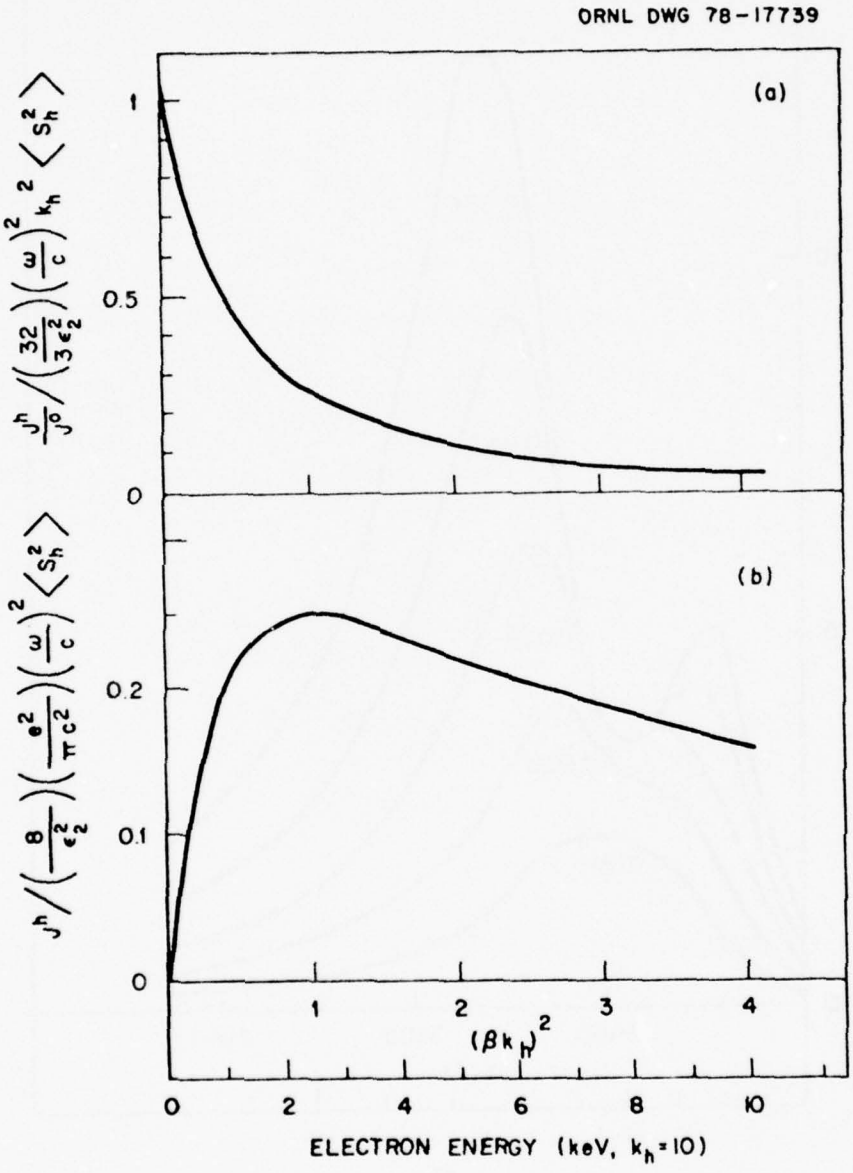
ORNL DWG 78-17739
(a)
(b)
$\frac{J^h}{J^0}/\left(\frac{32}{3\epsilon_2^2}\right)\left(\frac{\omega}{c}\right)^2 k_h^2 \langle S_h^2 \rangle$
$J^h/\left(\frac{8}{\epsilon_2^2}\right)\left(\frac{e^2}{\pi c^2}\right)\left(\frac{\omega}{c}\right)^2 \langle S_h^2 \rangle$
1
0.5
0
0.2
0.1
0
1
2
3
4
$(\beta k_h)^2$
0
2
4
6
8
10
ELECTRON ENERGY (keV, k_h=10)

Fig. 1

ORNL DWG 78-17743

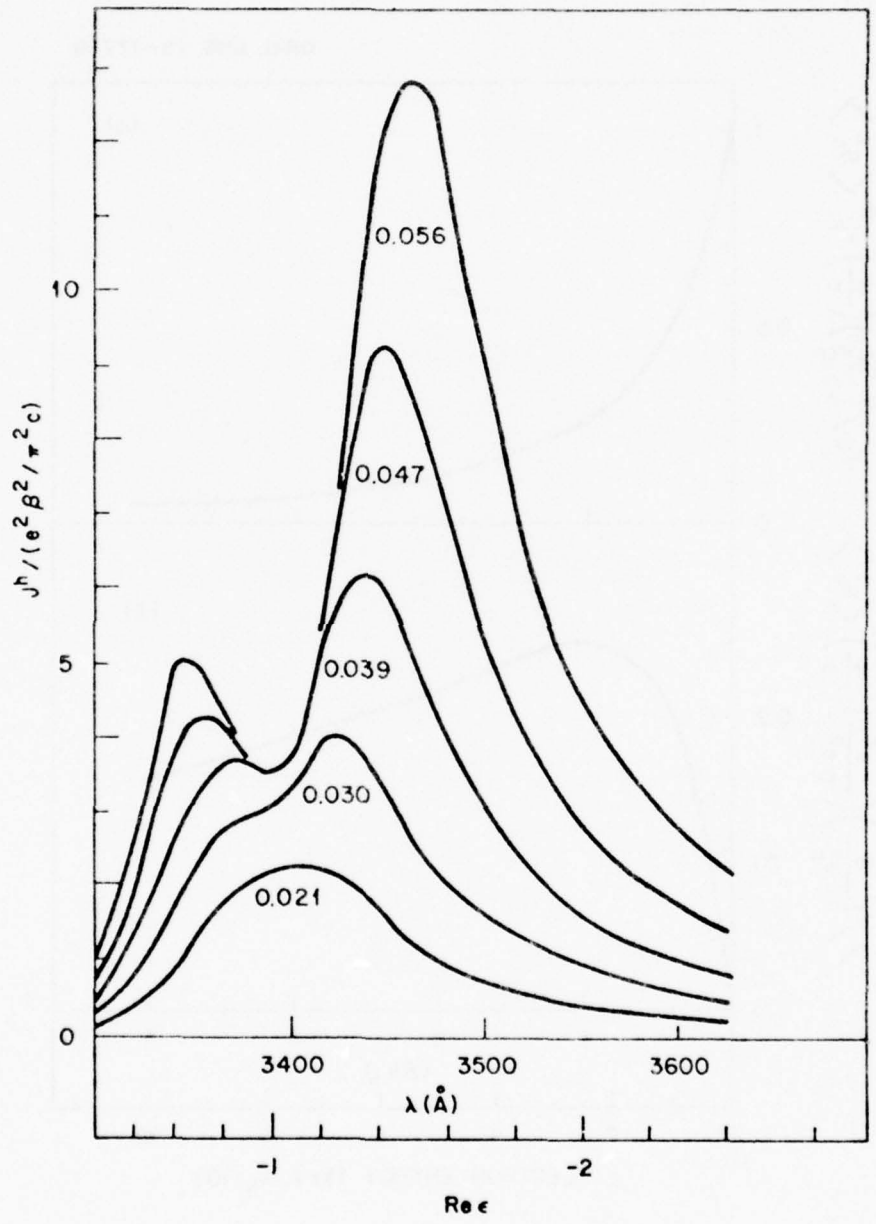

Fig. 2

CHAPTER II-C

A SPLITTING OF THE DISPERSION RELATION OF SURFACE PLASMONS ON A ROUGH SURFACE*

E. Kretschmann,† T. L. Ferrell,†† and J. C. Ashley

Health and Safety Research Division
Oak Ridge National Laboratory
Oak Ridge, TN 37830

Abstract

The dispersion relation for surface plasmons on a statistically slightly rough surface is shown to display a splitting under certain conditions. For a simple model of the correlation function of the surface roughness, explicit calculations are made which explain experimental results not previously interpreted.

*Research sponsored jointly by the Deputy for Electronic Technology, Air Force Systems Command, under Interagency Agreement DOE No. 40-226-70 and the Division of Biomedical and Environmental Research, U. S. Department of Energy, under contract W-7405-eng-26 with the Union Carbide Corporation.

†Permanent address: Schäferstr. 28, Hamburg 6, West Germany

††Also, Physics Dept., Appalachian State University, Boone, NC 28608

The dispersion relation for surface plasmons on a statistically slightly rough surface is of continuing interest in surface physics as attempts are made to characterize more closely actual surfaces. The present paper considers this dispersion relation for surface plasmon wave vectors $\underset{\sim}{K}$ large relative to ω/c, where ω is the surface plasmon frequency.

The dispersion relation for surface plasmons on a smooth solid-vacuum boundary can be written

$$n_s(K) \equiv \varepsilon K_2 + K_1 \equiv \varepsilon \sqrt{K^2 - 1} + \sqrt{K^2 - \varepsilon} = 0, \tag{1a}$$

or simply

$$\varepsilon + \frac{1}{1 - \frac{1}{K^2}} = 0. \tag{1b}$$

In these equations, K is the (magnitude of the) surface plasmon wave vector in units of ω/c. The function $\varepsilon = \varepsilon(\omega)$ is the complex dielectric function of the solid. The dispersion relation is shown in Fig. 1 for Im $\varepsilon = 0$.

If the surface is rough, the dispersion relation, Eq. (1), must be modified. Equations for the modified dispersion relation have been given by several authors.[1-4] The most convenient form for the present purposes is given by Toigo, Marvin, Celli, and Hill.[3] We have verified the equivalence of their results to those of Kröger and Kretschmann.[1] The dispersion relation for a surface with statistically small roughness may be written as

$$n_R(\underset{\sim}{K}) = n_s(K) - \frac{\omega^2}{c^2}(\varepsilon - 1)^2 \langle s^2 \rangle I(\underset{\sim}{K}) = 0, \tag{2}$$

where $\langle s^2 \rangle$ is the "mean-square roughness height," and

$$I(\underset{\sim}{K}) = \frac{\omega^2}{c^2} \int d^2K' g(\tfrac{\omega}{c}|\underset{\sim}{K} - \underset{\sim}{K}'|) \frac{(\underset{\sim}{K}\cdot\underset{\sim}{K}' - K_2K_1')\ (\underset{\sim}{K}\cdot\underset{\sim}{K}' - K_2'K_1)}{n_s(K')} \quad , \qquad (3)$$

with $g(\frac{\omega}{c}|\underset{\sim}{K} - \underset{\sim}{K}'|)$ the surface-roughness correlation function, $K_1' \equiv K_1(K')$, and $K_2' \equiv K_2(K')$.

Equation (2), or an equivalent form, has been discussed qualitatively in connection with the broadening of the surface plasmon resonance (increased damping), and the increase of the wave vector of "low wave vector" surface plasmons.[1,5] The "low wave vector" region corresponds to $K \lesssim 2$. Good agreement of these expectations with the experimental changes in the dispersion on a grating has been found.[6]

In the "high wave vector" region, $K > 2$, the dispersion relation for a *smooth surface* simplifies to $\varepsilon(\omega) \approx -1$, as can be seen from Eq. (1b) or Fig. 1. When surface roughness is included, a new feature arises in the dispersion relation in this wave vector region, in addition to the obviously different dependence on K, which prevents a simple extrapolation of the results described for $K < 2$ to values of $K > 2$. This new feature in the "high wave vector" region is a splitting of the dispersion relation for surface plasmons on a rough surface. This effect is demonstrated and described in the remainder of this paper.

If the surface wave vector has a large enough magnitude so that one neglects terms of order K^{-1} compared to K, one may put $K_1 \approx K_2 \approx K$ in Eq. (1a) to obtain

$$n_s(K) \approx K(\varepsilon + 1). \qquad (4)$$

For the present purposes we divide $I(\underset{\sim}{K})$ of Eq. (3) into two integrals, I_1 and I_2, given by $I = K[I_1/(\varepsilon + 1) + I_2]$, where I_2 (I_1) is restricted the region $K' < 2$ ($K' > 2$). In the "high wave vector" region of I, n_s is approximated by the limiting form in Eq. (4), and Eq. (2) becomes

$$\frac{n_R}{K} \approx \varepsilon + 1 - \frac{\omega^2}{c^2}(\varepsilon - 1)^2 \langle s^2 \rangle \left[\frac{I_1}{(\varepsilon + 1)} + I_2 \right] = 0, \tag{5}$$

where, for $K > 2$,

$$I_1 \approx \frac{\omega^2}{c^2} \int_{K'>2} d^2K' g(\tfrac{\omega}{c}|\underset{\sim}{K} - \underset{\sim}{K'}|) KK'(1 - \cos\phi)^2 , \tag{6}$$

$$I_2 \approx \frac{\omega^2}{c^2} \int_{K'<2} d^2K' g(\tfrac{\omega}{c}|\underset{\sim}{K} - \underset{\sim}{K'}|) K \frac{(K'\cos\phi - K_2')(K'\cos\phi - K_1')}{n_s(K')} , \tag{7}$$

and

$$\cos\phi = \frac{\underset{\sim}{K}\cdot\underset{\sim}{K'}}{KK'} . \tag{8}$$

For large K and $\varepsilon \approx -1$, one finds

$$I_2 \ll \frac{I_1}{\varepsilon + 1} . \tag{9}$$

Thus, neglecting I_2, Eq. (5) leads to two solutions for ε as shown by the equation

$$[\varepsilon(\omega) + \alpha] \quad [\varepsilon(\omega) + \beta] \quad = 0, \tag{10}$$

where

$$\alpha = \frac{1 - a}{1 + a} , \tag{11}$$

with

$$a^2 = \frac{\omega^2}{c^2} \langle s^2 \rangle I_1 , \tag{12}$$

and $\beta = 1/\alpha$. Equation (10) yields the splitting. This surprisingly simple result has the consequence that, under the conditions dictated by the above approximations, one may observe a double peak near the surface plasma resonance. The separation of the peaks, or the splitting, is determined by the difference in the roots of Eq. (10) and is given by

$$\Delta\varepsilon = \beta - \alpha \approx 4\sqrt{\frac{\omega^2}{c^2}\langle s^2\rangle I_1} = 4a. \tag{13}$$

In Fig. 2 we plot the response function $|K/n_R|^2$, from Eq. (5) with $I_2 = 0$, as a function of Re ε. To be more specific we have chosen Im ε = 0.1, corresponding to potassium, and the wavelength scale at the top of the figure is for potassium with $\hbar\omega_s = 2.8$ eV.[7] These curves give the values of $\varepsilon(\omega)$ at which surface plasmon excitation is possible (positions of the maxima) and the damping of these modes (half-width). The curve labeled $a^2 = 0$ corresponds to surface waves on a smooth surface. The curves for $a^2 > 0$ show the splitting found in the response function (or the dispersion relation) when surface roughness is included in the description of "high wave vector" surface waves. For a given value of $a^2 > 0$, the surface waves at a lower ε value (larger vacuum wavelength) always have a larger intensity than those with a higher ε value (smaller vacuum wavelength.

In order to analyze Eqs. (3)-(12) in more detail, we choose a special form of the correlation function $g(\omega K/c)$. It is likely that most metal samples have a roughness wavelength which peaks around a given value λ_R.[8,9] Therefore, we assume

$$g(\omega K/c) \approx \frac{c^2}{2\pi K_R \omega^2}\,\delta(K - K_R), \tag{14}$$

where the factor $2\pi K_R$ in the denominator of Eq. (14) has been chosen so that

$$\frac{\omega^2}{c^2} \int d^2K \; g(\omega K/c) \;=\; 1. \tag{15}$$

In general the correlation function may be given by a linear superposition of functions like that of Eq. (14), and there is always a maximum in $g(\omega K/c)$ for $K = 0$.

As the case $K_R << K$ below shows, the choice of a form for g under the above simple conditions has very little effect on the dispersion relation for long roughness wavelengths.

Inserting Eq. (14) into Eq. (6) for I_1, we calculate the integral for the cases $K_R << K$, $K_R = K$, and $K_R >> K$. These cases respectively imply a surface roughness wavelength, λ_R, larger, equal to, or smaller than the surface plasmon wavelength. The results are given in Table 1.

Table 1. *Numerical Examples* (λ = 4000 Å, $K = 10$, $\langle s^2 \rangle^{1/2} = \lambda_R/20$)

	I_1	K_R	$\langle s^2 \rangle^{1/2}/\lambda_R$	$\Delta\varepsilon$
$K_R << K$	$\frac{3K_R^4}{32K^2}$	2	100/2000	0.077
$K_R = K$	$\left(\frac{20}{3\pi} - 2\right)K_R^2$	10	20/400	0.44
$K_R >> K$	$1.5\, KK_R - 2K^2$	40	5/100	0.63

The table also contains the splitting $\Delta\varepsilon$ for K_R = 2, 10, and 40 if electromagnetic waves with a vacuum wavelength λ = 4000 Å are involved in the surface plasmon excitation process. We have taken the surface plasmons to have K = 10 and the surface to have a roughness height $\langle s^2 \rangle^{1/2}$ given by $\langle s^2 \rangle^{1/2} = \lambda_R/20$.

The numerical examples show that even a small roughness height can produce a remarkable splitting of the dispersion relation. If one wishes to describe properly the behavior of electromagnetic waves at a rough surface for frequencies near the surface plasma resonance, the change in the dispersion relation should be included. However, this has not been done in the analysis of reflection measurements on rough surfaces.[10,11]

The splitting of the dispersion relation should be experimentally observable. There is, in fact, a report of a double peak near the surface plasma frequency in reflection measurements on sodium and potassium.[7] For their potassium sample this splitting was observed to be approximately 0.2 eV, implying that $\Delta\varepsilon \approx 0.3$. From our calculations above for $K = K_R$, this would mean $\langle s^2 \rangle^{1/2}/\lambda_R \approx 1/30$, which is quite reasonable.

Recently, in the light-emission spectra from films bombarded by low-energy electrons ($\sim$ 1 keV), a doublet structure at the surface plasma energy was found for some potassium films.[12] This structure is readily explained in terms of the theory presented here.

In an experiment in which surface plasma waves of a variety of wave vectors are involved, the splitting may not be detectable. This is due to the fact that the superposition of the associated response functions $|K/n_R|^2$, each with its own splitting, may smear the results into a broad maximum with a lower ε value (< -1). Additionally, there will be a substantial amount of response for $-1 < \varepsilon < 0$, which comes from the branch at the higher ε values.

References

1. E. Kröger and E. Kretschmann, Phys. Status Solidi B 76, 515 (1976).
2. A. A. Maradudin and W. Zierau, Phys. Rev. B 14, 484 (1976).
3. F. Toigo, A. Marvin, V. Celli, and N. R. Hill, Phys. Rev. B 15, 5618 (1977).
4. D. G. Hall and A. J. Braundmeier, Jr., Phys. Rev. B 17, 3808 (1978).
5. D. Hornauer, H. Kapitza, and H. Raether, J. Phys. D 7, 2100 (1974).
6. I. Pockrand and H. Raether, Appl. Opt. 16, 2784 (1977).
7. R. E. Palmer and S. E. Schnatterly, Phys. Rev. B 4, 2329 (1971).
8. J. Endriz and W. E. Spicer, Phys. Rev. B 4, 4144 (1971).
9. P. Dobberstein, Phys. Lett. A 31, 307 (1970).
10. J. L. Stanford, H. E. Bennett, J. M. Bennett, E. J. Ashley, and E. T. Arakawa, Bull. Am. Phys. Soc. 12, 399 (1961).
11. L. J. Cunningham and A. J. Braundmeier, Phys. Rev. B 14, 479 (1976).
12. E. Kretschmann, T. A. Callcott, M. S. Chung, E. T. Arakawa, and M. W. Williams (to be submitted to Phys. Lett.)

Figure Captions

Fig. 1. Dispersion relation of surface plasma waves on a smooth surface.

Fig. 2. The response function $|K/n_R|^2 = \left|(\varepsilon + 1) - \frac{(\varepsilon - 1)^2 a^2}{\varepsilon + 1}\right|^{-2}$ for surface plasmons on a rough surface ($a > 0$). The response function for a smooth surface is given by the curve labeled $a^2 = 0$. Each curve is scaled so that the maximum value of $|K/n_R|^2$ is equal to one.

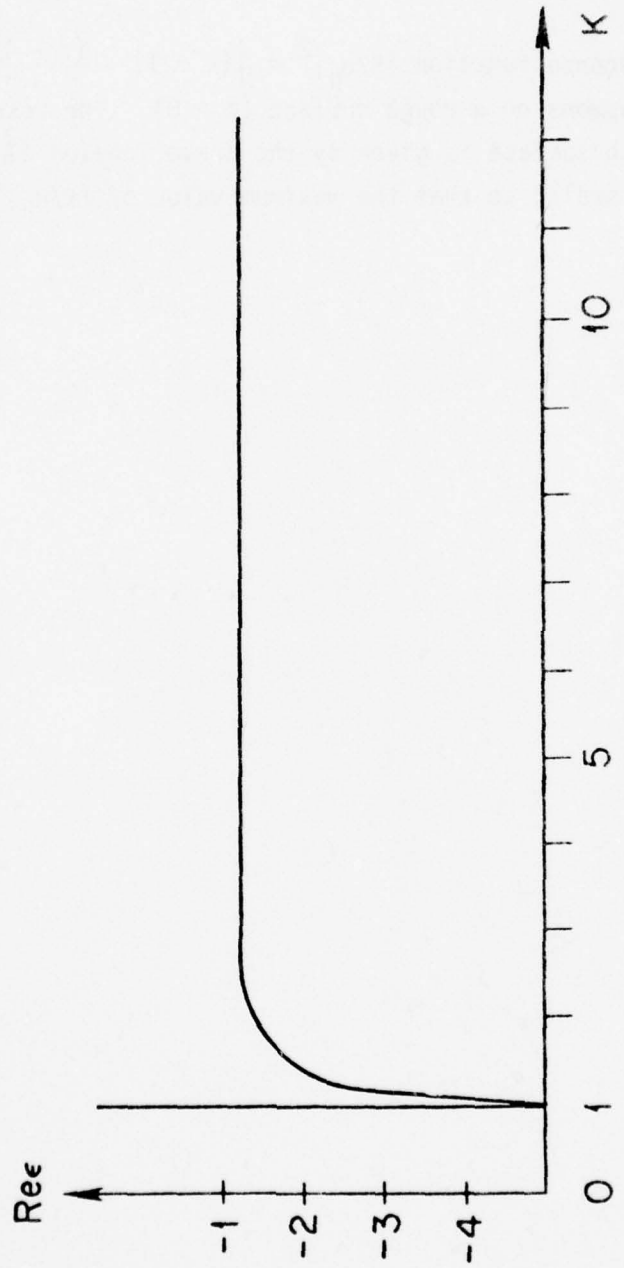

Fig. 1

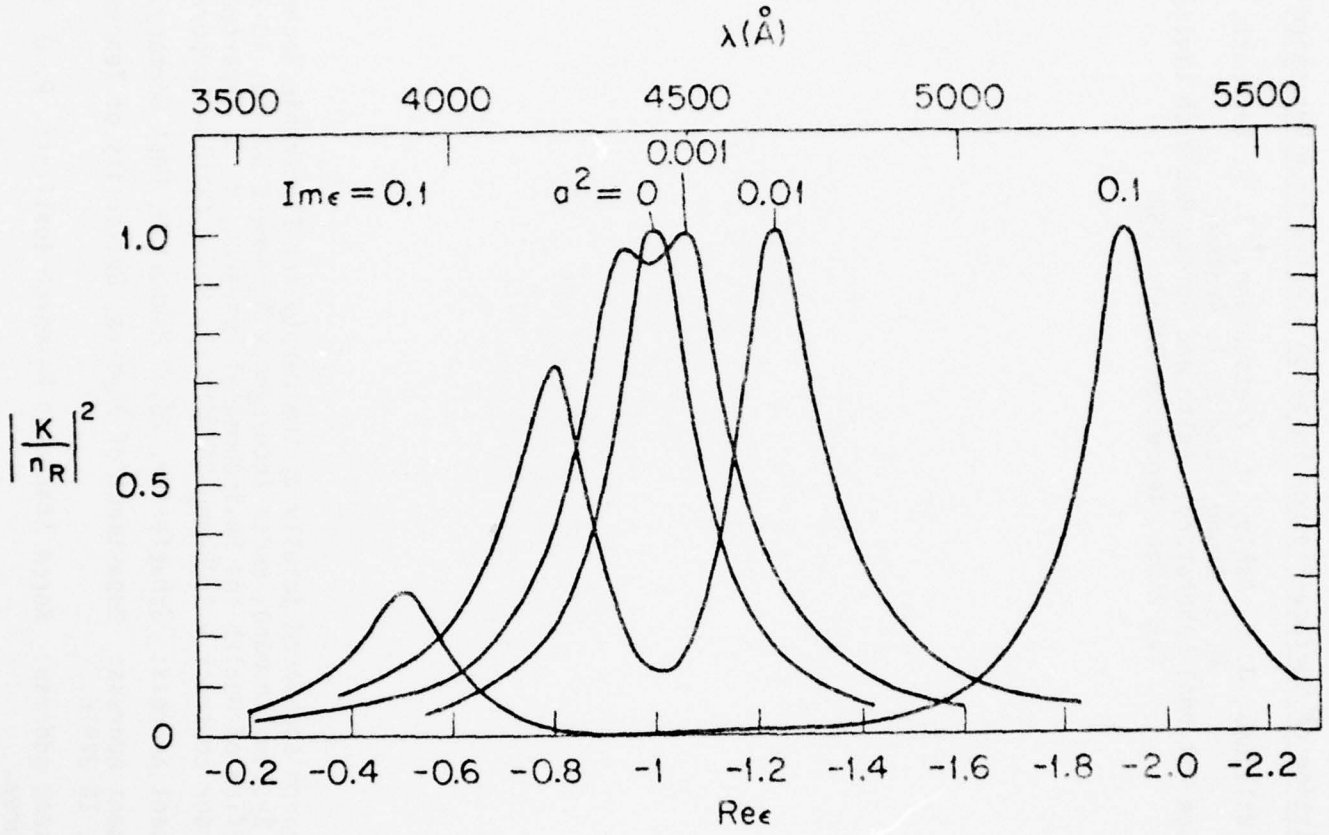
ORNL-DWG 78-15381R
λ(Å)
3500
4000
4500
5000
5500
0.001
Imε = 0.1
a² = 0
0.01
0.1
1.0
0.5
0
|K/nR|²
-0.2
-0.4
-0.6
-0.8
-1
-1.2
-1.4
-1.6
-1.8
-2.0
-2.2
Reε

Fig. 2

CHAPTER II-D

Splitting of Surface-Plasmon Emission Spectra from Potassium*

M. W. Williams, J. C. Ashley, E. Kretschmann,[+] T. A. Callcott,[++]
M. S. Chung,[§] and E. T. Arakawa
Oak Ridge National Laboratory, Health and Safety Research Division,
Oak Ridge, Tennessee 37830, USA

*Research sponsored jointly by the Deputy for Electronic Technology, Air Force Systems Command, under Interagency Agreement DOE No. 40-226-70 and the Office of Health and Environmental Research, U. S. Department of Energy, under contract W-7405-eng-26 with the Union Carbide Corporation.

[+]Present address: Schaeferstr. 28, 2 Hamburg 6, West Germany.

[++]Present address: Department of Physics, University of Tennessee, Knoxville, TN 37916.

[§]Present address: Korea Standards Research Institute, P. O. Box 33, Daejon, Korea.

Abstract

Emission spectra from potassium films irradiated with 1.5-keV electrons have shown a splitting of the roughness-coupled surface-plasmon radiation into two peaks, as predicted by a recently developed theory.

It has been shown theoretically [1,2] that high-wavevector components in the roughness spectrum for a surface should cause the roughness-coupled surface-plasmon radiation curve to split into two peaks lying above and below the normally observed asymptotic surface-plasmon energy. This splitting was looked for, but not resolved, in emission spectra from electron-irradiated Ag films [3]. This letter demonstrates its existence in the emission spectra from electron-irradiated "smooth" K films.

High-wavevector components in the surface-roughness spectrum arise from small-scale irregularities or structures which may be superimposed on, and independent of, the larger scale surface roughness usually characterized from reflectance measurements in terms of a low-wavevector distribution. It seemed that it would be easier to observe splitting in the surface-plasmon emission for a given material if the effects of the low-wavevector components were minimized. This can be achieved in two ways. For low-energy electrons incident normal to the surface, relatively few small-wavevector surface plasmons are excited [1,4]. This reduces the possible coupling between low-wavevector surface plasmons and the corresponding low-wavevector part of the surface-roughness spectrum, thus

reducing its effect on the surface-roughness coupled radiative decay spectrum. In addition, the low-wavevector components of the surface-roughness spectrum can be made as small as possible, which means that on a large scale the film should be as smooth as possible.

Potassium is a nearly-free-electron metal with a volume-plasmon energy of (3.8 ± 0.1) eV [5,6]. When K films were irradiated with low-energy electrons at near-normal incidence [6], the surface-plasmon radiation was found to be very sensitive to the temperature of the film and to the pressure in the experimental chamber. If the K films were not cooled, no surface-plasmon radiation peak was observed. K has a relatively low melting point of 62.3°C, and it was thought that the smooth liquid K surface produced by electron beam heating could not couple surface plasmons to the radiation field. The same result was obtained when the K film was cooled to liquid nitrogen temperature, and the electron beam current was increased from 12 to 200 μA.

Since, in order to resolve the splitting in the surface-plasmon radiative decay due to high-wavevector components in the surface-roughness spectrum, the surface should, on a large scale, be smooth, it appeared that K was a good candidate. In addition, K has the added advantage of being free-electron-like which provides a larger separation of the volume and surface plasmon energies than in silver. To provide the high-wave-vector components, this surface must possess a periodic irregularity, or roughness, with a stepping height of the order of a few angstroms. It was felt that K solid surfaces allowed to solidify close to the melting point might be free of stress-induced large-scale irregularities and, hence, show the desired characteristics.

Details of the experimental arrangement have been described previously [6]. A McPherson Model 218 scanning monochromator was used to measure the spectral distribution of p-polarized radiation emitted from vacuum-evaporated thick K films bombarbed by low-energy electrons. A thick K film was vacuum evaporated in situ directly onto a clean, shiny Cu substrate which was cooled by liquid nitrogen. The evaporator consisted of a copper tube which was attached to the experimental chamber through a copper flange gasket and sealed off at its other end. A glass ampoule containing K was mounted in the copper tube. With the experimental system at 7×10^{-8} torr the glass ampoule was crushed by squeezing the copper tube. The K was first outgassed for about 10 minutes and then evaporated by a heating coil wound around the copper tube. The pressure rose as high as 10^{-6} torr during the evaporation but afterwards dropped rapidly to 2×10^{-8} torr. 1.5-keV electrons with a beam current in the 10 → 20 μA range were incident on the K film at 35° from the film normal, and the photons emitted along the normal were observed over the wavelength range from 3000 to 5500 Å. This range of beam currents minimized heating of the film, while still producing emission with a reasonable intensity. Following the evaporation, during which the K film was cooled with liquid nitrogen, the coolant was removed and the film annealed at room temperature. This process of cooling the sample by liquid nitrogen and then removing the coolant was repeated. At each stage of this temperature cycle, emission spectra were recorded. During the second period of annealing, evidence was seen of splitting in the surface-plasmon emission. Additional K was then evaporated onto the

sample which was now water cooled and the emission spectrum recorded as a function of time after deposition. Figure 1 shows the original recorder trace obtained 30 minutes after the second K deposition. Figure 2 shows the spectrum after correcting the spectrum in Fig. 1 for grating efficiency and photomultiplier response. The peak at 3250 Å (3.82 eV) is the volume-plasmon, or transition radiation, peak. When this is subtracted, peaks are seen at 3980 Å (3.12 eV) and 4790 Å (2.59 eV) as indicated. These results are representative of the eight spectra recorded, four before and four after the second K deposition. The relative magnitudes of the peaks varied slightly from one spectrum to the next, the 3980 Å peak generally growing with time relative to the other two peaks. The peak wavelengths were in the ranges (3250 ± 20) Å, (3980 ± 40) Å, and (4790 ± 40) Å with no systematic variation with time within these ranges. It is thought that the peaks at 3980 Å and 4790 Å are due to surface-plasmon radiative decay, on either side of the expected position of the asymptotic surface-plasmon radiation at 4320 Å.

The splitting of the dispersion relation for surface plasmons on a rough solid-vacuum boundary for high wavevectors can be expressed in terms of the two values of ε_1, the real part of the dielectric function $\varepsilon(\omega)$, at which surface plasmons are generated. It has been shown [2] that peaks occur at values of ε_1 given by α and β where $\alpha = 1/\beta$. For ready reference, ε_1 as a function of wavelength, taken from Ref. 5, is shown in Fig. 2. It is seen that at the 3980 Å peak, $\varepsilon_1 = -0.665 = \alpha$; while at the 4790 Å peak, $\varepsilon_1 = -1.50 = \beta$. Hence, the predicted relationship between the values of ε_1 at the peaks, given by $\alpha = 1/\beta$, is satisfied for the peaks observed at 3980 Å and 4790 Å in potassium.

It has also been shown [2] that

$$|\Delta\varepsilon_1| = |\alpha-\beta| \tilde{\approx} 4a$$

where a is a function of the surface-plasmon wavevector and of the high-wavevector components of the surface-roughness spectrum. If $a = 0$, then $\alpha = \beta = -1$ and there is no splitting of the dispersion relation. Figure 2 in Ref. 2 gives the values of ε_1 at which surface-plasmon excitation is possible. The curve for $a^2 = 0$ shows a single peak at the asymptotic surface-plasmon wavelength. However, surface plasmons generated at a smooth surface cannot radiate. The curves in Fig. 2, Ref. 2, for $a \neq 0$ illustrate the expected splitting for surfaces having a high-wavevector component in the surface-roughness spectrum. For our sample

$$|\Delta\varepsilon_1| = |-0.67 - (-1.50)| = 0.83.$$

Hence, $a \tilde{\approx} 0.2$.

A calculation of the predicted shape of the surface-plasmon excitation spectrum for $a^2 = 0.04$ was performed as in Ref. 2 using the published values of ε_1 and ε_2 for K given by Palmer and Schnatterly [5]. This is shown in Fig. 2 for comparison with our experimental spectrum.

Palmer and Schnatterly [5, Fig. 8] observed some structure in an absorption peak attributed to surface-plasmon excitation in K. This structure was small and was located at 2.7 eV and 2.9 eV, on either side of the 2.8-eV surface-plasmon absorption. It is suggested that this could be splitting due to coupling to a high-wavevector surface roughness, superimposed on a surface-plasmon peak due to coupling to the low-

AD-A079 054 OAK RIDGE NATIONAL LAB TN HEALTH AND SAFETY RESEARCH DIV F/G 9/5
STUDIES OF PHOTON AND ELECTRON INTERACTIONS WITH COMMUNICATIONS--ETC(U)
OCT 79 J C ASHLEY , M W WILLIAMS

UNCLASSIFIED RADC-TR-79-234 NL

2 OF 2
AD-
A079054

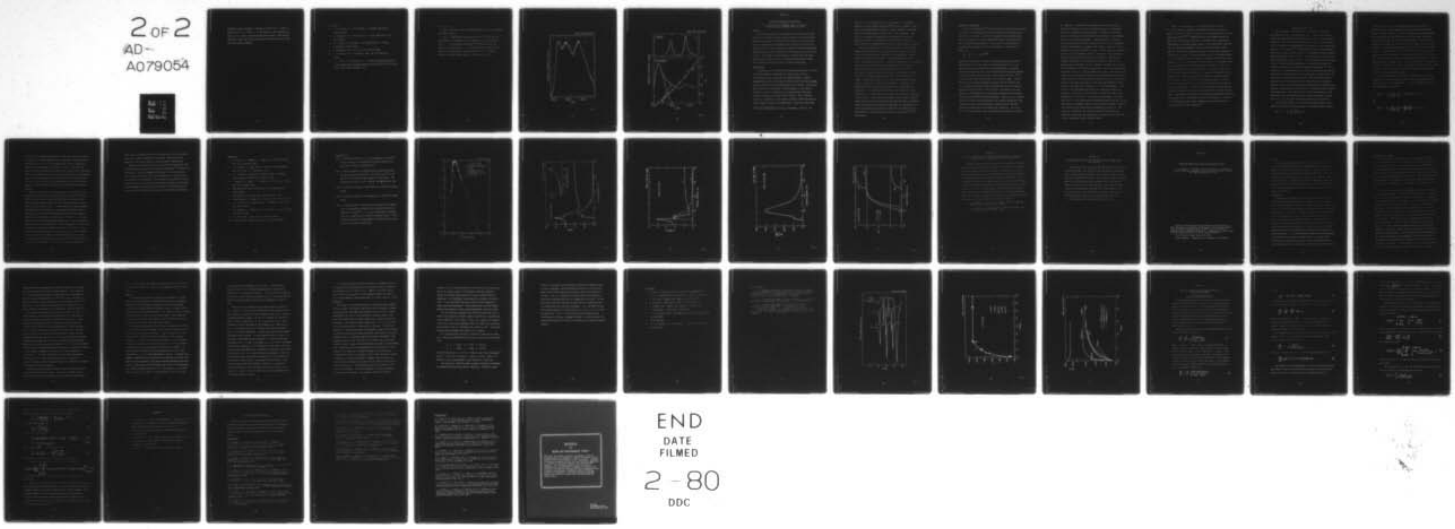

END
DATE
FILMED
2-80
DDC

wavevector surface roughness. From Fig. 2, at 2.7 eV $\varepsilon_1 = -1.28 = \alpha$, while at 2.9 eV $\varepsilon_1 = -0.96 = \beta$. In this case α is only approximately equal to $1/\beta$. However, considering the uncertainties in the measured quantities, their data are not inconsistent with splitting due to high-wavevector surface roughness.

References

1. E. Kretschmann, T. A. Callcott and E. T. Arakawa, submitted to Surface Science.
2. E. Kretschmann, T. L. Ferrell and J. C. Ashley, submitted to Phys. Rev. Letters.
3. M. S. Chung, T. A. Callcott, E. Kretschmann, and E. T. Arakawa, submitted to Surface Science.
4. P. Dobberstein, Phys. Stat. Solidi 38, 649-655 (1970).
5. R. E. Palmer and S. E. Schnatterly, Phys. Rev. B 4, 2329-2339 (1971).
6. M. S. Chung, T. A. Callcott and E. T. Arakawa, Radiation from Ag and K Films Bombarded by Low Energy Electrons, Oak Ridge National Laboratory Report, ORNL-TM-6527 (October, 1978).

Figure Captions

Fig. 1. Recorder trace of emission spectrum from K film irradiated by 1.5-keV electrons.

Fig. 2. Experimental emission spectrum from K held at near room temperature and irradiated by 1.5-keV electrons at 35° from the film normal; —— total measured intensity, —— estimated transition radiation contribution, and ----- surface plasmon contribution. Also shown are the experimental ε_1 values from Ref. 5 (•——•) and the theoretical surface-plasmon spectrum calculated as in Ref. 2.

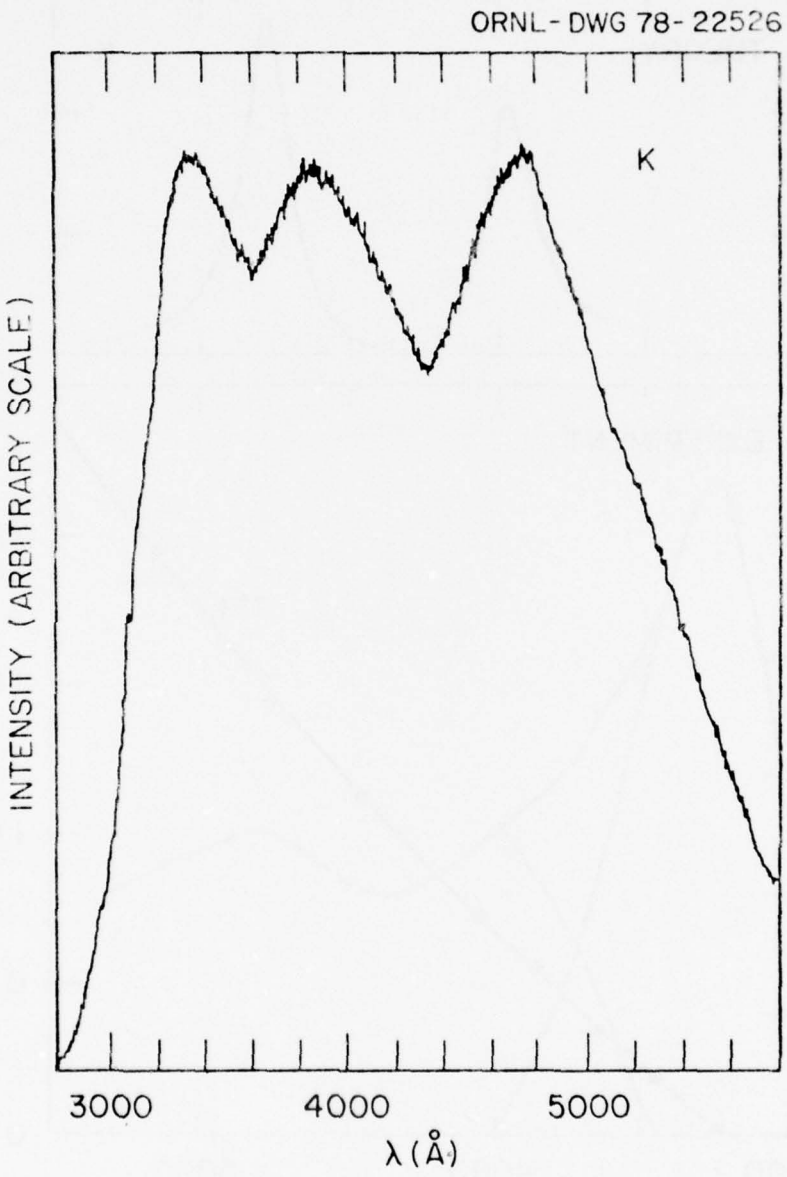
ORNL-DWG 78-22526
K
INTENSITY (ARBITRARY SCALE)
3000
4000
5000
λ(Å)

Fig. 1

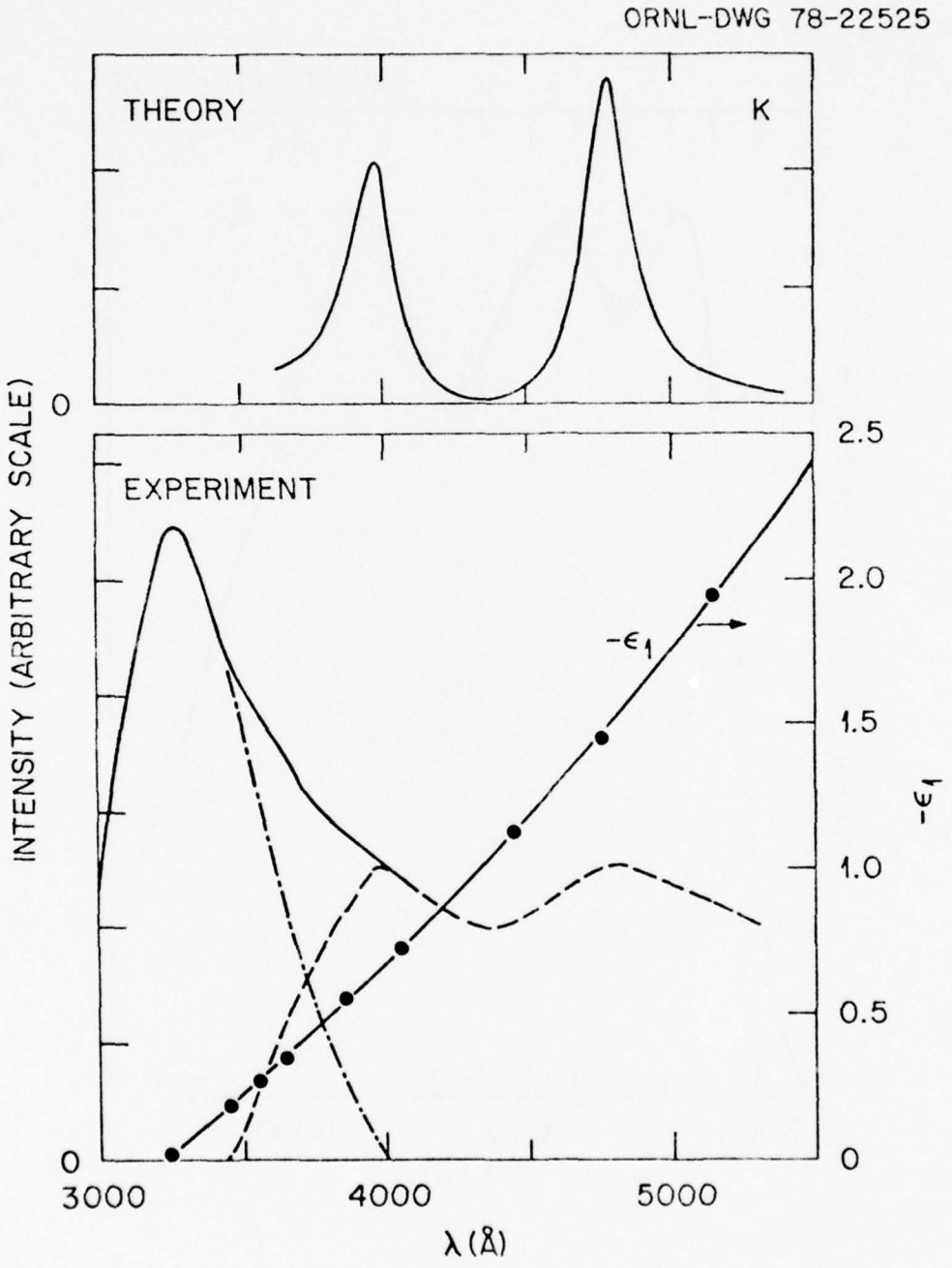
ORNL-DWG 78-22525
THEORY
K
EXPERIMENT
INTENSITY (ARBITRARY SCALE)
0
0
3000
4000
5000
λ(Å)
2.5
2.0
1.5
1.0
0.5
0
$-\epsilon_1$
$-\epsilon_1$

Fig. 2

CHAPTER III

Optical Properties of Polyethylene

L. R. Painter,[+] E. T. Arakawa, and M. W. Williams
Health and Safety Research, ORNL, TN 37830

Abstract

The optical properties of polyethylene in the form of thin films have been determined for photon energies from 0.5 to 76 eV from transmission measurements. The results for the extinction coefficient, k, have been combined with calculated values in the soft and hard x-ray regions and their internal consistency, and their consistency with data obtained previously for polystyrene, verified through a sum rule calculation. It is hoped to use these data to calculate mean free paths, stopping powers, and "continuous-slowing-down-approximation" ranges for low-energy electrons (~10 eV to 10 keV) in polyethylene.

Introduction

Polyethylene is used extensively for high-voltage cable insulation. It is also employed in communications systems, many of which are miniaturized for use in the space and defense programs. Hence an understanding of the interactions of photons and of high-energy charged particles with thin films of polyethylene is of interest. A convenient way to obtain this information is by measurements of the optical properties of thin film samples over an energy range sufficiently large to include all of the oscillator strength. From a chemical viewpoint, polyethylene is the simplest synthetic hydrocarbon polymer, with a monomeric repeat unit of $\{CH_2\text{-}CH_2\}$. It has only single bonds

[+]Also Physics Department, University of Tennessee, Knoxville, TN.

and hence all its valence electrons are designated as σ electrons. We have previously studied polystyrene[1]—one of the simplest of the hydrocarbon polymers which includes an aromatic component in the monomeric unit and which thus has both π and σ valence electrons. Comparison of the optical properties of polyethylene with those for polystyrene extends our knowledge and understanding of the way in which electrons in hydrocarbon solids react to electromagnetic radiation.

Previous measurements of the optical properties of polyethylene have been mainly restricted to the IR and visible regions. In this study, we report the optical properties of polyethylene in the form of thin solid films over the range of photon energies from 0.5 to 76 eV. The measured results for the extinction coefficient, k, are combined with values calculated from those for polystyrene,[1] to obtain a combined k spectrum which covers substantially all of the total oscillator strength, including the carbon core excitations starting at ∿282 eV. A Kramers-Kronig analysis then yields the refractive index, n, from 0.5 to 76 eV, and a sum-rule calculation verifies the internal consistency of these optical properties. Comparisons are drawn between the measured optical properties of polyethylene and polystyrene. It is hoped that differential inverse mean free paths (DIMFP's) can be calculated for the excitation of inner-shell electrons in polyethylene. These combined with DIMFP's from the model insulator theory would be used to calculate electron mean free paths and stopping powers for comparison with the Bethe-Bloch theory at high energies. If these comparisons are satisfactory a complete set of tabulations for polyethylene, as has been done previously for polystyrene,[2,3] will be prepared.

Experimental Techniques

Transmission techniques[4] were used to obtain values of the extinction coefficient, k, of polyethylene films over essentially the whole energy range from 0.5 to 76 eV. Up to 6.6 eV, transmission measurements were made on free-standing, 0.5 mil, Glad Wrap[5] using a Cary spectrometer and a Seya-Namioka monochromator. In this case, the transmittance, T, yielded absolute values of k since the thickness, t, of the film was known, and

$$T = \frac{I}{I_o} = (1 - R)^2 e^{\frac{-4\pi kt}{\lambda}} .$$

I_o was the intensity of the radiation incident normally on the polyethylene, while I was the intensity transmitted by the film. R was the normal incidence reflectance for the polyethylene-air interface and was calculated from the n values measured on evaporated polyethylene films, using methods described later. Below about 4.9 eV ($k = 10^{-4}$) k was too small to be measured using a 0.5 mil thick sample. The use of thicker free-standing polyethylene samples (0.9 mil Glad Wrap and 4 mil Nalgene polyethylene) showed weak absorption below ~1 eV but no measurable absorption from ~1 eV to ~4.5 eV. Data above 6.6 eV were obtained on evaporated films of polyethylene prepared by vacuum deposition from Dow Corning[6] polyethylene pellets. However, since it proved difficult to obtain vacuum-evaporated, free-standing polyethylene films suitable for transmission measurements, techniques were used which allowed the polyethylene to be supported by a substrate. For use in the 7.7 to 10.6 eV energy range, polyethylene was evaporated over half

of a MgF_2 disc. Transmission measurements were made by recording I_o through the MgF_2 disc alone and I through the MgF_2 plus polyethylene film, using a Seya-Namioka monochromator. Two separate films were used with thicknesses of 460 and 504 Å as determined by interferometric and by quartz crystal measurements. These measurements, limited by the absorption edge of the MgF_2 substrate at ∿10.6 eV, also allowed an absolute determination to be made of the k values. Above 10.6 eV the fluorescent substrate method[7] was used. A glass slide was coated with a thick layer of p-terphenyl, which is fluorescent. Polyethylene was then vacuum evaporated over half of the p-terphenyl. Radiation was incident normally on this sample and the fluorescent radiation from the p-terphenyl monitored. For the uncovered p-terphenyl the intensity of the fluorescent radiation was $\propto I_o$, while for the polyethylene-covered p-terphenyl it was $\propto I$. Since p-terphenyl fluoresces in the visible, the intensity of the fluorescent radiation was not attenuated on passing out through the glass slide and hence the measured intensities from the two halves of the sample were subject to the same proportionality constant and their ratio gave the transmittance, T, of the polyethylene. From 10.6 to 76 eV observations were made using a grazing-incidence monochromator. From 10.6 to ∿35.5 eV where k is relatively large, a thin polyethylene film was used. Its thickness was estimated as ∿100 Å by normalizing k to the experimentally determined absolute value at 10.6 eV. This process was repeated from 35.5 to 76 eV, using a thicker film which was estimated to be ∿590 Å thick, by normalizing k at 35.5 eV. The values of k obtained by the fluorescent substrate method that are presented in this paper were confirmed on a number of other films with similar thicknesses to those described above.

Values of the real part, n, of the complex refractive index, $\tilde{n} = n + ik$, were also determined experimentally in the energy range from 1.77 to 8.4 eV. From 1.77 to 5.8 eV, n was determined from critical angle measurements.[8,9] Polyethylene was vacuum evaporated onto the plane face of a sapphire semicylinder. Radiation from a Seya-Namioka monochromator was incident along a radius of the semicylinder, reflected from the sapphire-polyethylene interface, and exited along a radius. Scans of reflectance vs angle of incidence at the sapphire-polyethylene interface were recorded. For photon energies where the refractive index, n_s, of the material of the semicylinder is greater than that of the polyethylene, n, $\sin\theta_c = n/n_s$ where the critical angle, θ_c, is defined as the angle which marks the onset of total internal reflection. Thus if n_s is known and θ_c measured, n can be calculated. In this case values of n_s were obtained before the polyethylene was deposited on the semicylinder from scans of reflectance vs angle of incidence at the plane sapphire-air interface. From 7.3 to 8.4 eV reflectance vs angle of incidence scans were obtained at the CaF_2-polyethylene interface for polyethylene on a CaF_2 semicylinder. In this case critical angles were not observed, and the reflectance vs θ data were least squares fit to Fresnel's equations. Interference fringes were also analyzed for the polyethylene films on the MgF_2 discs to yield both n and the film thicknesses. The values of n obtained from each of these techniques agree well with the two values available in the literature.[10]

Results and Discussion

The experimental results obtained for k between 4.6 and 76 eV are presented in Fig. 1 on a logarithmic plot. The best smooth curve through the experimental points is also shown in Fig. 1. The same data is presented in Fig. 2 on a linear plot from 0.5 to 76 eV. Also presented in Fig. 2 are the n values determined experimentally in the present study and from the literature.[10] A Kramers-Kronig analysis was performed on these data in order to obtain values of n for polyethylene over the whole experimental range from 0.5 to 76 eV. The k values from ~30 eV to 76 eV were extrapolated as shown in Fig. 1. Since absorption measurements above 76 eV were unavailable for polyethylene, the contribution due to the carbon 1s electrons was estimated from data for polystyrene.[1] It was assumed that in hydrocarbons, which contain only carbon and hydrogen, the experimental k associated with the C 1s electrons is proportional to the number of C 1s electrons per unit volume. The contribution to k for polyethylene due to core electrons was calculated on this assumption above the carbon K-shell absorption edge from experimental data for polystyrene, assuming densities of 1.05 $g.cm^{-3}$ for polystyrene and 0.92 $g.cm^{-3}$ for polyethylene. The calculated core electron contribution to k was then added to the extrapolated valence electron contribution as shown in Fig. 1 to give the total estimated k-spectrum for polyethylene.

The refractive index, n, as a function of photon energy, E, was determined from the k-spectrum by means of the Kramers-Kronig relation

$$n(E) - 1 = \frac{2}{\pi} \int_0^\infty \frac{E'k(E')}{E'^2 - E^2} \, dE' \, .$$

In the region below ∿1 eV, where photoabsorption due to molecular vibrations occurs, the k values were so small that the contributions to the integrals of E'k(E'), in this low-energy region, were neglected. At high energies the cut-off for the integral was chosen so that the values of n obtained from the Kramers-Kronig analysis agreed with those determined experimentally in the 1.77 to 8.4 eV range. The values of n obtained for polyethylene by this analysis, from 0.5 to 76 eV, are shown in Fig. 2. Then assuming $\tilde{n} = n + ik$ and $\tilde{n}^2 = \tilde{\varepsilon} = \varepsilon_1 + i\varepsilon_2$, the n and k values were used to calculate the real and imaginary parts ε_1 and ε_2 of the complex dielectric function, $\tilde{\varepsilon}$, and the energy loss function $\mathrm{Im}(-1/\tilde{\varepsilon})$. These quantities are shown in Figs. 3 and 4, respectively. The estimated error on the experimental k values is $\leq \pm 6\%$ and on the experimental n values is $\leq \pm 0.5\%$. The possible errors on the other quantities depend on the validity of the Kramers-Kronig analysis.

A check was performed on the internal consistency of the optical properties derived for polyethylene and on their consistency with data obtained previously for polystyrene. For ε_2 and $\mathrm{Im}(-1/\tilde{\varepsilon})$, there exist the well-known f sum rules[11]

$$N_1(E) = \frac{2}{\pi} \frac{m}{4\pi n_o e^2 \hbar^2} \int_o^E E'\varepsilon_2(E')dE' \to N, \; E \to \infty ,$$

and

$$N_2(E) = \frac{2}{\pi} \frac{m}{4\pi n_o e^2 \hbar^2} \int_o^E E' \mathrm{Im}\left(\frac{-1}{\tilde{\varepsilon}(E')}\right) dE' \to N, \; E \to \infty ,$$

where n_o is the molecular density and N is the total number of electrons in a molecule. Taking a monomeric unit $-(CH_2 \cdot CH_2)-$ of polyethylene as a molecular unit, N is 16. The calculated values of $N_1(E)$ and $N_2(E)$ as functions of photon energy, E, are shown in Fig. 5. Both $N_1(E)$ and $N_2(E)$ are seen to saturate at 16 electrons per molecular unit, indicating internal consistency of the optical constants determined for polyethylene. Since the core contribution to k was calculated from polystyrene data, this also shows the validity of our assumptions concerning the general behavior of core electrons in hydrocarbons containing only carbon and hydrogen.

Further evaluations of N(E) were made on the k values due to the valence and core excitations, separately. The results for $N^V(E)$ and $N^C(E)$, the contributions to $N_1(E)$ or $N_2(E)$ above the carbon K-shell absorption edge from the valence and core electron excitations, respectively, are also shown in Fig. 5. A redistribution of electron numbers corresponding to 0.5 electrons is found between the valence and core excitations. $N^V(E)$ and $N^C(E)$ should tend to 12 and 4, the numbers of valence and core electrons, respectively, in the limit $E \to \infty$, if there were no oscillator strength coupling between them. A similar result was found previously for polystyrene.[1] As for polystyrene, it should also be noted that the effective numbers of electrons as plotted in Fig. 5 as functions of photon energy E do not saturate until a few thousand eV. This is so even for the valence electrons showing that even at these high energies the contribution of valence excitations to the oscillator strength is not negligible. For both polyethylene and polystyrene,

these results demonstrate that sum rule calculations can only be applied to the total number of electrons in the system. Partial sum rules, employed in some other situations, cannot be used for hydrocarbons.

Comparison of the plots of $\tilde{n}$, $\tilde{\varepsilon}$, and $\mathrm{Im}(-1/\tilde{\varepsilon})$ for polyethylene with the corresponding variations with energy for polystyrene[1] shows striking similarities. The only fundamental difference is the sharp structure seen in polystyrene below $\sim$10 eV associated with the π electrons which is not present in polyethylene. Thus the general conclusions[1] arrived at from analysis of sum rules for polystyrene concerning the interaction of electromagnetic radiation with the electrons in a hydrocarbon solid over essentially the whole energy range, can be applied to polyethylene.

References

1. T. Inagaki, E. T. Arakawa, R. N. Hamm, and M. W. Williams, Phys. Rev. B 15, 3243-3253 (1977).
2. J. C. Ashley, C. J. Tung, and R. H. Ritchie, to be published in IEEE Trans. Nucl. Sci. NS-25 (Dec. 1978).
3. J. C. Ashley, C. J. Tung, R. H. Ritchie, and V. E. Anderson, Air Force Report RADC-TR-78-32 (February, 1978).
4. T. Inagaki, R. N. Hamm, E. T. Arakawa, and L. R. Painter, J. Chem. Phys. 61, 4246-4250 (1974).
5. Registered trade name for polyethylene film manufactured by Union Carbide.
6. Dow Chemical Co., 2020 Dow Center, Midland, Mich. 48640.
7. Pon-Wei Hou and R. P. Rampling, J. Appl. Phys. 47, 4572-4573 (1976).
8. L. R. Painter, R. D. Birkhoff, and E. T. Arakawa, J. Chem. Phys. 51, 243-251 (1969).
9. R. A. MacRae, E. T. Arakawa, and M. W. Williams, J. Chem. Eng. Data 23, 189-190 (1978).
10. R. H. Partridge, J. Chem. Phys. 45, 1679-1684 (1966).
11. P. Nozières and D. Pines, Phys. Rev. 113, 1254-1267 (1959).

Figure Captions

Fig. 1. Extinction coefficient, k, for polyethylene as a function of photon energy. The calculated values were obtained from experimental values for polystyrene.[1]

Fig. 2. Optical properties of polyethylene over the energy range of the experimental measurements. The smooth curve for n was derived from a Kramers-Kronig analysis of the k values. The experimental values of n are: -Δ- ORNL, and -●- from Ref. 10.

Fig. 3. Dielectric functions of polyethylene as a function of photon energy.

Fig. 4. Energy loss function of polyethylene as a function of photon energy.

Fig. 5. Effective number of electrons $N_1(E)$ and $N_2(E)$ per monomeric unit of polyethylene obtained from the imaginary part of the dielectric function $\tilde{\varepsilon} = \varepsilon_1 + i\varepsilon_2$, and the energy-loss function $\mathrm{Im}(-1/\tilde{\varepsilon})$, respectively, as functions of photon energy E. $N^V(E)$ and $N^C(E)$ represent the contributions from the valence and core electron excitations, respectively.

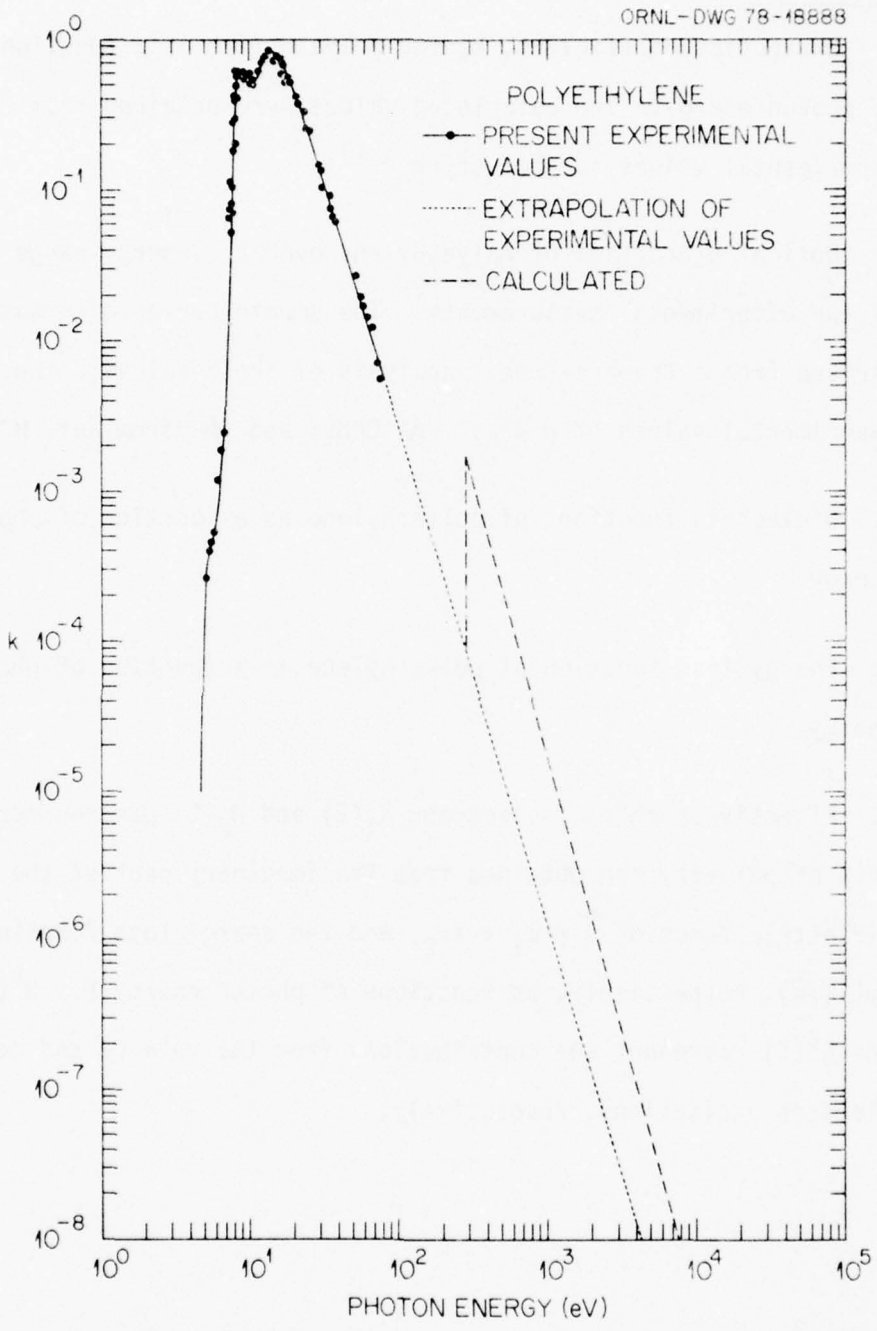
ORNL-DWG 78-18888
POLYETHYLENE
PRESENT EXPERIMENTAL VALUES
EXTRAPOLATION OF EXPERIMENTAL VALUES
CALCULATED
k
PHOTON ENERGY (eV)

Fig. 1

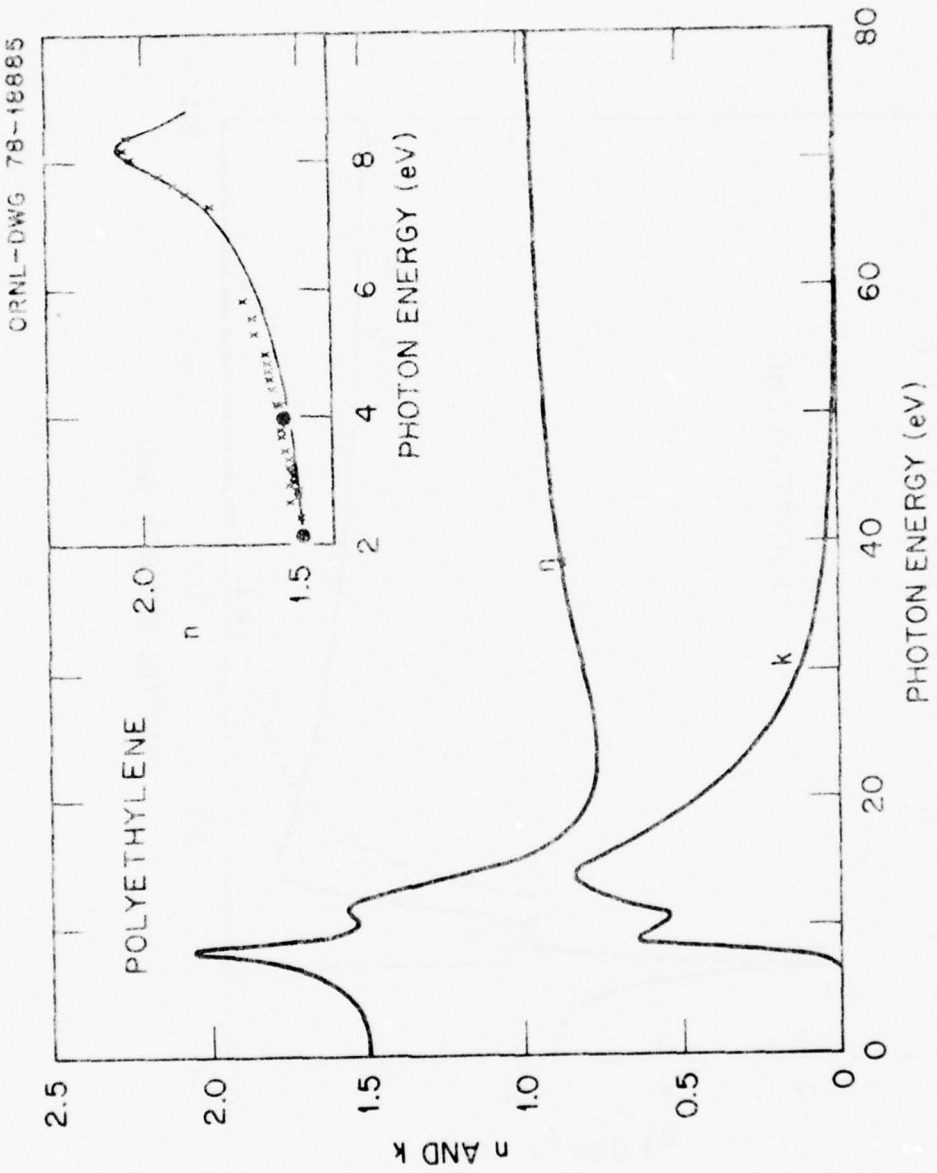
ORNL-DWG 78-10885
POLYETHYLENE
n
k
n AND k
PHOTON ENERGY (eV)
PHOTON ENERGY (eV)
2.5
2.0
1.5
1.0
0.5
0
20
40
60
80
2.0
1.5
2
4
6
8

Fig. 2

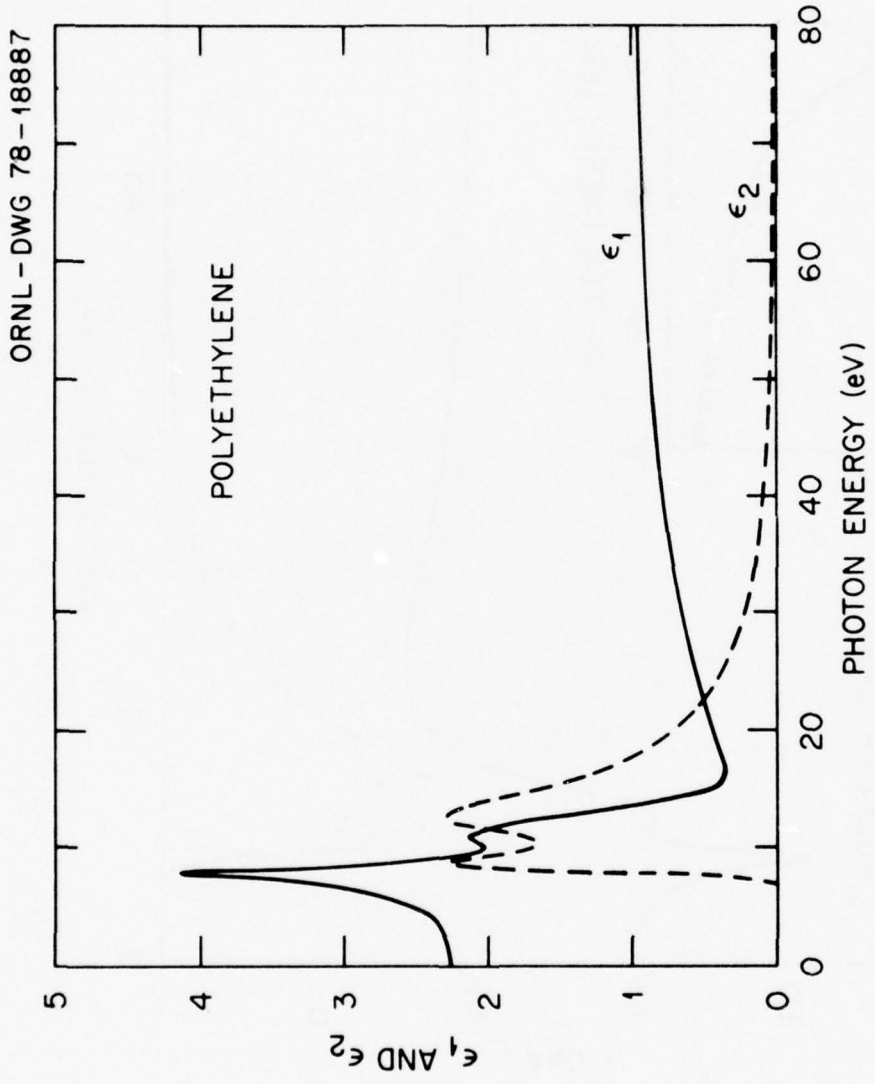
ORNL-DWG 78-18887
POLYETHYLENE
ϵ_1
ϵ_2
ϵ_1 AND ϵ_2
PHOTON ENERGY (eV)
0
1
2
3
4
5
0
20
40
60
80

Fig. 3

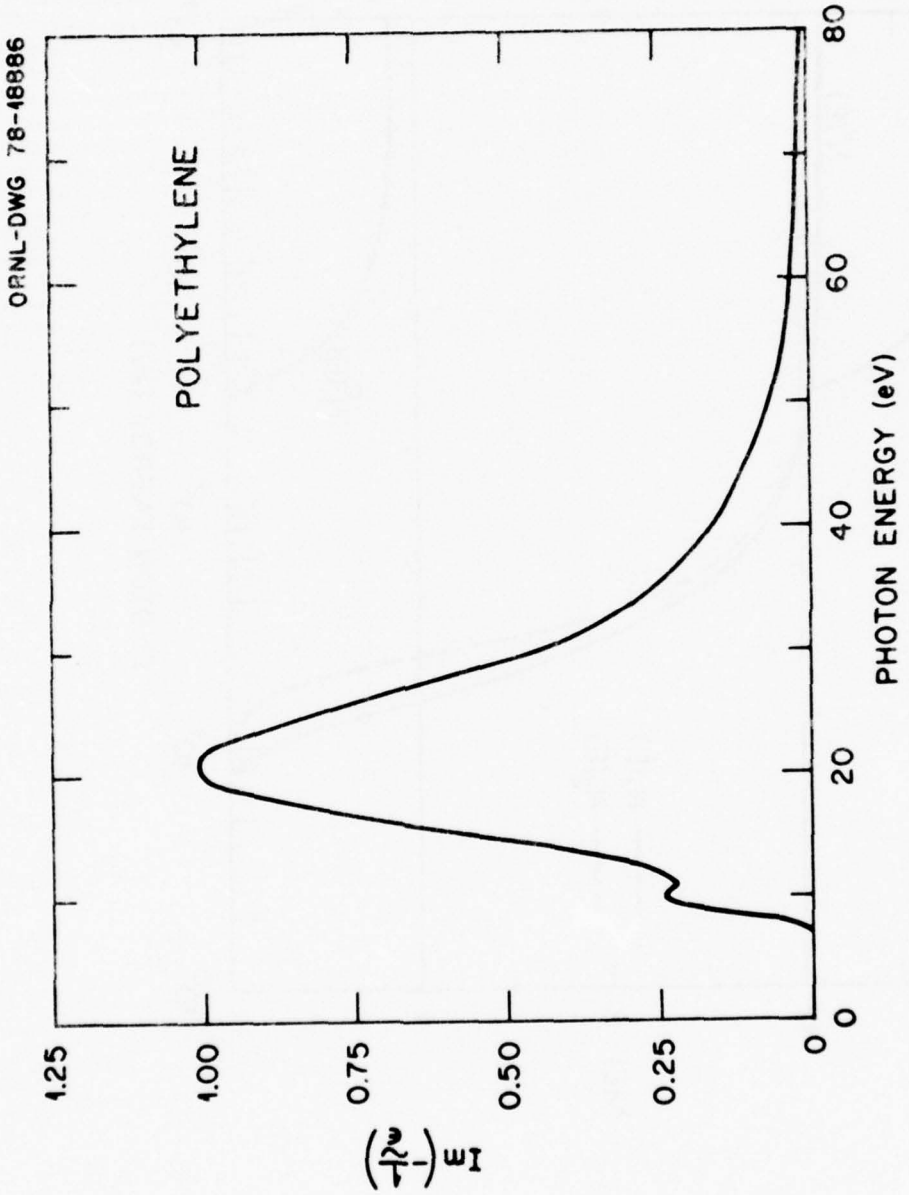
ORNL-DWG 78-18886
POLYETHYLENE
PHOTON ENERGY (eV)
0
20
40
60
80
0
0.25
0.50
0.75
1.00
1.25
Im(-1/ε)

Fig. 4

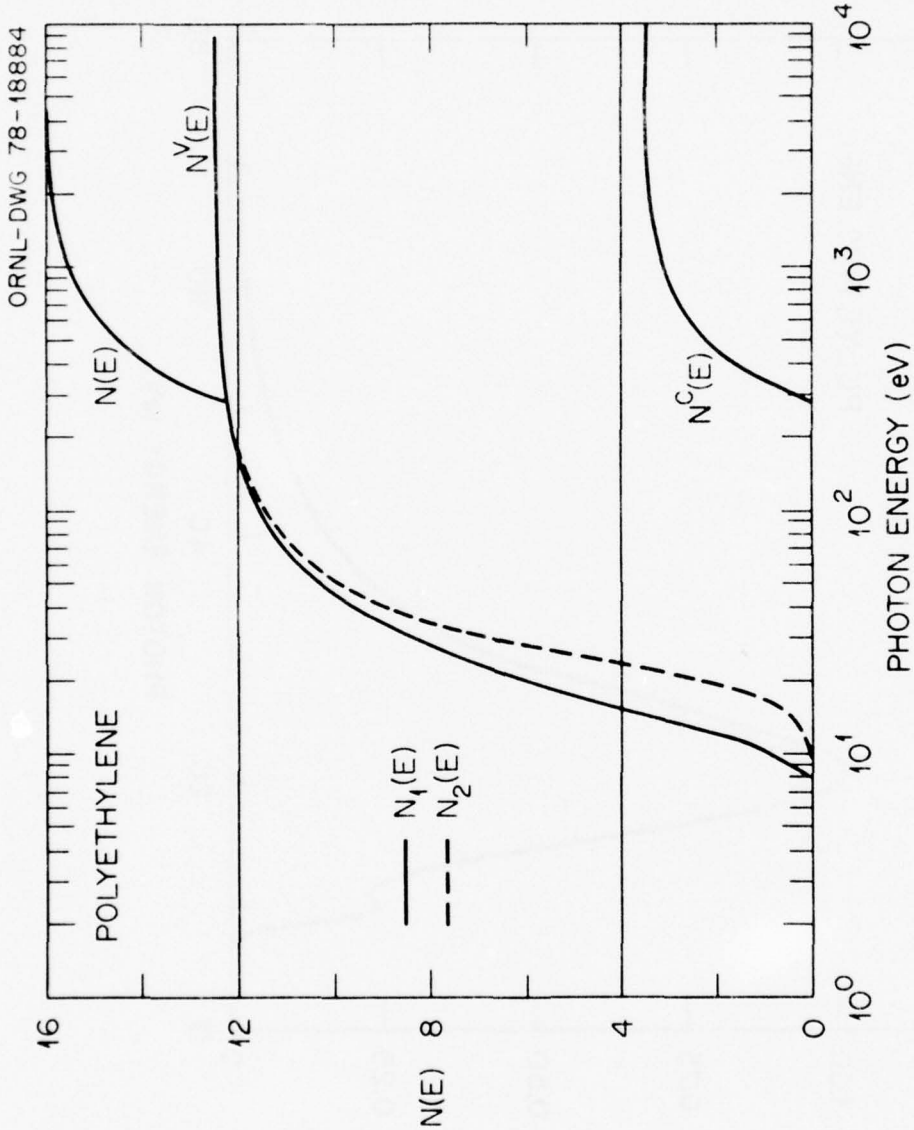
ORNL-DWG 78-18884
POLYETHYLENE
N(E)
$N^V(E)$
$N^C(E)$
$N_1(E)$
$N_2(E)$
N(E)
16
12
8
4
0
10^0
10^1
10^2
10^3
10^4
PHOTON ENERGY (eV)

Fig. 5

CHAPTER IV

Inelastic Interactions of Electrons with Polystyrene: Calculations of Mean Free Paths, Stopping Powers, and CSDA Ranges

A theoretical description of the inelastic interactions of electrons with solid polystyrene has been presented. The response of the valence electrons to energy and momentum transfers was determined by a model insulator theory; carbon K-shell ionization cross sections were derived from atomic, generalized oscillator strengths. Contributions to the inverse mean free paths and stopping powers due to these two excitation processes were derived and tabulated for incident electrons with energies from 10 eV to 10 keV. Electron ranges in the continuous-slowing-down approximation were calculated and tabulated for electrons with energies from 15 eV to 10 keV. Complete descriptions of this calculational method and these results may be found in the following references:

1. J. C. Ashley, C. J. Tung, R. H. Ritchie, and V. E. Anderson, RADC-TR-78-32 (February, 1978), A057881.

2. J. C. Ashley, C. J. Tung, and R. H. Ritchie, IEEE Trans. Nucl. Sci. NS-25, 1566-1570 (December, 1978).

CHAPTER V-A

The ATR Method with Focused Light--Application to Guided Waves on a Grating

The attenuated total reflection (ATR) method has been modified by using focused light. The reflected light cone contains information about a large portion of wavevector space instead of only one point as in the conventional ATR method. The dispersion relation of guided modes can be found directly from the image of the light cone on a screen. When applied to guided waves on a grating, the dispersion relation of the waves with "band gaps" and discontinuities can be seen on the screen. This application, with further discussion of the ATR method using focused light, has been published. See:

E. Kretschmann, Opt. Commun. 26, 41-44 (July, 1978).

CHAPTER V-B

Refractive Index of LiF Films as a Function of Time*

T. L. Haltom,† E. T. Arakawa, M. W. Williams and E. Kretschmann††
Oak Ridge National Laboratory, Health and Safety Research Division,
Oak Ridge, Tennessee 37830, USA

*Research sponsored jointly by the Southern College University Union the Deputy for Electronic Technology, Air Force Systems Command, under Interagency Agreement DOE No. 40-226-70 and the Division of Biomedical and Environmental Research, U. S. Department of Energy, under contract W-7405-eng-26 with the Union Carbide Corporation.

†Also Millsaps College, Jackson, MS 39202.

††Present address: Schaeferstr. 28, 2 Hamburg 6, West Germany

Abstract

The optical properties and thickness of evaporated LiF films on silver or aluminum were determined by attenuated total reflection techniques as a function of time after deposition. With the LiF films maintained in vacuum, the refractive index increased from ~1.3 to ~1.4, or close to the crystalline value, in the course of a few days. This implies that the LiF, loosely packed when first deposited, anneals over a period of time to the more closely packed crystalline configuration. The LiF films were found to be optically isotropic in contrast to earlier reports of anisotropy.

Introduction

Attenuated total reflection (ATR) techniques employing various experimental configurations have been reviewed by Otto.[1] More specifically, such techniques have been used to study light modes in evaporated films of LiF and the results analyzed in terms of the optical properties and thickness of the films.[2-4] However, the behavior of these properties with time after deposition has not previously been studied for LiF films. The changes in the refractive index, n, reported here for LiF indicate that changes take place in the film structure after deposition. These results become significant when, for example, an optical system involving reflection or antireflection coatings must be designed for maximum efficiency. It is then necessary to know the correlation between the properties of the coating as deposited and in its final state. Deterioration of coatings on exposure to certain anticipated environmental conditions could also be studied experimentally by this technique.

Experimental Techniques

The experimental arrangement was similar to that used previously by Hornauer and Raether[4] for LiF. A transparent semicylinder was mounted in a reflectometer in such a way that a narrow beam of monochromatic light entered the semicylinder along a radius and hence normal to the curved surface, was reflected at the plane semicylinder-vacuum interface, and exited from the semicylinder along a radius. The incident light was plane polarized using a polaroid filter, and the reflected light was detected with a photomultiplier. The pressure in the system was $\sim 10^{-6}$ torr.

A thin metallic layer was vacuum evaporated in situ onto the plane face of the semicylinder. A scan of reflectance vs angle of incidence for p-polarized light showed a strong dip in reflectance at an angle of incidence just above the critical angle due to the generation of surface plasmons at the metal-vacuum interface. A thick LiF film was then deposited by vacuum evaporation over the thin metal film. Scans of reflectance vs angle of incidence, recorded individually for p- and s-polarized light, then showed several strong dips at angles above the critical angle. There are two types of resonances possible in the semicylinder/metal/LiF system: surface plasmons and optical guided waves. The surface plasmon mode, which now occurs at the metal-LiF interface is shifted to a larger angle of incidence than its value for the metal-vacuum interface. In both systems the dip corresponding to the surface plasmon mode shows broadening resulting mainly from the energy absorption associated with the non-zero value of the extinction coefficient of the metal. Several sharper dips in reflectance showing slight instrumental broadening only and corresponding to resonant

conditions for optical guided modes of different orders, occur between the critical angle and the surface plasmon resonance. The thicker the LiF film, the greater the number of guided modes that can be supported. With the system maintained under the $\sim 10^{-6}$ torr vacuum, reflectance vs angle of incidence scans were repeated at different times after LiF film deposition. It was found that the characteristic reflectance minima always shifted to larger angles of incidence with increasing age of the LiF film, each minimum going asymptotically with time to its final angular position. Observations were repeated until the characteristic minima were effectively no longer changing position with time. Representative reflectance vs angle of incidence scans obtained using p-polarized light incident on a semicylinder/metal/LiF system are shown in Fig. 1. In this case the semicylinder was of fused silica, the metal was Ag, the LiF was calculated to have a thickness of 855 nm, and the wavelength of the light was 500 nm. The scan for time zero was recorded immediately after deposition of the LiF and shows both optical guided modes and the surface plasmon mode (labelled m = 0). For the semicylinder/Ag film alone the surface plasmon mode was excited at an angle of incidence of $\sim 46°$, whereas it appeared initially for this semicylinder/Ag/LiF system at $\sim 75°$. The scans recorded after two and after thirteen days illustrate that for a particular optical mode (e.g., labelled m = 1) the shift to higher values of the observed angle of incidence for resonance is most rapid in the first few days.

Observations were obtained on several systems, for various periods of time lasting from one to 26 days. In each case a Suprasil (high-purity fused silica) semicylinder was used, and the metal layer was Ag

or Al. The thin metal films ranged in thickness from 20 to 50 nm for Ag and from 15 to 30 nm for Al. The LiF films ranged from 855 to 2,100 nm thick.

Analysis

The reflectance vs angle of incidence scans obtained on the thin metal films were analyzed by a method used previously by Kretschmann.[5] Through the use of approximate relationships involving the angular position of the surface plasmon reflectance minimum, its depth, and its half-width the real and imaginary parts of the complex dielectric constant and the thickness of each metal film were obtained. These quantities are required in a proper interpretation of the bulk properties of the LiF from the positions of the guided mode resonances.

The guided mode resonances in the LiF were analyzed using relationships, given by Hornauer and Raether,[4] which allow for the possibility of the LiF being optically anisotropic. Small corrections, $\delta\theta_o$, were first made[6] to the observed angles of incidence at which resonance occurred, θ, in order to obtain the correct values, θ_o, in the absence of coupling between the LiF and the semicylinder. It is the thickness of the metal film which determines the extent of this coupling. We chose the metal thickness to produce good coupling with only slight distortion ($\delta\theta_o << \theta_o$) of the guided modes in the LiF. In Hornauer and Raether's experiment this correction was not necessary as their Ag films were ~80 nm thick and the LiF was almost completely decoupled from their prism. A least squares fitting procedure was used to fit simultaneously the corrected angular positions of all of the observed p- and s-guided mode resonances, for a given film and wavelength, to Eqs. (3) in Ref.

(4) to yield the film thickness D, and $n_{\perp}$ and $n_{\parallel}$, the refractive indices of the LiF for light polarized perpendicular and parallel, respectively, to the plane of incidence. The only mode not included in this analysis was the surface plasmon mode, which is associated with the metal-LiF interface rather than with the bulk properties of the LiF film.

The results of our observations on several systems are shown in Figs. 2 and 3. For all the films studied the LiF was essentially optically isotropic, any deviation from isotropicity being <0.2%. Hence the calculated refractive index, n, of the LiF is graphed as a function of time, t, after LiF deposition. In Fig. 2 the values of n vs t for a wavelength of 500 nm correspond to the reflectance vs θ data shown in Fig. 1. Also shown are the n vs t data for three other wavelengths. Figure 3 shows data, obtained at λ = 500 nm, for several Suprasil/Ag/LiF and Suprasil/Al/LiF systems. For each sample the value of n was $\sim$1.3 when the film was deposited and increased to $\sim$1.4 after several days. Also shown in Fig. 3 is the LiF thickness, D vs t, for one of the samples. In each system a decrease in LiF thickness of $\sim$1% was seen in the first one to two days after deposition, after which the thickness was constant with time to $\sim\pm$0.2%. As a check on the results presented, a thick LiF film was deposited directly onto the plane face of a semicylinder and the refractive index of the LiF calculated from observations of the critical angle at the semicylinder/LiF interface. The variation of refractive index with time after deposition for this system is also shown in Fig. 3 and is seen to be consistent with data obtained on the semicylinder/metal/LiF systems.

For a single resonance, uncertainties due to instrumental factors, including some slight deviation from the described geometry, account for an uncertainty in n of ± 0.002 or $<0.2\%$. However, since each n value results from a least squares fit to the observed angular positions of six or more resonances, the estimated error in a given n value is $<\pm 0.001$.

Discussion

Any change in the angular position of a given guided mode resonance implies a change in the optical path within the film caused by a change in the refractive index and/or the thickness of the LiF film. We have demonstrated that for LiF films maintained in vacuum, changes in the optical path within the film result mainly from a change in the refractive index. The refractive index increases from $\sim$1.3 to $\sim$1.4, or close to the crystalline value, in the course of a few days. This implies that the LiF, loosely packed when first deposited, anneals over a period of time to the more closely packed crystalline configuration. We saw no evidence of the $\sim$1% anisotropy reported by Hornauer and Raether.[4] Any anisotropy present in our films was $<0.2\%$ as long as the LiF was maintained in vacuum. However, when observations were made on a semicylinder/Ag/LiF system exposed to the atmosphere and the reflectance *vs* θ scans analyzed in the same way as the data presented in this paper, the refractive index of the LiF appeared to show a small anisotropy[7] similar to that seen by Hornauer and Raether. However, these data could be explained more satisfactorily in terms of a thin barrier layer with an index of refraction $\lesssim$ 1.15 separating an optically isotropic LiF film from the Ag substrate. All of the resonances, including the surface plasmon mode, are included in this analysis, whereas the analysis

leading to the ∿1% anisotropy does not include the surface plasmon mode. Our Ag/LiF samples exposed to the atmosphere eventually peeled, or flaked, off, whereas those maintained in vacuum remained stable in appearance. The intermediate layer apparently originates from the Ag films. It has been found[8] that when silver films were annealed in oxygen-containing atmospheres, surface agglomeration occurred rapidly; whereas when annealed in other selected atmospheres, they were stable.

The time required to approach the crystalline refractive index is found to vary among the different samples, and the factor governing the rate of change of n is not known. In each case, however, the change in n with time is most rapid immediately after film deposition, decreasing with increasing time as n approaches the crystalline value. Differences between systems presumably are inherent to the samples.

For comparison with the values of refractive index that we report here, Hornauer and Raether[4] gave the following results for two different films:

$$\text{(i)}\quad n_{\perp} = 1.3086,\quad n_{\parallel} = 1.3175,\quad D = 3093\ \text{nm}$$

$$\text{(ii)}\quad n_{\perp} = 1.3090,\quad n_{\parallel} = 1.3160,\quad D = 3143\ \text{nm}$$

Otto and Sohler[3] gave n = 1.31 for D = 3000 nm, while Holst and Raether[2] gave n = 1.22 for D < 20 nm and n = 1.40 for D > 50 nm. There is no mention in any of these reports of any variation of n with time.

Our results are significant when an optical system must be designed for maximum efficiency under specific conditions. Dielectric layers

which act as reflection or antireflection coatings are frequently used on optical components, and the thickness desired for a given function depends on the final value of the refractive index of the material of the layer. Thus it is necessary to know the correlation between the properties as deposited and the final properties of the layer. In most applications the exact time taken to reach the final crystalline-like, or annealed conditions, would be unimportant. It is sufficient to know that an approximately 10% increase occurs in n, from $\sim$1.3 to $\sim$1.4, after film deposition. Thus if films are monitored during deposition by interferometric techniques, subsequent changes in n should be taken into account when choosing the initial film thickness for a particular desired property.

References

1. A. Otto, in "Optical Properties of Solids--New Developments," Ed. B. O. Seraphin (North Holland Pub. Co., 1976), pp. 677-729.
2. K. Holst and H. Raether, Opt. Commun. 2, 312-316 (1970).
3. A. Otto and W. Sohler, Opt. Commun. 3, 254-258 (1971).
4. D. Hornauer and H. Raether, Opt. Commun. 7, 297-301 (1973).
5. E. Kretschmann, Z. Physik 241, 313-324 (1971).
6. E. D. Kretschmann and M. W. Williams, Bull. Am. Phys. Soc. Ser. II 22, 1269 (1977).
7. To be published.
8. A. E. B. Presland, G. L. Price, and D. L. Trimm, Surf. Sci. 29, 424-434 (1972).

Figure Captions

Fig. 1. Measured reflectance as a function of angle of incidence, θ, on a semicylinder/Ag/LiF system, recorded for p-polarized light of a wavelength of 500 nm. The characteristic minima are seen to shift to larger angles with increasing time after LiF deposition.

Fig. 2. The refractive index, n, of one LiF film as a function of time after deposition and of the wavelength, λ, of the incident light.

Fig. 3. The refractive index, n, for several LiF samples as a function of time after deposition, for a wavelength of 500 nm. —— Suprasil/Ag/LiF systems. – – – – Suprasil/Al/LiF systems. . . . . Suprasil/LiF system. The thickness of the LiF film is recorded on each curve. Also shown is the thickness as a function of time of one LiF sample.

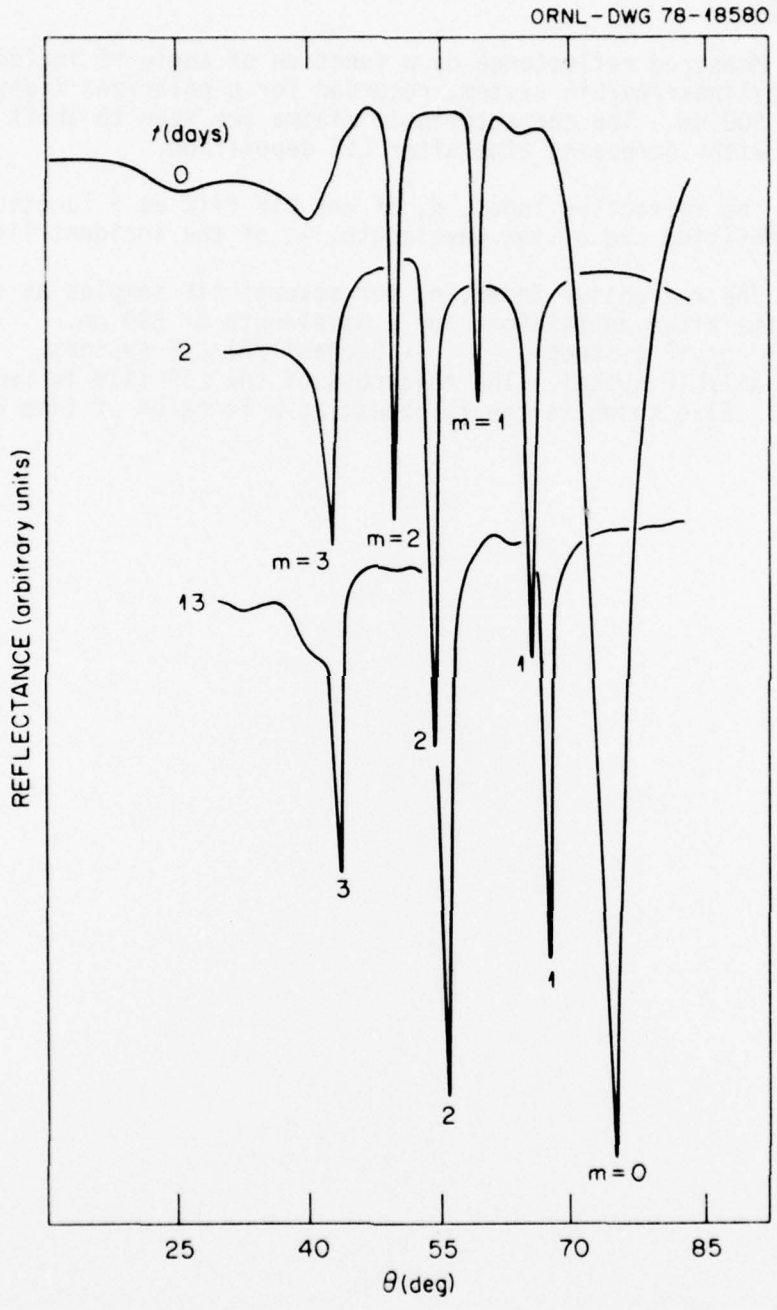
ORNL-DWG 78-18580
t(days)
0
2
13
m=3
m=2
m=1
m=0
3
2
2
1
1
REFLECTANCE (arbitrary units)
25
40
55
70
85
θ(deg)

Fig. 1

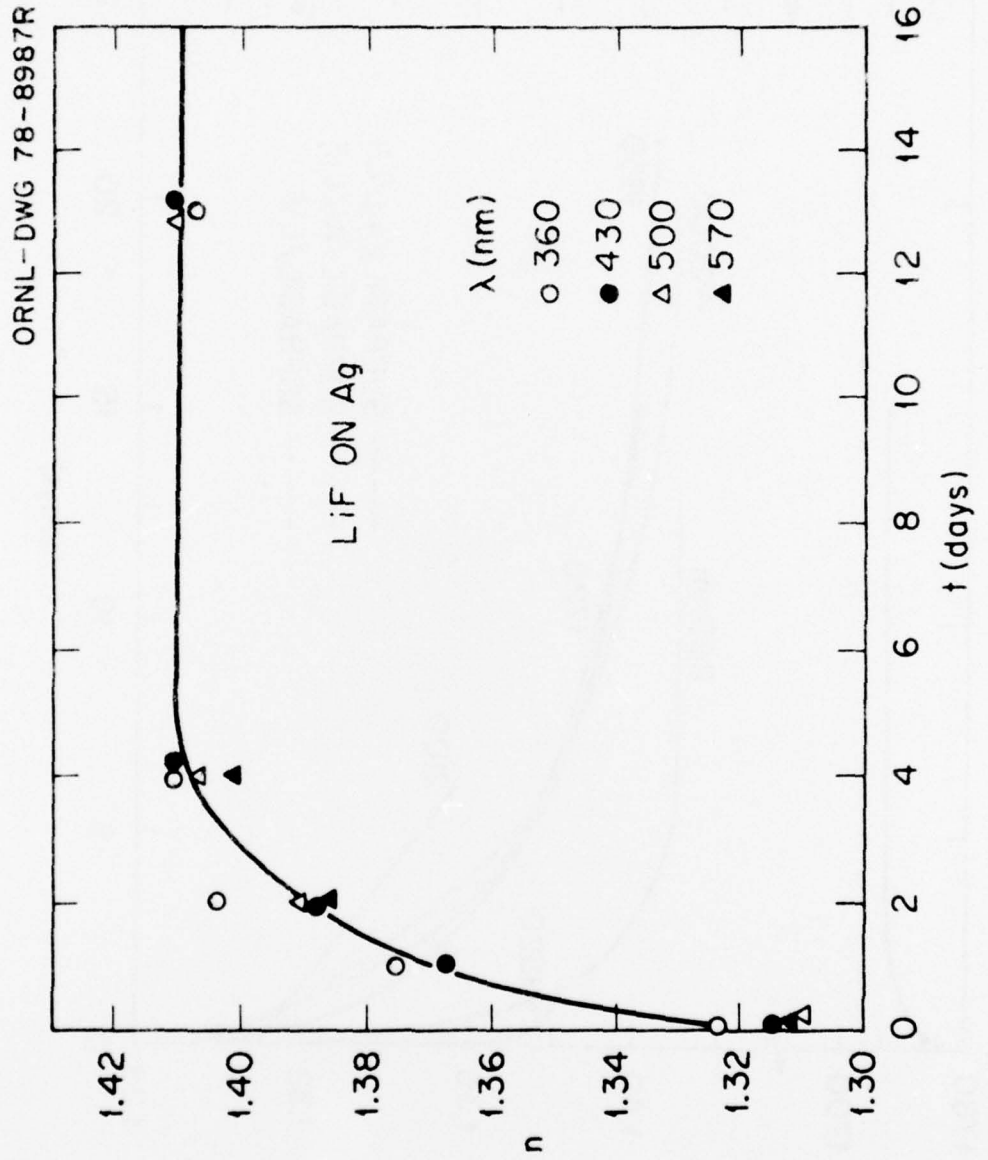
ORNL-DWG 78-8987R
LiF ON Ag
λ (nm)
o 360
● 430
Δ 500
▲ 570
n
t (days)
1.42
1.40
1.38
1.36
1.34
1.32
1.30
0
2
4
6
8
10
12
14
16

Fig. 2

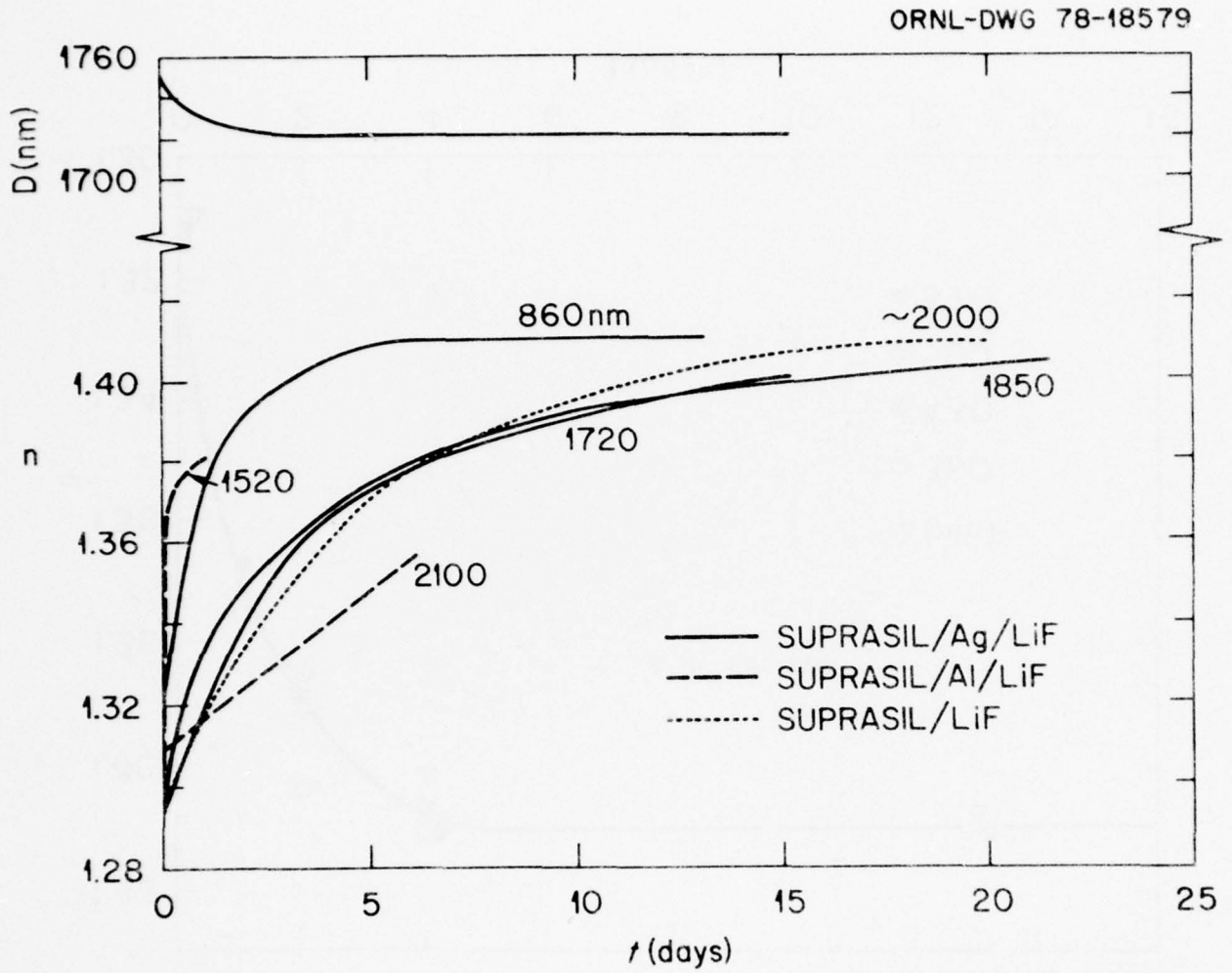
ORNL-DWG 78-18579
1760
1700
D(nm)
860nm
~2000
1850
1720
1520
2100
1.40
1.36
1.32
1.28
n
SUPRASIL/Ag/LiF
SUPRASIL/Al/LiF
SUPRASIL/LiF
0
5
10
15
20
25
t (days)

Fig. 3

CHAPTER VI

A MODEL CALCULATION OF CROSS SECTIONS FOR INNER-SHELL IONIZATION BY ELECTRONS

J. C. Ashley and R. H. Ritchie
Health and Safety Research Division

Inverse mean free paths (or cross sections) for inner-shell ionization of atoms by electrons form part of the basic input for detailed electron transport calculations. Thus it is important to have a simple, reliable method for obtaining such cross sections for a wide variety of materials. We propose a scheme for predicting cross sections for inner-shell ionization based on binary encounter theory and experimental photoelectric cross sections. Background material for this calculation can be found in our earlier study entitled "Classical Binary Collision Cross Sections of Atomic Systems" (see Ref. 1).

The hydrogenic oscillator strength (GOS) corresponding to the classical-binary-collision model is given by[1]

$$\frac{df}{d\varepsilon} = \frac{2^8}{3\pi} \cdot \frac{\varepsilon\eta^3\,\Theta(\varepsilon-\varepsilon_i)}{[(\varepsilon-\eta^2)^2+4\eta^2]^3} \quad , \tag{1}$$

where $\eta = q/\sqrt{2mE_{oi}}$, $\varepsilon = \epsilon/E_{oi}$, and $\varepsilon_i = E_i/E_{oi}$ are dimensionless variables related to, respectively, momentum transfer q, energy transfer ϵ, and "ionization energy" E_i for the given shell i. Here E_{oi} is the mean kinetic energy of the electrons in the shell. As shown earlier,[1] this GOS suffers from an oscillator strength deficiency at small momentum transfers, η, which is clearly related to the factor η^3 in the numerator. This deficiency may be remedied by adding a simple polynomial expression $g(\varepsilon)$ to the numerator of the GOS, viz.,

$$\frac{df}{d\varepsilon} = \frac{2^8}{3\pi} \cdot \frac{\varepsilon[\eta^3+g(\varepsilon)]\,\Theta(\varepsilon-\varepsilon_i)}{[(\varepsilon-\eta^2)^2+4\eta^2]^3} \quad . \tag{2}$$

The form

$$g(\varepsilon) = A_0 + A_1\varepsilon + A_2\varepsilon^2 + A_3\varepsilon^3 \qquad (3)$$

is convenient and should be flexible enough to fit experimental data over a fairly wide range of energy. In the limit $\eta \to 0$, Eq. (2) becomes

$$\frac{df_o}{d\varepsilon} = \frac{2^8}{3\pi} \cdot \frac{g(\varepsilon)}{\varepsilon^5}\, \Theta(\varepsilon - \varepsilon_i) \quad . \qquad (4)$$

Note that the integral $\int_{\varepsilon_i}^{\infty} \frac{df}{d\varepsilon}\, d\varepsilon$ would diverge if $g(\varepsilon)$ contained a power of ε higher than the third. If terms with negative powers had been included, the integral of Eq. (2) over ε would become very cumbersome to obtain in analytical form.

The constants required to specify $g(\varepsilon)$, and thus the optical oscillator strength, Eq. (4), can be obtained from data on photoelectric cross sections, $\sigma_p(\epsilon)$, through the relation

$$\frac{df_o}{d\epsilon} = \frac{\sigma_p(\epsilon)}{2\pi^2 \alpha a_o^2 (e^2/a_o)} \quad , \qquad (5)$$

where a_o is the Bohr radius and α is the fine structure constant, or

$$\frac{df_o}{d\epsilon}\,[eV^{-1}] = 9.11 \times 10^{-9}\, \sigma_p[\text{barns}] \quad . \qquad (6)$$

The compilations of photoabsorption cross sections produced by Biggs and Lighthill[2] and by Storm and Israel[3] are useful for fitting purposes. Biggs and Lighthill give analytical fits to experimental data for

a wide range of elements ($1 \leq Z \leq 100$). Unfortunately their fits have the form $\sigma_p = \sum_{k=1}^{4} B_k \epsilon^{-k}$, including a power ϵ^{-1} which is inadmissible since the integral of $df_0/d\varepsilon$ (and σ_p as well) must converge. (In fitting their expressions by polynomials of the form of Eq. (3) one should use only the range of energy over which experimental data are available. This range may be read from their graphs.)

Once the task of fitting σ_p for a given inner shell to obtain the constants A_i has been accomplished, one can obtain the predicted cross section for ionization of that shell by fast electrons by carrying out the double integral[1]

$$\sigma_e^i(E_1) = \int_{\sqrt{\beta}-\sqrt{\beta-\varepsilon_i}}^{\sqrt{\beta}+\sqrt{\beta-\varepsilon_i}} d\eta \int_{\varepsilon_i}^{2\eta\sqrt{\beta}-\eta^2} d\varepsilon \; \frac{d^2\sigma}{d\varepsilon\, d\eta} \quad , \tag{7}$$

where $\beta = E_1/E_0$ and E_1 is the energy of the incident electron. Since the doubly-differential cross section $d^2\sigma/d\varepsilon d\eta$ is related to the GOS through

$$\frac{d^2\sigma}{d\varepsilon\, d\eta} = \frac{2\pi e^4}{E_0 \beta} \cdot \frac{1}{\varepsilon\eta} \cdot \frac{df}{d\varepsilon} \quad , \tag{8}$$

Eqs. (2) and (7) lead to

$$\sigma_e^i(E_1) = \frac{2^9 e^4}{3E_0\beta} \int_{\sqrt{\beta}-\sqrt{\beta-\varepsilon_i}}^{\sqrt{\beta}+\sqrt{\beta-\varepsilon_i}} \frac{d\eta}{\eta} \int_{\varepsilon_i}^{2\eta\sqrt{\beta}-\eta^2} d\varepsilon \; \frac{\eta^3 + g(\varepsilon)}{[(\varepsilon-\eta^2)^2 + 4\eta^2]^3} \quad , \tag{9}$$

with $g(\varepsilon)$ given by Eq. (3) with the constants A_i determined from experimental data.

The integration over ε in Eq. (9) may be carried out analytically. The basic integral to be evaluated may be written

$$I_n(\varepsilon) = \int_{\varepsilon}^{\infty} \frac{dx\; x^n}{[(x-\eta^2)^2 + K\eta^2]^3} \quad , \tag{10}$$

where $\kappa = 4$ in Eq. (9), but could be taken as a fitting parameter in some calculations. Equation (10) can also be expressed as

$$I_n = \int_{\lambda}^{\infty} \frac{dy\,(y+\eta^2)^n}{(y^2+\zeta)^3} = \sum_{s=0}^{n} \frac{n!}{s!(n-s)!}\,\eta^{2s}\,J_{n-s} \quad , \tag{11}$$

where $\lambda = \varepsilon - \eta^2$, $\zeta = \kappa\eta^2$, and

$$J_k = \int_{\lambda}^{\infty} \frac{dx\,x^k}{(x^2+\zeta)^3} \quad . \tag{12}$$

For k = 0, 1, Eq. (12) gives

$$J_0 = \frac{1}{4\zeta^{5/2}}\left[\frac{3}{2}\left(\frac{\pi}{2} - \tan^{-1}\mu\right) - \frac{3}{2}\frac{\mu}{1+\mu^2} - \frac{\mu}{(1+\mu^2)^2}\right] \quad , \tag{13a}$$

$$J_1 = \left[4\zeta^2(1+\mu^2)^2\right]^{-1} \quad , \tag{13b}$$

where $\mu = \lambda/\zeta^{1/2}$. The recursion relation

$$J_k = \frac{1}{3}\left[\zeta J_{k-2} + \frac{\zeta^{(k-5)/2}\,\mu^{k-1}}{(k-1)(1+\mu^2)^2}\right] \tag{14}$$

may be used to find any of the J_K once J_0 and J_1 have been found.

In terms of the integrals I_n in Eq. (10), Eq. (9) becomes

$$\sigma_e^{\,i}(E_1) = \frac{2^9 e^4}{3E_0\beta}\int_{\sqrt{\beta}-\sqrt{\beta-\varepsilon_i}}^{\sqrt{\beta}+\sqrt{\beta-\varepsilon_i}} \frac{d\eta}{\eta}\left[(\eta^3+A_0)\,I_0(\varepsilon) + A_1 I_1(\varepsilon) + A_2 I_2(\varepsilon) + A_3 I_3(\varepsilon)\right]\Bigg|_{\varepsilon=2\eta\sqrt{\beta}-\eta^2}^{\varepsilon=\varepsilon_i} . \tag{15}$$

The remaining integration over momentum transfer η may be carried out numerically.

The procedure outlined here gives a reasonable approach for obtaining GOS's and hence inner-shell ionization cross sections, from the relatively abundant photoionization data[2,3] covering a wide range of elements. There remains, however, the task of comparing the results obtained by this procedure with differential inverse mean free paths calculated using theoretical GOS values, e.g., for aluminum[4], and experimental data on inner-shell ionization by electrons.[5]

REFERENCES

1. R. H. Ritchie, J. C. Ashley, and Dayashankar in "Studies of Electron Interactions with Communications Materials," Rome Air Development Center Report RADC-TR-77-74 (February, 1977) pp. 25-43.
2. F. Biggs and R. Lighthill, Sandia Laboratories Research Report No. SC-RR-71-0507.
3. E. Storm and H. I. Israel, Nuclear Data Tables A7, 565-681 (1970).
4. J. C. Ashley, C. J. Tung, and R. H. Ritchie, IEEE Trans. Nucl. Sci. NS-22, 2533-2536 (1975).
5. See, e.g., C. J. Powell, Rev. Mod. Phys. 48, 33-47 (1976).

PUBLICATIONS AND PRESENTATIONS

During the course of this work, several papers were published, or prepared for publication, and presentations were given at conferences, which described work related to this project and for which partial support by the Air Force was acknowledged. A list of these items follows.

Publications

J. C. Ashley, C. J. Tung, R. H. Ritchie, and V. E. Anderson, *"Calculations of mean free paths and stopping powers of low energy electrons ($\leq$ 10 keV) in solids using a statistical model,"* IEEE Trans. Nucl. Sci. NS-23, 1833-1837 (December, 1976).

J. C. Ashley and R. H. Ritchie, *"The influence of damping on the mean free path of low energy electrons in an electron gas,"* Phys. Status Solidi B 83, K159-K163 (October, 1977).

C. J. Tung, J. C. Ashley, R. D. Birkhoff, R. H. Ritchie, and L. C. Emerson, *"Electron slowing-down flux spectrum in Al_2O_3,"* Phys. Rev. B 16, 3049-3055 (October, 1977).

C. J. Tung and R. H. Ritchie, *"Electron slowing-down spectra in aluminum metal,"* Phys. Rev. B 16, 4302-4313 (November, 1977).

J. C. Ashley, C. J. Tung, R. H. Ritchie, and V. E. Anderson, *"Inverse mean free path, stopping power, CSDA range, and straggling in polystyrene for electrons of energy $\leq$ 10 keV,"* Air Force Report, RADC-TR-78-32 (February, 1978).

E. Kretschmann, *"The ATR method with focused light--Application to guided waves on a grating,"* Opt. Commun. 26, 41-44 (July, 1978).

M. S. Chung, T. A. Callcott, and E. T. Arakawa, *"Radiation from Ag and K films bombarded by low energy electrons,"* Oak Ridge National Laboratory Report, ORNL-TM-6527 (October, 1978).

J. C. Ashley, C. J. Tung, and R. H. Ritchie, *"Inelastic interactions of electrons with polystyrene: Calculations of mean free paths, stopping powers, and CSDA ranges,"* IEEE Trans. Nucl. Sci. NS-25, 1566-1570 (December, 1978).

J. C. Ashley, C. J. Tung, and R. H. Ritchie, *"Electron inelastic mean free paths and energy losses in solids: I. Aluminum metal,"* Surf. Sci. (to be published).

C. J. Tung, J. C. Ashley, and R. H. Ritchie, *"Electron inelastic mean free paths and energy losses in solids: II. Electron gas statistical model,"* Surf. Sci. (to be published).

J. C. Ashley, V. E. Anderson, J. J. Cowan, R. H. Ritchie, and J. Hoelzl, *"Straggling and plasmon excitation in the energy loss spectra of electrons transmitted through carbon,"* Thin Solid Films (submitted for publication).

T. L. Haltom, E. T. Arakawa, M. W. Williams, and E. Kretschmann, *"Refractive index of LiF films as a function of time,"* Appl. Opt. (submitted for publication).

M. S. Chung, T. A. Callcott, E. T. Arakawa, and E. Kretschmann, *"Radiation from silver films bombarded by low-energy electrons,"* Surf. Sci. (submitted for publication).

E. Kretschmann, T. A. Callcott, and E. T. Arakawa, *"Theory of emission spectra from metal films irradiated by low-energy electrons near normal incidence,"* Surf. Sci. (submitted for publication).

E. Kretschmann, T. L. Ferrell, and J. C. Ashley, *"A splitting of the dispersion relation of surface plasmons on a rough surface,"* Phys. Rev. Lett. (submitted for publication).

M. W. Williams, J. C. Ashley, E. Kretschmann, T. A. Callcott, M. S. Chung, and E. T. Arakawa, *"Splitting of surface-plasmon emission spectra from potassium,"* Phys. Lett. A (submitted for publication).

Presentations

C. J. Tung, R. H. Ritchie, and J. C. Ashley, *"Electron slowing-down spectra in Al and Al_2O_3,"* American Physical Society, Southeastern Section, Virginia Beach, Va., November 11-13, 1976.

M. W. Williams, T. Inagaki, R. N. Hamm, and E. T. Arakawa, *"Optical properties of polystyrene and optical sum rules,"* American Physical Society, Southeastern Section, Virginia Beach, Va., November 11-13, 1976.

J. C. Ashley and R. H. Ritchie, *"Influence of plasmon damping on the mean free path of electrons for plasmon excitation,"* American Physical Society, Southeastern Section, Virginia Beach, Va., November 11-13, 1976.

J. C. Ashley, C. J. Tung, R. D. Birkhoff, and R. H. Ritchie, *"Electron slowing-down spectra in aluminum metal,"* IEEE Annual Conference on Nuclear and Space Radiation Effects, Williamsburg, Va., July 12-15, 1977.

J. C. Ashley, C. J. Tung, and R. H. Ritchie, *"Mean free path and energy loss of electrons in polystyrene,"* American Physical Society, Miami Beach, Florida, November 21-23, 1977.

M. S. Chung, T. A. Callcott, and E. T. Arakawa, *"Radiation from silver films irradiated by low energy electrons,"* American Physical Society, Miami Beach, Florida, November 21-23, 1977.

E. D. Kretschmann and M. W. Williams, *"Approximate Fresnel coefficients for a multilayer system near the resonance condition for optical guided modes,"* American Physical Society, Miami Beach, Florida, November 21-23, 1977.

T. L. Haltom, E. T. Arakawa, R. N. Hamm, E. D. Kretschmann, and M. W. Williams, *"Optical properties and thickness of a dielectric layer from attenuated total reflection,"* American Physical Society, Miami Beach, Flordia, November 21-23, 1977.

J. C. Ashley, C. J. Tung, and R. H. Ritchie, *"Mean free paths and energy losses of electrons in polystyrene,"* IEEE Annual Conference on Nuclear and Space Radiation Effects, Albuquerque, New Mexico, July 18-21, 1978.

J. C. Ashley, J. J. Cowan, R. H. Ritchie, and V. E. Anderson, *"Energy spectra of electrons transmitted thru thin solid films of carbon,"* IEEE Annual Conference on Nuclear and Space Radiation Effects, Albuquerque, New Mexico, July 18-21, 1978.

MISSION
of
Rome Air Development Center

RADC plans and executes research, development, test and selected acquisition programs in support of Command, Control Communications and Intelligence (C^3I) activities. Technical and engineering support within areas of technical competence is provided to ESD Program Offices (POs) and other ESD elements. The principal technical mission areas are communications, electromagnetic guidance and control, surveillance of ground and aerospace objects, intelligence data collection and handling, information system technology, ionospheric propagation, solid state sciences, microwave physics and electronic reliability, maintainability and compatibility.

Printed by
United States Air Force
Hanscom AFB, Mass. 01731